The Dissertation Committee for Jason Henry Stephens Certifies that this is the approved version of the following dissertation:

TECTONIC AND DEPOSITIONAL HISTORY OF AN ACTIVE FOREARC BASIN, SANDINO BASIN, OFFSHORE NICARAGUA

Committee:

Craig S. Fulthorpe, Supervisor

Kirk D. McIntosh, Co-Supervisor

Robert H. Tatham

Ronald J. Steel

Brian K. Horton

TECTONIC AND DEPOSITIONAL HISTORY OF AN ACTIVE FOREARC BASIN, SANDINO BASIN, OFFSHORE NICARAGUA

by

Jason Henry Stephens, B.S.

Dissertation

Presented to the Faculty of the Graduate School of

The University of Texas at Austin

in Partial Fulfillment

of the Requirements

for the Degree of

Doctor of Philosophy

The University of Texas at Austin

May 2014

Dedication

To my wife, Carissa, for her love and understanding
and our three amazing children, Jasper, Penelope, and Dean
who fill each day with wonder and elation.
And to my parents who never wavered in their support.

Acknowledgements

I would like to thank the National Science Foundation for generously funding much of my involvement in the NicStrat project. Additional funding for my graduate studies was provided by the Jackson School of Geosciences at the University of Texas at Austin, the ConocoPhillips SPIRIT Scholar program, as well as the Gale White Fellowship from the University of Texas Institute for Geophysics Fellowship Committee. I am very grateful to have received such an abundance of financial support from these institutions.

I would like to thank both Craig Fulthorpe and Kirk McIntosh for giving me the tremendous opportunity to be involved with such an incredible project and showing me the ropes as a seafaring geoscientist aboard the *R/V Maurice Ewing*. Furthermore, I would like to thank Craig especially for his ceaseless encouragement and for always making himself available for discussions, not limited to the intricacies of seismic stratigraphy or the Sandino basin. I would like to thank Kirk who helped tremendously to create a deeper understanding of the myriad complex geological processes underway in Central America. I would also like to thank Bob Tatham for his guidance and for giving me such a great education in geophysics when I first arrived at the Jackson School. I greatly appreciate the efforts of my other dissertation committee members Ron Steel and Brian Horton as well as former member Randy Marrett. I would also like to thank Jack Sharp who served on my qualifying committee.

I would also like to thank the crew of the *R/V Ewing* during cruise EW04-12 from Lamont-Doherty Earth Observatory including Ted Koczynski, Anthony Johnson, Dietmar Kathman, Carlos Gutierrrez, and Justin Walsh for making the acquisition phase run so

smoothly. I am also thankful for the efforts of Kirk and Craig as co-Chief Scientists during the NicStrat cruise and their tremendous leadership at sea. I would also like to recognize the efforts of the watchstanders at sea, Matthew McDonald, Carlos Venegas, Julius Doruelo, Manuel Trana, Manuel Alvarez, and Luis Castillo.

There have been a great number of research scientists, staff, and students at UTIG that have been enormously helpful during my time at 'The Institute.' Steffan Saustrup was a great teacher of seismic data processing and his contributions during the acquisition and processing phases of our NicStrat data were indispensable. I also want to thank Chaoshun Hu and Mike Hanson who made tremendous contributions during the data processing phase. The technical support staff at UTIG, including Mark Weiderspahn, Kevin Johnson, and John Gerboc, are superb and I want to sincerely thank them for doing such a fantastic job each and every day.

I have been very fortunate to attend the Jackson School alongside so many wonderfully helpful and incredibly bright people through the years, including Paresh Patel, Matt MacDonald, Craig Calkins, Russell Young, Katherine Young, Kimberley Kumar, Lindsay Lowe Worthington, Carla Sanchez, Carolina Gomez, Carlos Venegas, Guy Fitz, Justin Funk, David Gorney, and many, many others. Thank you all for being such good friends during my time in Austin.

Finally, I would like to thank my family. I must thank my children Jasper, Penelope, and Dean who are especially adept at dissolving any frustrations I might have brought home after days when the Sandino basin may have gotten the best of me. I am grateful to have had such great parents. My mother, Larraine, taught me to love the act of learning and offers exactly what I need before I even know to ask. My father, Henry, taught me to make improvements rather than excuses after my failures. I want to thank my siblings who will always be my best friends and, for better or worse, never stop

making fun of me. I am indebted to my sister Kate who gave me courage and lent a compassionate ear whenever it was needed. Thanks are due to my brother Rob with whom I share such a strong bond. Last but not least, a very special thank you is extended to my wife Carissa to whom I am deeply indebted for her continued patience, encouragement, and inspiration. Without her support and sacrifices, I am certain that there is no way I would have accomplished this.

TECTONIC AND DEPOSITIONAL HISTORY OF AN ACTIVE FOREARC BASIN, SANDINO BASIN, OFFSHORE NICARAGUA

Jason Henry Stephens, Ph.D.

The University of Texas at Austin, 2014

Supervisors: Craig F. Fulthorpe and Kirk D. McIntosh

High-resolution (20-250 Hz) multichannel seismic (MCS) reflection data with record lengths of 4-8 s TWT, totaling approximately 4620 line km on the shelf and slope of the Sandino forearc basin of offshore western Nicaragua, were acquired in November-December 2004 (cruise EW04-12) and subsequently processed at the University of Texas Institute for Geophysics. Seismic stratigraphic interpretation was conducted using these MCS data in conjunction with deeper penetration (16-20 s TWT) MCS profiles from a previous survey (cruise EW00-05). Age estimates were based on cuttings from intersecting industry wells. Structure and isochron maps were created for 16 sequences and used to identify structural and depositional trends within the Sandino basin. The tectonostratigraphic evolution of the basin varies considerably along-strike and is divided into five general stages from Late Cretaceous to recent. Evidence for multiple episodes of terrane accretion is observed from Late Eocene to Late Oligocene and potentially during Mid- to Late Miocene as well. Stratal stacking patterns suggest the Nicaraguan margin has not been dominated by subduction erosion during its history and extensional features beneath the slope are interpreted to have also been affected by processes related to the collision of allochthonous terrane of the downgoing plate, sediment underplating, and slab roll-back. With more precise age control, the stable northwestern region of the

Sandino basin, where sediment is relatively undeformed since Late Oligocene and measures ≥ 16 km thick, offers a unique convergent margin setting for investigations of forcings on sequence development.

Table of Contents

List of Tables

List of Figures

Chapter 1: Introduction

The main research objective of this study of the offshore Sandino forearc basin is to refine the tectonic and depositional history of the basin through detailed seismic stratigraphic analysis. This investigation establishes the extent of both offshore depositional sequences and major structural features within the basin. The relationships between the stratigraphic sequences and structural features are analyzed to establish the relative timing of tectonic events and the roles which major regional tectonic events and eustasy may have played in the formation of this complex and actively deforming basin. The results of this offshore study are also compared to previous studies from onshore Nicaragua and Costa Rica to investigate the relationships between geologic processes in both settings.

Few published multi-channel seismic (MCS) reflection profiles from the Sandino basin exist in the literature and this investigation is the first non-industry MCS study of the basin to examine its seismic stratigraphy using data that have regional coverage (Fig. 1.1). McIntosh et al. (2007) explored the Nicaraguan Pacific margin using several lower resolution deep-penetration MCS data in an effort to better understand the region's subduction processes and seismogenic zone. Acquired in 2000, this earlier data set from the NicSeis survey (most of which is incorporated into this study) imaged the forearc basin and the underlying margin wedge but detailed stratigraphic analysis on the shelf was limited due to insufficient vertical and horizontal resolution. Outside of industry, the most comprehensive previous seismic stratigraphic study of the Sandino basin is based on one composite profile created by reprocessing three overlapping dip profiles of relatively low-frequency seismic data (Ranero et al., 2000).

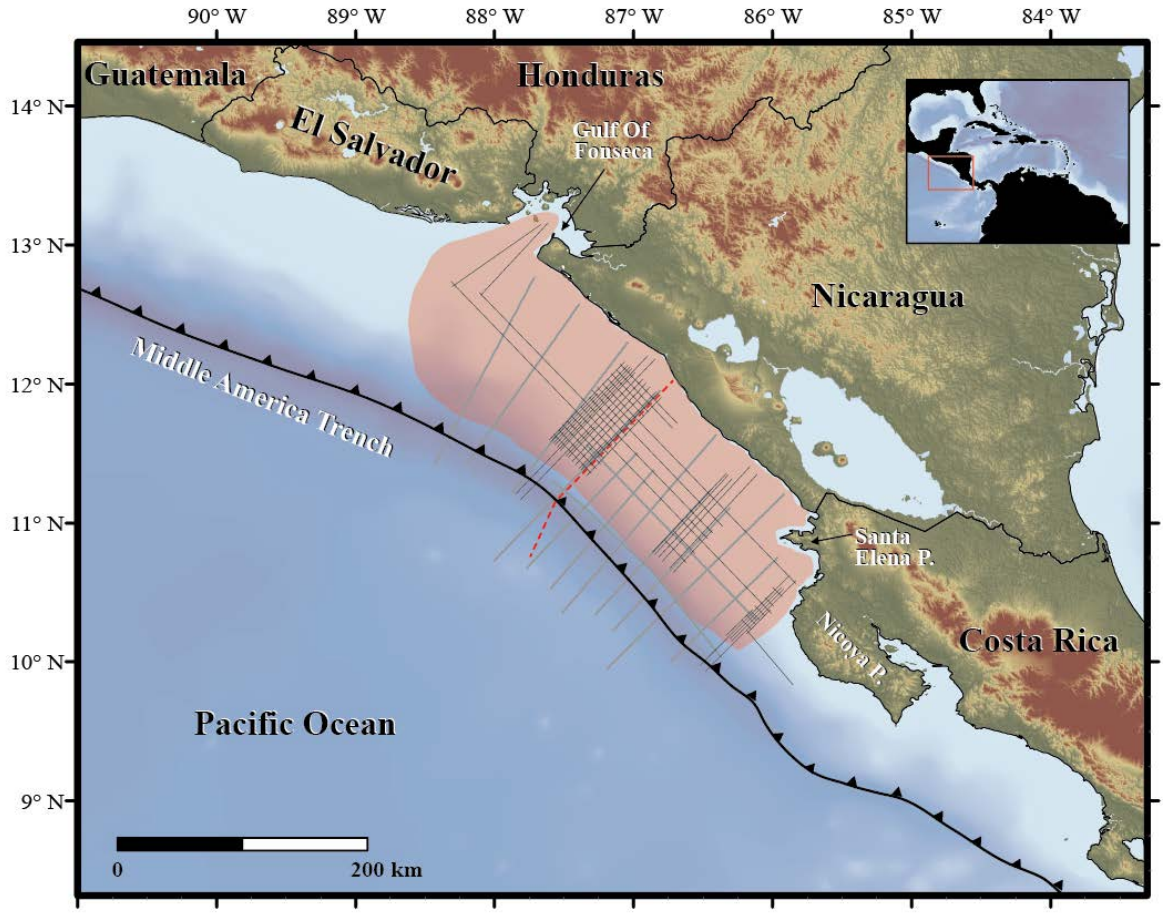

Figure 1.1: General location map of study area. Brown shading marks the approximate boundary of the offshore Sandino basin, which is bounded by the Middle America Trench to the southwest, the Santa Elena Peninsula (Santa Elena P.) and Nicoya Peninsula (Nicoya P.) to the southeast, the Nicaraguan coast to the northeast, and (approximately) the seaward projection of the Gulf of Fonseca to the northwest. Profile locations for the primary data used for this study, the EW04-12 NicStrat MCS survey, are shown as thin black lines. Profiles of the deeper penetration NicSeis MCS data that were also incorporated into this study are shown as thicker gray lines. The approximate location of the composite MCS profile used by Ranero et al. (2000) is represented by the dashed red line. Bathymetry data is from GEBCO (2008). Topography is from Shuttle Radar Topography Mission (SRTM) data set (Jarvis et al., 2006).

The MCS data acquired for the this study in 2004 (R/V *Maurice Ewing* cruise EW04-12; also referred to here as the "NicStrat" survey) presents many advantages over previous surveys for the purpose of constructing a detailed geologic history of the forearc basin including its broad coverage coupled with the existence of three separate regions of closely spaced grids, long regional strike lines, and high vertical resolution (~5 m).

In addition to recording the regional stratigraphic and tectonic history, the unique setting of the Sandino basin offers insights into the relative roles that different forcings, such as tectonics and changes in global sea level, play into the development of stratigraphic sequences. In the northwestern portion of the study area and farther northward in the forearc regions offshore El Salvador and Guatemala, previous studies have shown that the shelf has been dominated by subsidence throughout the Cenozoic allowing development of a sedimentary section with a maximum thickness that is at least 14 km and possibly as great as 22 km (Ladd and Schroder, 1985; McIntosh et al., 2007). Conversely, the forearc regions of the southeastern Sandino basin and Costa Rica have relatively thin sedimentary sections due in part to erosion on the shelf caused by regional uplift of the area (Christeson et al., 1999; Hinz et al., 1996; Seyfried et al., 1991) that has exposed igneous basement onshore the Nicoya and Santa Elena Peninsulas (de Boer, 1979; Gazel et al., 2006; Hauff et al., 2000; Saginor et al., 2011). Therefore the Sandino basin transitions between two extreme regimes of vertical displacement along the Pacific margin of Nicaragua: (a) a more stable northwestern setting in the northwest dominated by long-term subsidence and where a primary eustatic signal may potentially be preserved despite the basin's location on an active margin, and (b) a southeastern setting where stratigraphically disruptive uplift and crustal deformation has eroded the sedimentary basin fill and overwhelms the potential for preserving a record of sea-level forcings.

This study is organized as follows: Chapter 2 gives an overview of previous studies in the region that describe the tectonic setting and geologic history of the Sandino forearc basin. Chapter 3 describes the data that are used in this study. Special attention is given to the MCS data acquired for this study including acquisition parameters and processing techniques. Chapter 4 presents the interpretation and mapping results of the seismic data. Chapter 5 is a synthesis of the tectonic and depositional history of the Sandino basin based on the offshore seismic stratigraphic analysis. The interpretation attempts to relate known major tectonic events and discusses the controls on seismic sequence formation. Chapter 6 presents specific conclusions about the evolution of the Sandino basin as well as broader implications related to our current understanding of how subduction processes affect deposition within forearc basins.

Chapter 2: Regional Geologic Background and Tectonic Setting of the Sandino Basin

2.1 TECTONIC HISTORY OF THE SANDINO BASIN

The Sandino forearc basin is located to the east of the plate boundary between the Caribbean plate and subducting oceanic Cocos plate (Molnar and Sykes, 1969). The tectonic history of the basin began in the Late Cretaceous with the initiation of eastward-dipping subduction of the Farallon plate beneath the western margin of the Chortis block (Elming et al., 2001; Mann, 2007) (Fig 2.1A). Subduction initiation is accompanied by uplift of the outer shelf and upper slope while rapid subsidence occurs within the forearc basin (Gurnis, 1992). Deposition in the Sandino basin likely began in this type of rapidly subsiding basin during its genesis on the western margin of the Chortis block while a basement high developed at the outer shelf (Ranero et al., 2000). This uplift of the outer forearc basement high may also have been a consequence of the accretion of an oceanic plateau during the Late Cretaceous to Early Paleocene, as inferred by modeling of seismic refraction and gravity data from a transect across the Sandino basin (Walther et al., 2000).

Plate reconstructions of the Early Eocene (49 Ma) configuration of the region show oblique subduction, ~25-30 degrees west of orthogonal, basinward of the Sandino basin (Mann, 2007) (Fig.2.1B). In addition, by Early Eocene, the ocean island arc Chorotega block was obducted at the trailing western edge of the Caribbean Large Igneous Province (CLIP) (Fig. 2.1B), directly adjacent to the southern boundary of the Chortis block (Fig. 2.1). Oblique subduction continued throughout the Oligocene, forming a volcanic arc associated with the Matagalpa Group found in the present day Nicaraguan and Honduran highlands (Ehrenborg, 1996) (Fig 2.2).

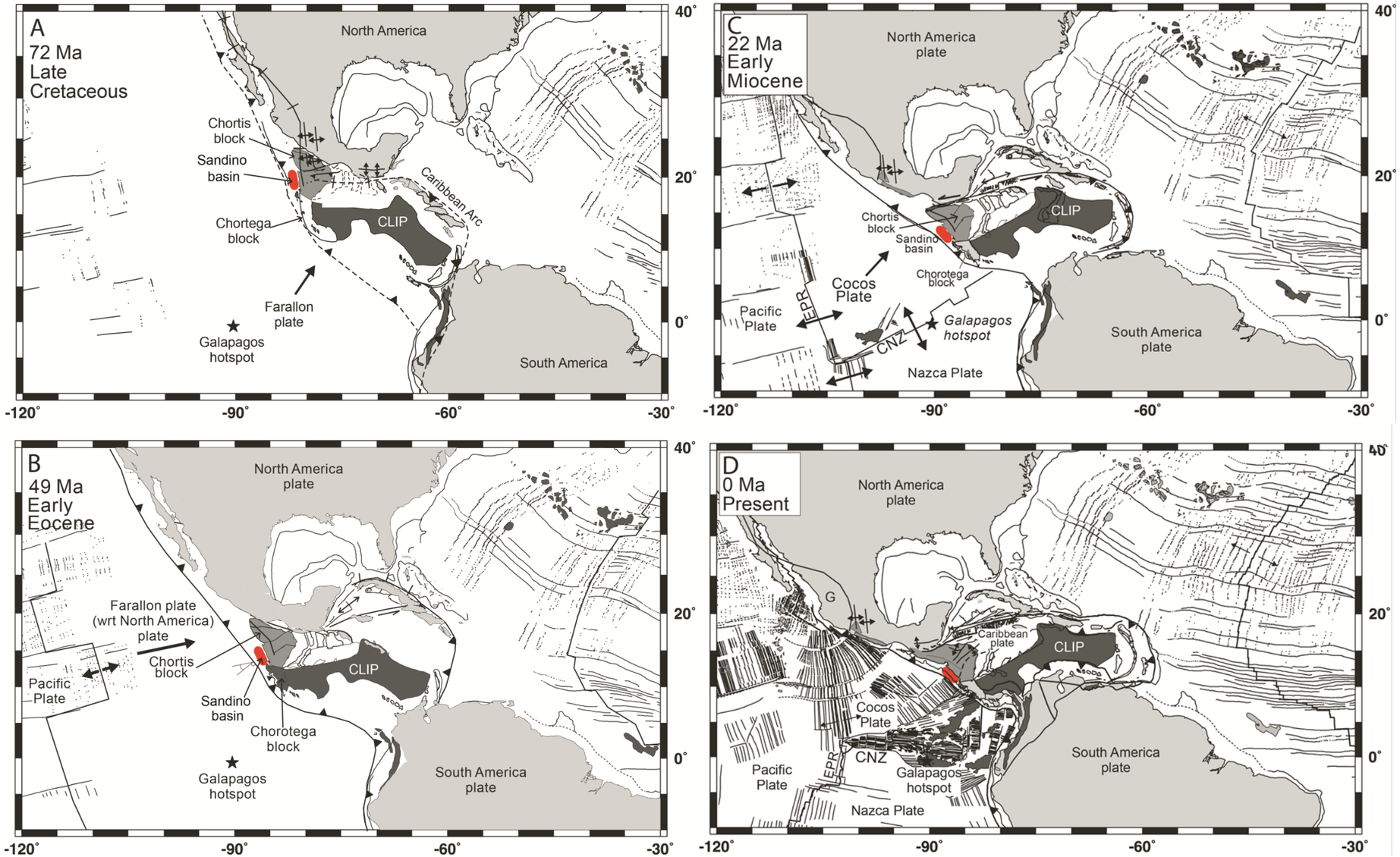
A
72 Ma
Late
Cretaceous
North America
Chortis
block
Sandino
basin
Caribbean Arc
CLIP
Chortega
block
Farallon
plate
Galapagos
hotspot
South America
B
49 Ma
Early
Eocene
North America
plate
Farallon plate
(wrt North America)
plate
Chortis
block
Pacific
Plate
Sandino
basin
CLIP
Chorotega
block
Galapagos
hotspot
South America
plate
C
22 Ma
Early
Miocene
North America
plate
Chortis
block
Sandino
basin
CLIP
Chorotega
block
Cocos
Plate
EPR
Pacific
Plate
CNZ
Galapagos
hotspot
Nazca Plate
South America
plate
D
0 Ma
Present
North America
plate
G
Caribbean
plate
CLIP
Cocos
Plate
Pacific
Plate
EPR
CNZ
Galapagos
hotspot
Nazca Plate
South America
plate
40˚
20˚
0˚
-120˚
-90˚
-60˚
-30˚

Fig. 2.1

Figure 2.1: Plate reconstruction for Caribbean and Central American region (modified from Mann et al., 2007). (A) Incipient subduction of Farallon plate along western margins of North American plate, Chortis block, Chorotega block, and South America plate as buoyant Caribbean Large Igneous Province (CLIP) wedges between North and South American plates during the Late Cretaceous. Deposition begins in forearc area of Chortis block in the Sandino basin (red oval). (B) North American and South American plates continue westward migration. Chortis block moves easterly along left-lateral strike-slip fault zone on its northern boundary. Subduction of Farallon plate is ENE outboard of Sandino basin, ~25-30° oblique from orthogonal. Chorotega and Chortis blocks converge. (C) In the Early Miocene, the Farallon plate is segmented by a rift that develops into the Cocos-Nazca spreading zone (CNZ). Plate reorganization leads to nearly orthogonal subduction beneath the Chortis block and, later, super-fast spreading at the East Pacific Rise (EPR). (D) At present, Chortis block is part of the Caribbean plate and subduction of EPR-derived Cocos plate continues eastward beneath it. CNZ-derived Cocos plate, including Galapagos hotspot tracks, converges with the subduction zone just to the southeast of the Sandino basin.

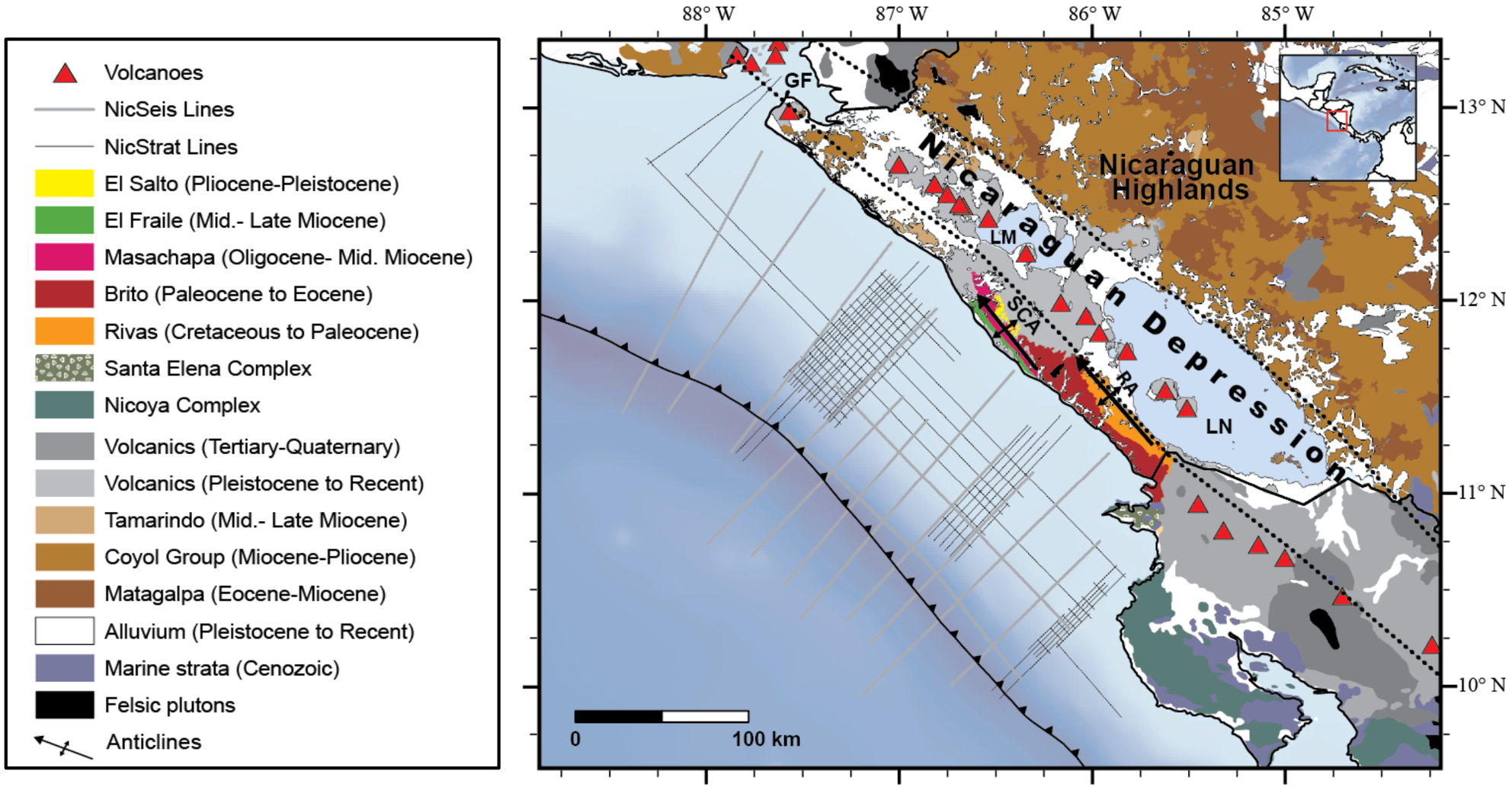

Figure 2.2: Onshore geologic map of the Sandino basin region. Approximate boundary of the Nicaraguan Depression is indicated by dotted lines extending from Gulf of Fonseca (GF) in the northwest, through Lake Managua (LM), Lake Nicaragua (LN) and the back arc region of Costa Rica. Sedimentary units of the Sandino basin outcrop on the southwestern coast of Nicaragua. Sandino basin basaltic basement outcrops to the south in Costa Rica in the Nicoya Complex and Santa Elena Complex. Paleoarc location is northeast of the Nicaraguan Depression in the Nicaraguan Highlands within deposits of the Matagalpa and Coyol Groups. Rivas (RA) and San Cayetano (SCA) anticlines are depicted on the isthmus of Nicaragua. Geologic map based on "Geological map of Nicaragua" 1:500 000, INETER Managua (1995) and mapping from Case and Holcombe (1980) and McBirney and Williams (1965). Bathymetry data are from GEBCO (2008).

During the Early Miocene, the Farallon plate underwent rifting at 22.7 Ma that divided it into the Cocos and Nazca plates (Barckhausen, 2001). This rifting was caused by high levels of tensional stresses related to its subduction to the north beneath the North American plate and to the south beneath the South American plate (Wortel and Cloetingh, 1981), giving rise to the precursor of the modern Cocos-Nazca spreading zone (Hey, 1977; Lonsdale and Klitgord, 1978; Meschede and Barckhausen, 2000). This plate reorganization during the Early Miocene forced the cessation of oblique subduction occurring at the western edge of the Chortis block as the convergence angle transitioned to nearly orthogonal (Mann, 2007) (Fig. 2.1). Shortly after the Farallon plate subdivided into the Cocos and Nazca plates, seafloor paleomagnetic data show that the East Pacific Rise (EPR) spreading center at the western boundary of the Cocos plate underwent a period of super-fast spreading between 18-10 Ma (Wilson, 1996) (Fig. 2.3). This rate of sea-floor spreading during the Miocene is the fastest known in the geologic record, reaching full-spreading rates of 180-210 mm/yr. The eastward spreading, EPR-derived, Cocos plate experienced half-spreading rates between 96-75 mm/yr during this period (Wilson, 1996). Coinciding with this anomalously high EPR spreading was the Miocene ignimbrite flare-up of Central America that occurred between 20-10 Ma based on the $^{40}Ar/^{39}Ar$ geochronology of tephra layers found in core samples collected from the western Caribbean Sea during Leg 165 of the Ocean Drilling Program (ODP) (Sigurdsson et al., 2000). These cored tephra layers have been linked by comparison of trace elements to the Central American Tertiary Ignimbrite Province which extends ~900 km from the southern highlands of Nicaragua to the border between Mexico and Guatemala (Jordan et al., 2006, 2007). In Nicaragua, the Miocene ignimbrite flare-up deposits are within the Coyol Group (Fig. 2.2) found along a trench-parallel arc that migrated ~60 km southwest

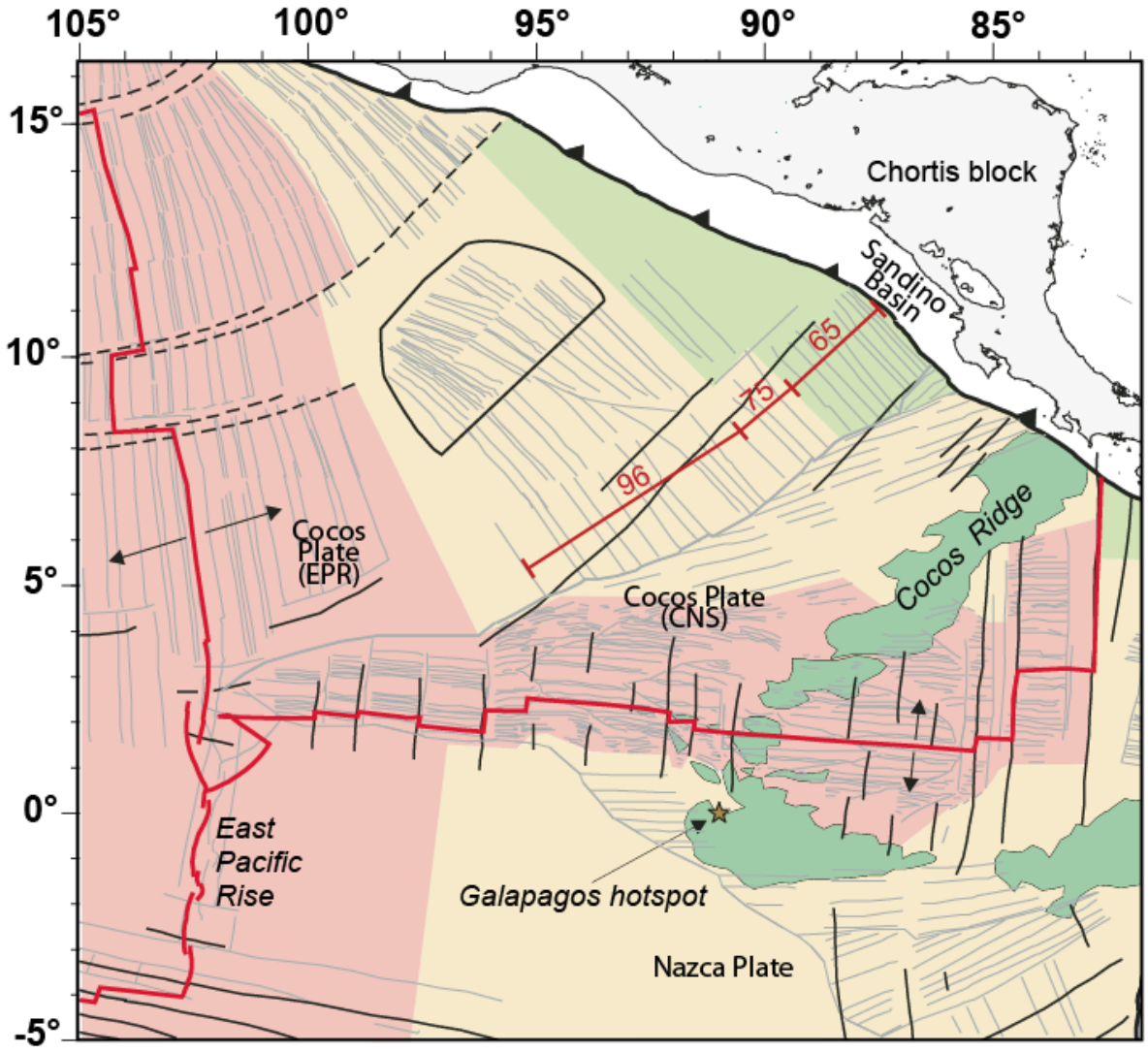

Figure 2.3: Seafloor spreading at the Cocos-Nazca and East Pacific Rise spreading zones. Ages of oceanic crust shown are 0-10 Ma (red), 10-20 Ma (yellow), and >20Ma (green) and are from marine magnetic anomalies and fracture zones in the UTIG PLATES database (2000), based on data and interpretation from Barckhausen et al. (2001), Wilson and Hey (1995), and Wilson (1996). Cocos plate lithosphere derived from the East Pacific Rise (EPR) and Cocos-Nazca spreading zones subducts at the Middle America Trench. The age of the EPR-derived Cocos plate at the trench west of the Sandino basin is approximately 25 Ma (modified from Rogers et al., 2002). The divergent Galapagos hotspot trail, including the Cocos Ridge, is shown in dark green. Red numbers indicate half-spreading rates from Wilson (1996) and Barckhausen et al. (2001).

from 25-7 Ma before becoming extinct at least 20 km northwest of the modern Central American Volcanic Front (CAVF) (Ehrenborg, 1996; McBirney and Williams, 1965; Plank et al., 2002; Saginor et al., 2011). The volcanic Tamarindo Group, geochemically distinct from the Coyol Group (Saginor et al., 2011), was also deposited onshore during the Middle Miocene (14.7-11.7 Ma) along a thin NW-SE band further west of the Coyol Group, seaward of the CAVF (Plank et al., 2002; Saginor et al., 2011).

As a consequence of the super-fast spreading at the EPR during the Miocene, relatively young, more buoyant lithosphere was delivered to the subduction zone at the ancient Middle America Trench. Rogers et al. (2002) suggested that this more buoyant lithosphere may have contributed to a slab tear and the eventual detachment of the subducted Cocos plate beneath the Caribbean and southern North American plate. The detachment has been imaged on tomographic profiles that transect the Cocos-Caribbean

and Cocos-North American margins (Rogers et al., 2002) (Fig. 2.4). The imaged slab gap allows upwelling of hot asthenospheric mantle through the tear beneath the continental western Caribbean margin including the Chortis block. This asthenospheric upwelling is proposed as the mechanism for the uplift of the Honduran and Nicaraguan Highlands that occurred sometime between 10-3.8 Ma (Rogers et al., 2002).

The Sandino basin region experienced a NE-SW compressional phase of deformation during the Miocene that generated folds found in the exposed Sandino basin on the isthmus of Nicaragua (Weinberg, 1992) (Fig. 2.2). The Rivas and San Cayetano anticlines, formed during this phase, strike roughly parallel to the trench and fold Late Miocene and older rocks which are then topped by unfolded Pliocene rocks overlying an unconformity (Fig. 2.2). The anticlines are described as having broad hinge zones (2-4 km) with wavelengths of 20-30 km.

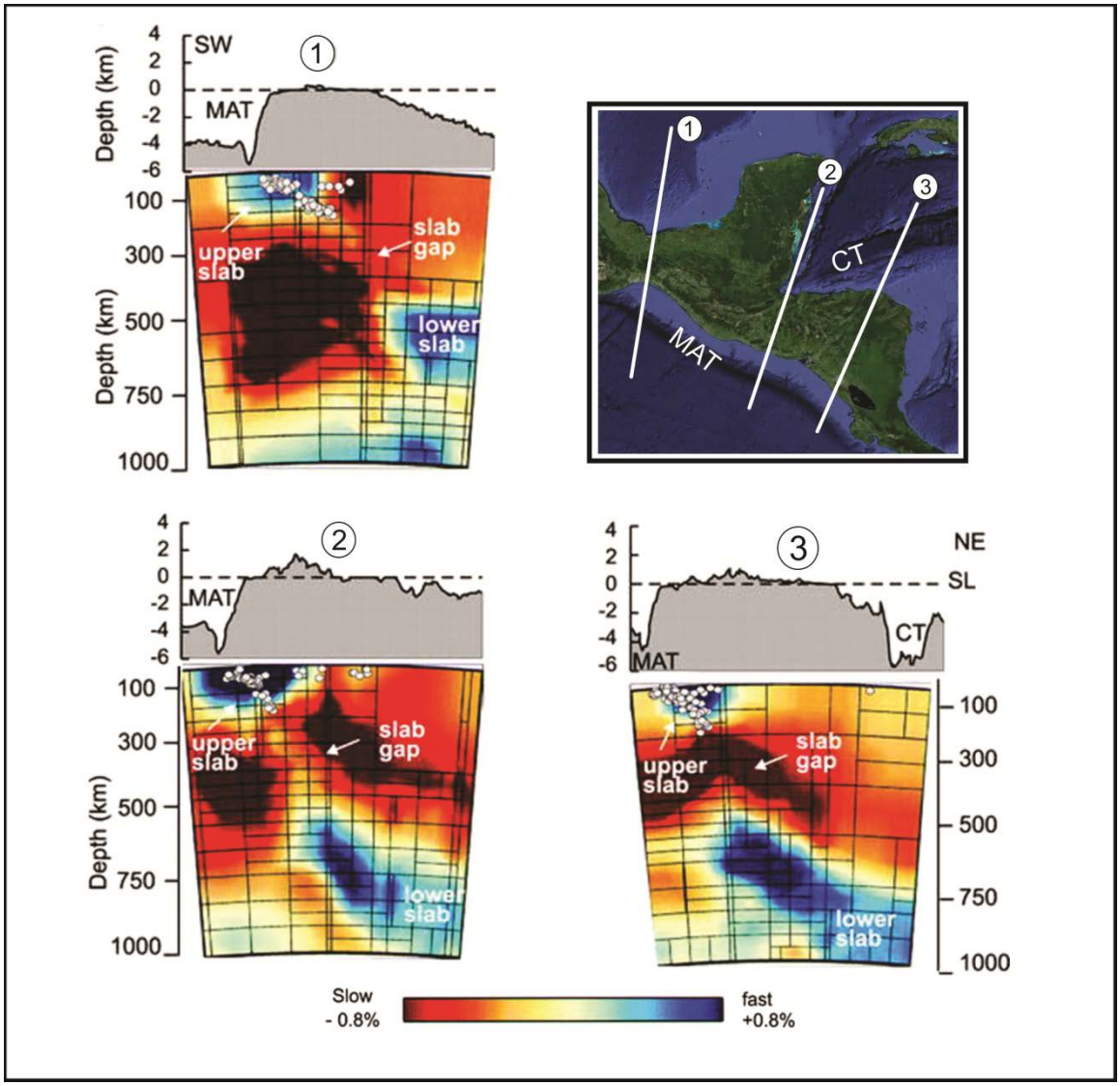

Figure 2.4: Tomographic profiles across southern Mexico and northern Central America showing Cocos slab detachment (modified from Rogers et al., 2002). Location of each numbered transect is shown on the map in the upper right of the figure. Above each tomographic profile is a transect representing topography and bathymetry. Sea level (SL) is represented by dashed line. Middle America Trench (MAT) and Cayman Trough (CT) are shown on map and transects. White circles on tomographic profiles are earthquake hypocenters. Tomographic profiles are from global mantle tomographic model of Karason and van der Hilst (2000). [Satellite imagery ©2013 TerraMetrics, NASA, Map data ©2013 INEGI.]

Based on structural analysis of outcrops onshore western Nicaragua, Weinberg (1992) proposed that a NE-SW extensional phase followed the Miocene shortening and created the large half-graben structure to the southwest of the Nicaraguan highlands known as the Nicaraguan Depression (Weinberg, 1992). The 50 km wide Nicaraguan Depression trends NW-SE and extends ~500 km from the Gulf of Fonseca, through Lake Managua and Lake Nicaragua, to the Median Trough of northern Costa Rica (McBirney and Williams, 1965; Weyl, 1980) (Fig. 2.2). The half-graben is bound to the southwest by a series of normal faults that strike parallel to the coast and dip to the northeast (Funk et al., 2009; McBirney and Williams, 1965; Weinberg, 1992). This proposed Pliocene extensional phase was thought to be a result of a steepening in the subduction dip angle or slab rollback, due to a decrease in plate convergence rates subsequent to the super-fast EPR spreading of 19-11 Ma (Weinberg, 1992). However, other research based on further investigation of upper-crustal deformation suggests the extensional deformation that developed into the Nicaragua Depression half-graben was the result of a time-transgressive footwall uplift that initiated as early as the Late Oligocene and propagated from southeast to northwest, (Funk et al., 2009).

Much of the active volcanic arc in Nicaragua is found within the Nicaraguan Depression rather than to its west. Therefore the Nicaraguan Depression is often described as an intra-arc basin, as opposed to the more common backarc basin (e.g. Phipps Morgan et al., 2008). A trenchward shift of the volcanic arc initiated in the Miocene and the arc migrated to its present position within the intra-arc basin during the Plio-Pleistocene. Slab rollback has also been hypothesized to explain this arc migration (Ehrenborg, 1996; Plank et al., 2002; Weinberg, 1992). Conversely, results from the geochemical analysis of Miocene ignimbrites from the Nicaraguan and Honduran highlands suggest that the geometry of the subduction zone which created the pre-

migration Miocene paleoarc was characterized by a steeply dipping subducted slab, similar to that which formed the modern arc (Jordan et al., 2007).

2.2 NEOTECTONICS

The rate of convergence of the subducting Cocos plate beneath the Caribbean plate outboard of the Sandino basin is estimated to range from ~75 mm/yr in the north to ~85 mm/yr in the south (DeMets, 2001). The angle of convergence is nearly orthogonal at the trench offshore El Salvador with obliquity of ~2-3° but obliquity increases to the southeast and is estimated to be ~20-25° at the trench offshore southern Nicaragua (DeMets, 2001; Harlow and White, 1985; Turner et al., 2007). For depths greater than 100 km, the dip of the subducting Cocos slab decreases from northwest to southeast along-strike, towards the flat slab subduction of the Cocos Ridge beneath southern Costa Rica, with dips of 84° beneath northwestern Nicaragua, 80° beneath northern Costa Rica, and 60° beneath central Costa Rica (Burbach et al., 1984; Protti et al., 1995; Protti et al., 1994)

Geodetic measurements reveal that the upper crustal forearc region in northern Central America is behaving as a microplate, or forearc sliver, and moving northwestward in a trench-parallel direction, independently of the Caribbean plate (Alvarado et al., 2011; Correa-Mora et al., 2009; Corti et al., 2005; DeMets, 2001; Funk et al., 2009; LaFemina et al., 2009; Norabuena et al., 2004; Turner et al., 2007) (Fig. 2.5). The rate of forearc sliver transport increases from 8.1 mm/yr in Costa Rica (Norabuena et al., 2004) to ~14-15 mm/yr in Nicaragua and El Salvador (Alvarado et al., 2011; Corti et al., 2005; DeMets, 2001; Turner et al., 2007).

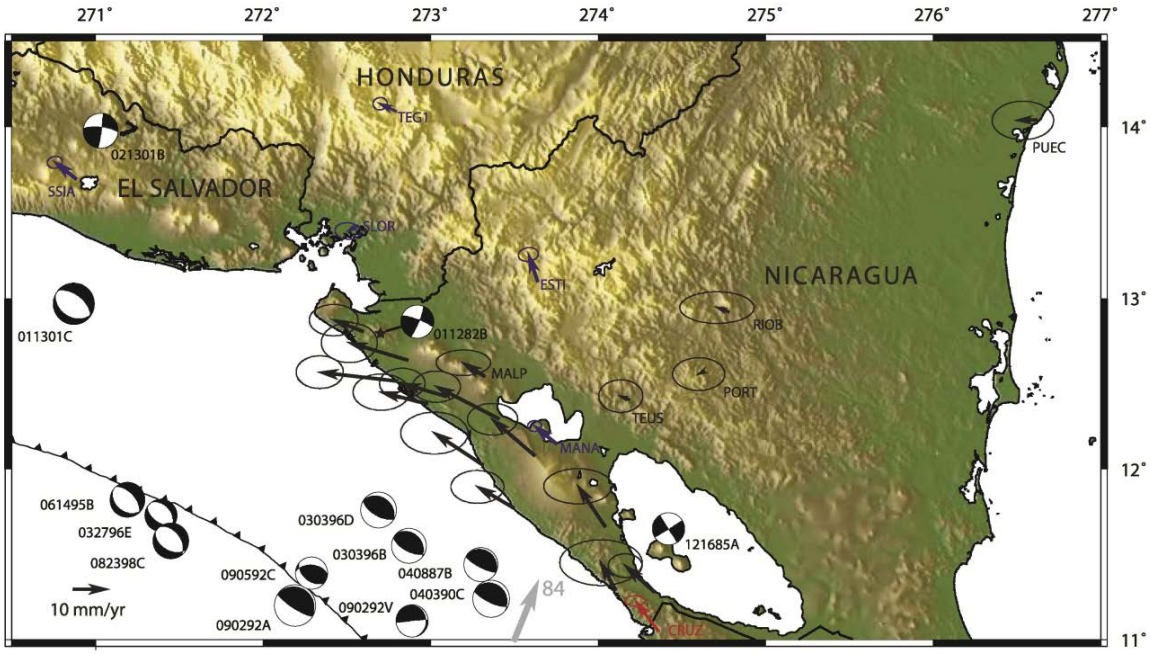

Figure 2.5: Global positioning system (GPS) velocity vector map from Turner et al. (2007) showing modern forearc sliver motion relative to a fixed Caribbean plate. Scale in bottom left corner is 10 mm/yr. Ellipses represent 95% confidence interval. GPS vectors in Nicaragua (black arrows) are from Turner et al. (2007) and are relative to the Caribbean reference frame of Demets et al. (2007). The red arrow near Costa Rica-Nicaragua border is a velocity vector from Norabuena et al. (2004) and uses the Caribbean reference frame of Sella et al. (2002). Blue arrows are velocities from continuous recording sites from Turner et al. (2007). Grey arrow is displaced from true location and not to scale. The grey arrow represents a Cocos plate location and refers to the Cocos-Caribbean convergence vector of Demets (2001). Focal mechanisms are displayed for events between 1976-2003 (mmddyy) with scalar moments of $\geq 10^{25}$ dyne cm from Harvard Central Moment Tensor catalog. Topography is from GTOPO30.

Oblique convergence along with a strongly-coupled plate interface within the subduction zone is generally thought to be the dominant driver of strain partitioning which results in forearc sliver motion (Jarrard, 1986). However, GPS-based models have determined coupling of the subduction interface along most of the Nicaragua forearc to be extraordinarily weak, < 3% of plate convergence rate, with the exception of the region west of the Nicoya Peninsula which has a maximum value of ~25% (Correa-Mora et al., 2009). Furthermore, forearc sliver transport continues in El Salvador where coupling remains weak and plate convergence is nearly orthogonal (Alvarado et al., 2011; Correa-Mora et al., 2009; Corti et al., 2005). Other mechanisms of forearc motion have therefore been proposed including northwestward tectonic escape of the forearc due to the combination of shallow subduction of the southern Cocos plate and the low coupling of the subduction interface (LaFemina et al., 2009) and long-term intra-arc extension (Phipps Morgan et al., 2008).

The trench-parallel motion of the forearc sliver is accommodated by a complex transtensional right-lateral shear zone focused along the active volcanic arc (Funk et al., 2009) (Fig. 2.6). This modern phase of deformation has persisted since approximately Mid-Pleistocene with E-W extension forming structures such as the N-S trending Managua Graben (Cowan et al., 2002; Frischbutter, 2002; Weinberg, 1992). Alternatively, forearc sliver motion has been described, based on focal mechanisms and previously mapped onshore faults, as the result of bookshelf faulting, such that the northwesterly right-lateral motion of the forearc is accommodated by strain on en echelon, northeast-striking, left-lateral strike-slips faults (LaFemina et al., 2002).

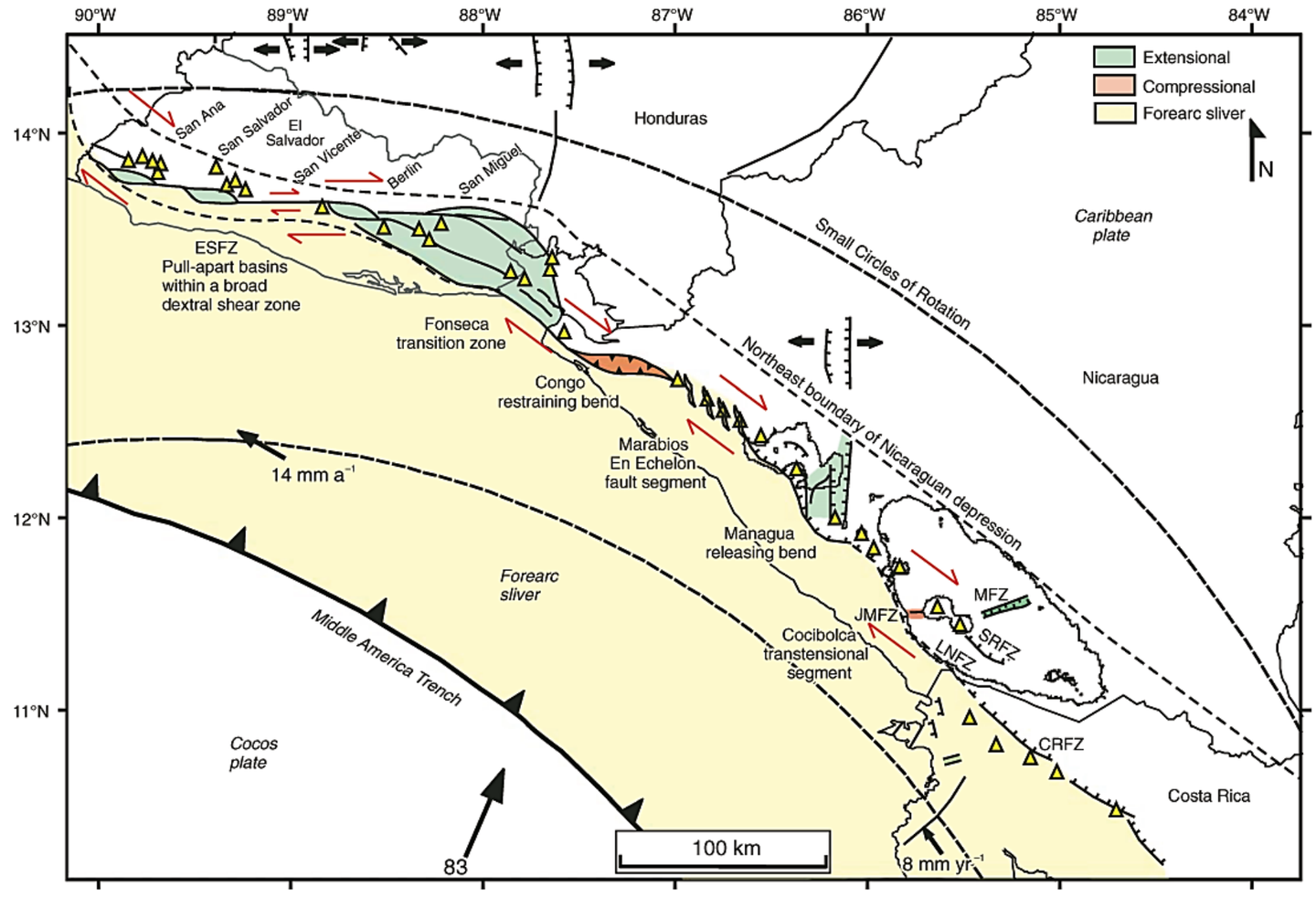

Figure 2.6: Neotectonic map of onshore northern Central American forearc sliver. The forearc sliver, highlighted in yellow, translates northwesterly at 14 mm/yr (Alvarado et al., 2011; Turner et al., 2007) as the Cocos plate converges towards the Middle America Trench at 83 mm/yr with ~15 degrees obliquity (DeMets, 2001; DeMets et al., 2000). The El Salvador fault zone (ESFZ) displays E-W right-lateral transtensional motion creating a series of en echelon pull-apart basins. The Fonseca transition zone is a broad releasing bend where the direction of forearc sliver motion changes from E-W to NW-SE. The Congo restraining bend uplifts a volcanic gap region between the Cosigüina volcano at the edge of the Gulf of Fonseca and the Maribios Cordillera. Within the Maribios Cordillera, the Maribios En Echelon fault segment is believed to lie within a series of volcanic centers. The Managua releasing bend displays E-W extension within the N-S striking Managua Graben. Right-lateral motion continues along the irregular southwestern boundary of the half-graben Nicaraguan Depression. The Lake Nicaragua fault zone (LNFZ) continues along this boundary southeastward into Costa Rica fault zone (CRFZ). The San Ramon fault zone (SRFZ) is interpreted as a synthetic normal fault. The Morrito fault zone (MFZ) and Jesus Maria fault zone (JMFZ) beneath Lake Nicaragua and adjacent to the Concepcion and Maderas island volcanoes are inferred to be E-W striking transverse faults. Small circles of rotation are from Turner et al. (2007) and centered on the Euler pole (8.9°N, 88.4°W) (adapted from Funk et al., 2009).

2.3 STRATIGRAPHY OF THE SANDINO BASIN

Sediments of the Sandino basin are exposed onshore west of Lake Nicaragua in southwestern Nicaragua and farther south in Costa Rica and depositional basement outcrops on both the Nicoya and Santa Elena peninsulas (Fig. 2.2). Analysis of the stratigraphy found in outcrops onshore has identified at least five distinct formations of marine sediments associated with the Sandino basin: the Rivas, Brito, Masachapa, El Fraile, and El Salto Formations (Weyl, 1980, and references therein). The depositional basement onshore consists of two discrete units: the Nicoya Complex and the Santa Elena Complex (Denyer et al., 2006; Gazel et al., 2006; Hauff et al., 2000).

2.3.1 Depositional Basement

Mafic igneous outcrops, to the southeast of the Sandino basin, in Costa Rica at the Santa Elena and Nicoya peninsulas are inferred to be the uplifted and exposed equivalents of the depositional basement that underlies the Sandino forearc basin (Fig. 2.2). These outcrops and have undergone extensive analysis (e.g. Bourgois et al., 1984; Calvo, 2003; Dengo, 1962; Denyer and Baumgartner, 2006; Gazel et al., 2006; Hauff et al., 2000; Hoernle et al., 2004; Kuijpers, 1980). The ophiolitic Nicoya Complex represents obducted oceanic lithosphere with a common mantle plume source that is geochemically similar to the Galapagos hotspot and the CLIP (Hauff et al., 2000). The igneous Nicoya outcrops consist mainly of gabbros and tholeiitic basalts and are accompanied by radiolarian chert (Denyer and Baumgartner, 2006; Sinton et al., 1997). To the north, the Santa Elena Complex comprises at least three units that are not genetically related to the Nicoya Complex: (a) Santa Elena Nappe, (b) Santa Rosa Accretionary Complex, and (c) Islas Murciélago (Gazel et al., 2006). The Santa Elena Nappe contains ultramafic components and is composed primarily of peridotites, gabbros,

and doleritic dikes formed in a volcanic island arc setting. The southwest- to south-directed thrusting of the nappe occurred atop the radiolaritic basalt assemblage of the Santa Rosa Accretionary Complex during the Late Cretaceous between late Cenomanian and Early Maastrichtian (Geldmacher et al., 2008; Hauff et al., 2000). The underlying Santa Rosa Accretionary Complex is mostly radiolarian chert and alkaline basalt from an enriched mantle source and likely represents an accreted seamount (Gazel et al., 2006; Hauff et al., 2000). The last unit, Islas Murcielago, is named for the archipelago at the western end of the Santa Elena peninsula where it outcrops. The structural relation is unclear but geochemical analysis found that the predominantly tholeiitic pillow and massive basalts are similar in composition to the doleritic dikes of the Santa Elena Nappe (Gazel et al., 2006).

The offshore forearc basement beneath the modern shelf varies significantly along-strike throughout the western Central American margin. Several wide-angle seismic refraction and multichannel seismic reflection studies which have imaged the margin wedge forearc basement have been conducted in the region, including offshore Guatemala (Ibrahim et al., 1979; Ladd and Schroder, 1985), Costa Rica (Christeson et al., 1999; Crowe and Buffler, 1985; Hinz et al., 1996; McIntosh et al., 1993; Sallarès et al., 1999; Shipley et al., 1990; von Huene et al., 2000), and within the Sandino forearc basin (Berhorst, 2006; McIntosh et al., 2007; Ranero et al., 2000; Sallarès et al., 2013; Walther et al., 2000). The general structural trend of the forearc basement is revealed by gravity anomaly data (Sandwell and Smith, 2009) (Fig. 2.7). In offshore Guatemala and northwestern Nicaragua, the depositional basement of the forearc basin is dominated by continuous long term subsidence beneath the middle shelf (Ladd and Schroder, 1985; McIntosh et al., 2007). Trenchward of this gravity low is a pronounced gravity high

representing the outer forearc high, a longitudinally oriented region of shallow forearc basement beneath the modern outer shelf and upper slope. Continuing along-strike to the southeast, the shelfal forearc basement shows an increasing amount of compressional strain giving rise to a progressively shallowing basement as well as fold-producing, southwest-directed, deep-seated basement thrusts (Berhorst, 2006; McIntosh et al., 2007; Ranero et al., 2000; Sallarès et al., 2013). Approaching Costa Rica, the gravity high associated with the outer forearc high diminishes, and may bifurcate, before the basement shallows basinwide, as illustrated by the prominent gravity high surrounding the Nicoya and Santa Elena peninsulas.

The mafic basement exposed at the Nicoya complex (Ranero et al., 2000) and Santa Elena complex (Geldmacher et al., 2008; Hauff et al., 2000) are both believed to represent portions of the Sandino forearc basement but the two complexes are of different ages and source mantle types and neither onshore or offshore trends are well understood (Alvarado et al., 2008). Mafic and ultramafic samples from the lower trench slope off Guatemala, collected during Deep Sea Drilling Program (DSDP) Leg 67 and Leg 84, have been linked to the Santa Elena Complex and may represent a geochemically similar assemblage, including both depleted volcanic island arc and enriched hotspot-derived ocean island basalt, that spans the western margin of the Chortis block (Bourgois et al., 1984; Geldmacher et al., 2008). The Chorotega block and its northernmost uplifted outer high segment, the Nicoya Complex, are understood to be obducted CLIP material emplaced during the initial transit of the CLIP between the North and South American plates (Denyer et al., 2006; Hoernle et al., 2004; Sinton et al., 1997). The terrane boundary between the Chortis and the Chorotega blocks resides between the two Costa Rican peninsulas, immediately south of the Santa Elena Complex, but its extent offshore has not been determined conclusively. However, the gravity data seem to suggest that the

E-W orientation of this boundary continues offshore to near the shelf edge (Fig. 2.7).

2.3.2 Rivas Formation

Outcropping along the western shore of Lake Nicaragua in the core of the Rivas anticline is the oldest stratigraphic unit in the Sandino basin, the Rivas Formation (McBirney and Williams, 1965). The earliest Rivas Formation was deposited contemporaneously with subduction initiation (~75 Ma) and overlies basaltic basement (INE, 1995; Weyl, 1980). Deposition of the Rivas Formation continued through Early Paleocene in an abyssal depositional environment (INE, 1995). The lithology consists mostly of turbidite deposits of tuffaceous sandstones, silty sandstones, and shales with an overall measured thickness that ranges from ~2,100-2,500 m onshore (Weyl, 1980).

2.3.3 Brito Formation

Overlying the Rivas Formation, and separated from it by a layer of conglomerates, is the Brito Formation. The Brito Formation is subdivided into two components based on age and lithology. The Late Paleocene to Eocene section of the Brito Formation consists of volcaniclastic turbidites and is believed to have been deposited in a deep-water to bathyal environment (Weyl, 1980). In contrast, deposits of the late Middle Eocene to Late Eocene section comprise carbonates and volcaniclastic turbidites and are believed to have been the product of a warm shallow marine environment (Weyl, 1980). The thickness of the Brito Formation is ~2,500 m in outcrop (McBirney and Williams, 1965; Weyl, 1980).

2.3.4 Masachapa Formation

The southernmost outcrops of the Masachapa Formation are found in coastal

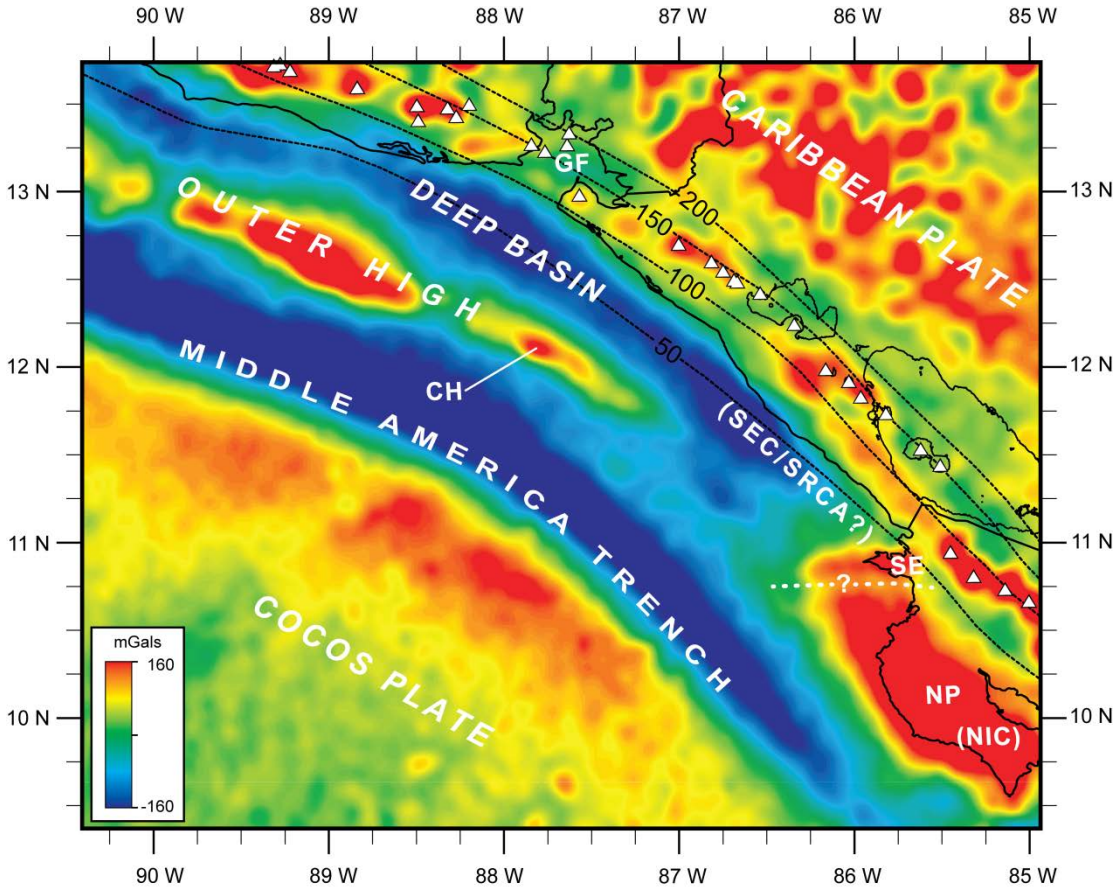

Figure 2.7: Global gravity anomaly map of the Sandino forearc basin using data from Smith and Sandwell (1997). White triangles represent volcano locations and black dashed lines are 50 km contour intervals for depth to the top of the subducted Cocos plate (Syracuse and Abers, 2006) The gravity data reveal the general structural trend of the forearc basement. The inner shelf gravity low southwest of the Gulf of Fonseca (GF) is a region where forearc basement is dominated by subsidence. Seaward, the outer high signifies a trench-parallel zone of shallow forearc basement beneath the outer shelf and upper slope. The Corinto High (CH) is a segment of this outer forearc high located within the NicStrat study area. The basement shallows basinwide to the southeast before eventually outcropping onshore in Costa Rica. Dotted white line is possible boundary between the Chortis and Chorotega blocks. The Chortis forearc basement north of the boundary is likely some combination of the island arc Santa Elena Complex (SEC) and the OIB Santa Rosa Accretionary Complex (SRAC) which outcrop at the Santa Elena peninsula (SE). South of the block boundary, the forearc basement is the CLIP-derived Nicoya Complex (NIC) which outcrops at the Nicoya peninsula (NP).

Nicaragua and extend to the northwest for nearly 75 km before being completely obscured by Quaternary alluvium and pyroclastics (Fig. 2.2). The beds of the Masachapa Formation dip seaward and were deposited unconformably over the gently folded Brito Formation. The age of the Masachapa Formation is Late Oligocene to early Middle Miocene (Weyl, 1980). Its depositional environment ranges from continental slope to neritic (INE, 1995). Thickness is estimated at 2,600 m with a lithology that consists primarily of tuffaceous mudstones and turbiditic volcaniclastic shales interbedded with minor siltstones and sandstones (McBirney and Williams, 1965; Weyl, 1980). Silicified wood is prevalent in some sections of the tuffaceous mudstone and the lower section of the unit contains an assemblage of carbonized tree trunks, volcanic debris and mollusk fragments (McBirney and Williams, 1965).

2.3.5 El Fraile Formation

The El Fraile Formation dates from Middle Miocene to Early Pliocene and is separated at its base by a layer of conglomerates from the Masachapa Formation (Kolb and Schmidt, 1991; Weyl, 1980). The middle and lower sections of the El Fraile Formation merge northwestward with the volcanic Tamarindo Group, with which it is believed to be contemporaneous (McBirney and Williams, 1965; Weyl, 1980), and which has been radiometrically dated to 14.7-11.7 Ma (Saginor et al., 2011). The depositional environment of the El Fraile Formation is nearshore neritic and it includes deltaic deposits and fossilized wood fragments (Kolb and Schmidt, 1991; Weyl, 1980).

Within the El Fraile Formation is a 0.5-1.0 m thick layer of shell lag and prominent amber nodules that is of basin-wide extent (Kolb and Schmidt, 1991). An equivalent shell lag layer also appears to the southeast in the Costa Rican forearc

(Schmidt and Seyfried, 1991). The amber layer is believed to represent a condensed section and displays a prominent hiatal concentration shell lag (sensu Kidwell, 1993) capping a transgressive systems tract (Kolb and Schmidt, 1991). The presence of numerous amber occurrences may be a consequence of increased resin production in flooded coastal forests (Kolb and Schmidt, 1991). The total thickness of the El Fraile Formation in outcrop is ~2,700 m (Weyl, 1980).

2.3.6 El Salto Formation

The El Salto Formation is the youngest formation of marine deposits in the Sandino basin. The base of the El Salto Formation is marked by an angular unconformity over folded Miocene and Oligocene beds of the Masachapa Formation at the San Cayetano anticline (McBirney and Williams, 1965; Weyl, 1980) (Fig. 2.1). The beds of the El Salto Formation are near-horizontal and do not appear to have undergone major deformation (McBirney and Williams, 1965). The El Salto Formation represents the entire period of marine Pliocene deposition within the Sandino basin. However, it has experienced significant erosion and is limited to < 100 m in thickness where preserved. The lithology consists of calcareous sediments, coquina, and sandy shale indicating a shoreface depositional environment (McBirney and Williams, 1965).

Chapter 3: Data and Methods

3.1 NicStrat Survey Design

The NicStrat survey was designed to provide regional coverage of the Sandino basin while also concentrating on key areas in detail (Fig. 3.1). The survey therefore comprises three grids of dense seismic coverage connected by longer regional strike-oriented profiles. From northwest to southeast the areas of closely spaced profiles are the Sandino, Salinas and Nicoya grids (Fig. 3.1). Each of the three grids extends from the inner shelf to upper slope with two dip lines in each grids extending basinward to the Middle America Trench. The spacing between profiles within each grid is either 2 or 4 km for the NE-SW margin-perpendicular (dip) profiles and 5 or 10 km for the NW-SE margin-parallel (strike) profiles. In addition, two dip-oriented profiles extend into the Gulf of Fonseca. The regional strike profiles connecting the grids and the Gulf of Fonseca profiles facilitate regional correlation of seismic stratigraphy throughout the Sandino basin.

3.2 Acquisition Parameters

The high-resolution MCS reflection profiles of the NicStrat survey were acquired during November to December 2004 aboard R/V *Maurice Ewing* (cruise EW04-12) off the Pacific coasts of Nicaragua and Costa Rica. The hydrophone streamer measured 2100 m in length and was towed at a depth of 2.5 m (Fig. 3.2). The seismic source was also towed at 2.5 m and comprised an array of three 45/45 in^3 generator-injector (GI) air guns that had a maximum frequency of ~300 Hz. The sampling rate for all lines was 1.0

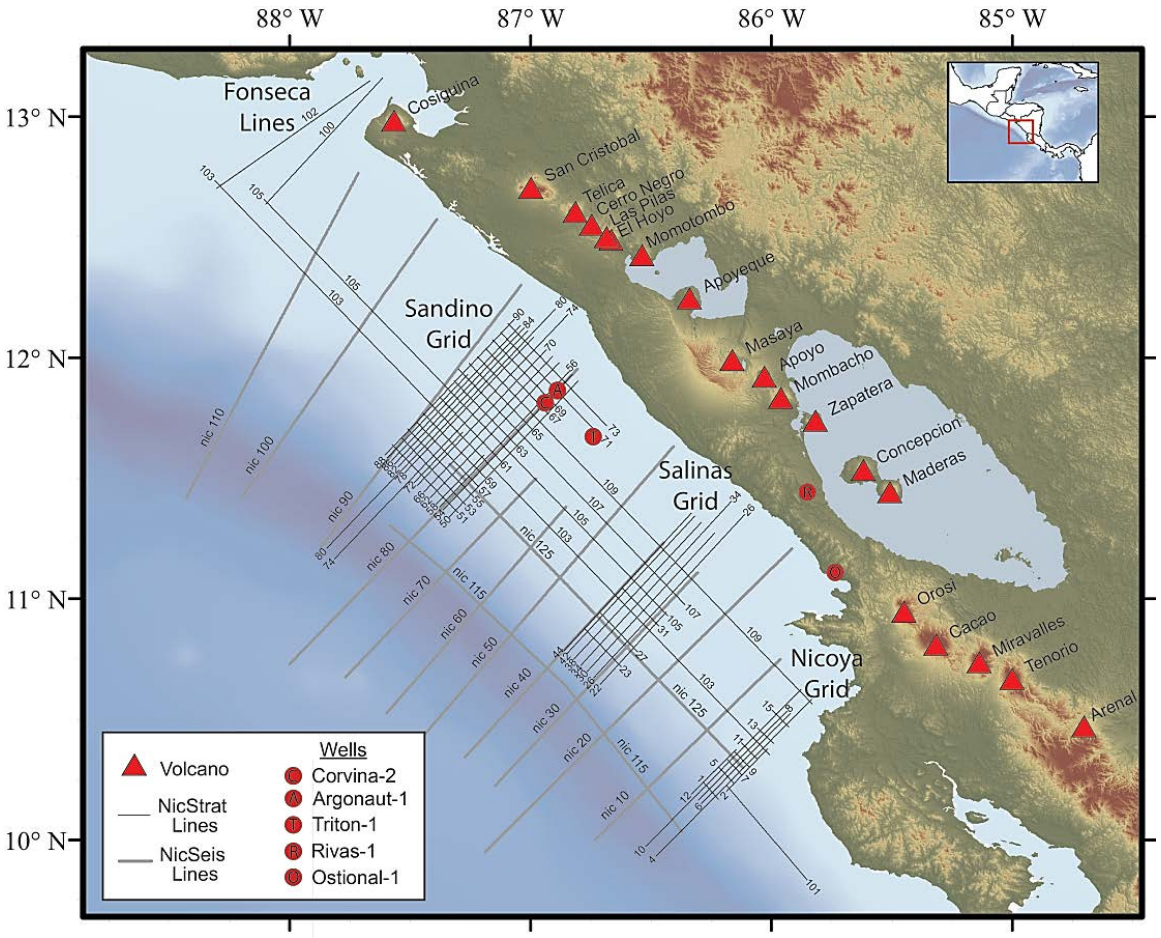

Figure 3.1: Location map showing NicStrat and NicSeis MCS surveys. Profiles from the NicStrat survey (thin black lines) are numbered according to the number in their line name (e.g. line ns054 = 54). Profiles from the NicSeis survey (thick gray lines) are labeled by their line name which includes the prefix "nic." The three grids of dense seismic coverage and the two Gulf of Fonseca lines from the NicStrat survey are labeled. Industry well locations from Instituto Nicaragüense de Energía (INE) (1995) are denoted by red circles with corresponding initial (see inset key). Active volcanic centers are represented by triangles and labeled with their common names. Bathymetry is from GEBCO (2008) and topographic relief image is from Shuttle Radar Topography Mission (SRTM) (Jarvis et al., 2006).

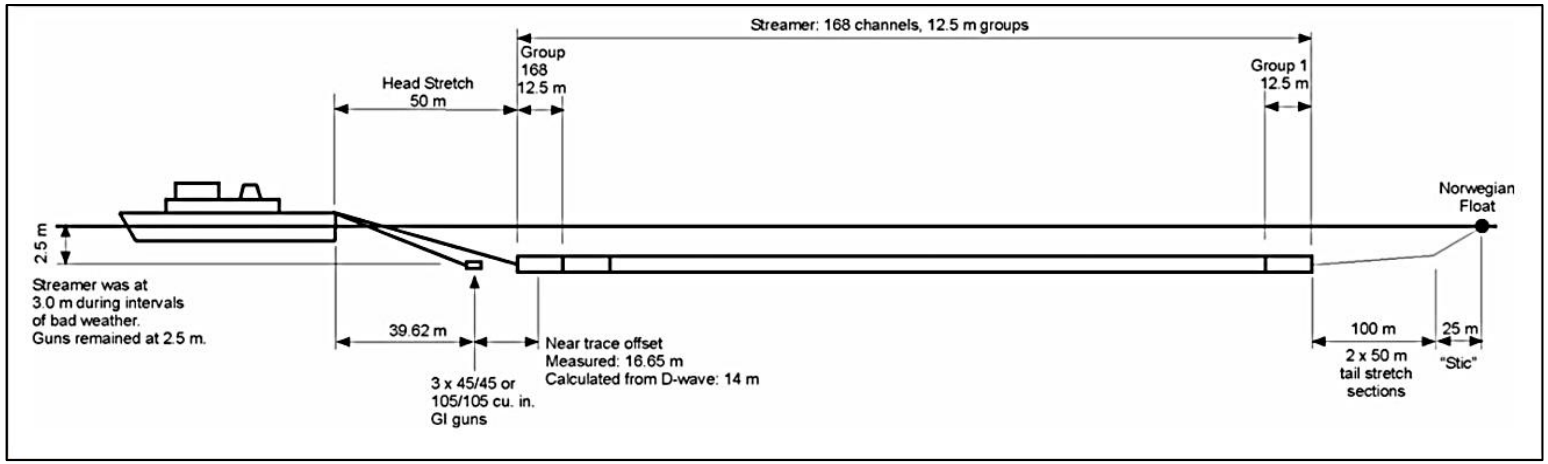

Figure 3.2: Diagram of acquisition parameters for cruise EW04-12 aboard R/V *Maurice Ewing*.

ms which is sufficient to eliminate aliasing in frequencies up to 500 Hz. Shot spacing was ~12.5 m and the source-receiver offset was calculated from the D-wave to be ~14.7 m. The streamer was subdivided into 168 channels with hydrophone groups spaced at 12.5 m, giving a maximum fold of 84 and yielding a common midpoint (CMP) spacing for shot gathers of 6.25 m. The record length for the vast majority of the NicStrat data was 4.0 s, but to account for increased water depth near the modern trench, the record lengths for dip profiles were increased to a maximum of 8.0 seconds.

3.3 PROCESSING OF MCS DATA

The NicStrat data were processed at the University of Texas Institute for Geophysics using Paradigm Focus© seismic processing software. Processing was completed in two phases (Fig. 3.3). The first phase began with reformatting SEG-Y data files to Paradigm format and then sorting the seismic traces into shot gathers. The dominant frequencies determined from raw shot gathers typically range from between 30 and 180 Hz (Fig. 3.4). A preliminary view of the unprocessed data was obtained by creating brutestack sections of the raw shot gathers with a constant velocity set to 1550 m/s. This was followed by the application of a trapezoidal minimum phase bandpass filter with coefficients of 10, 20, 250, and 300 Hz. The specific coefficients were chosen in order to retain as much bandwidth as possible, especially in the high-frequency portion of the spectrum, while removing low-frequency disturbances such as towing noise as well as high-frequency ambient noise. After filtering, a deconvolution with 15 channels of autocorrelation summed, a prediction gap of 12 ms, filter length of 100 ms, and 0.1% white noise added was applied to shot gathers. (A second bandpass filter was then applied in order to remove the artifact low frequency noise introduced by the deconvolution process.) Deconvolved shot gather results in shot-receiver coordinates

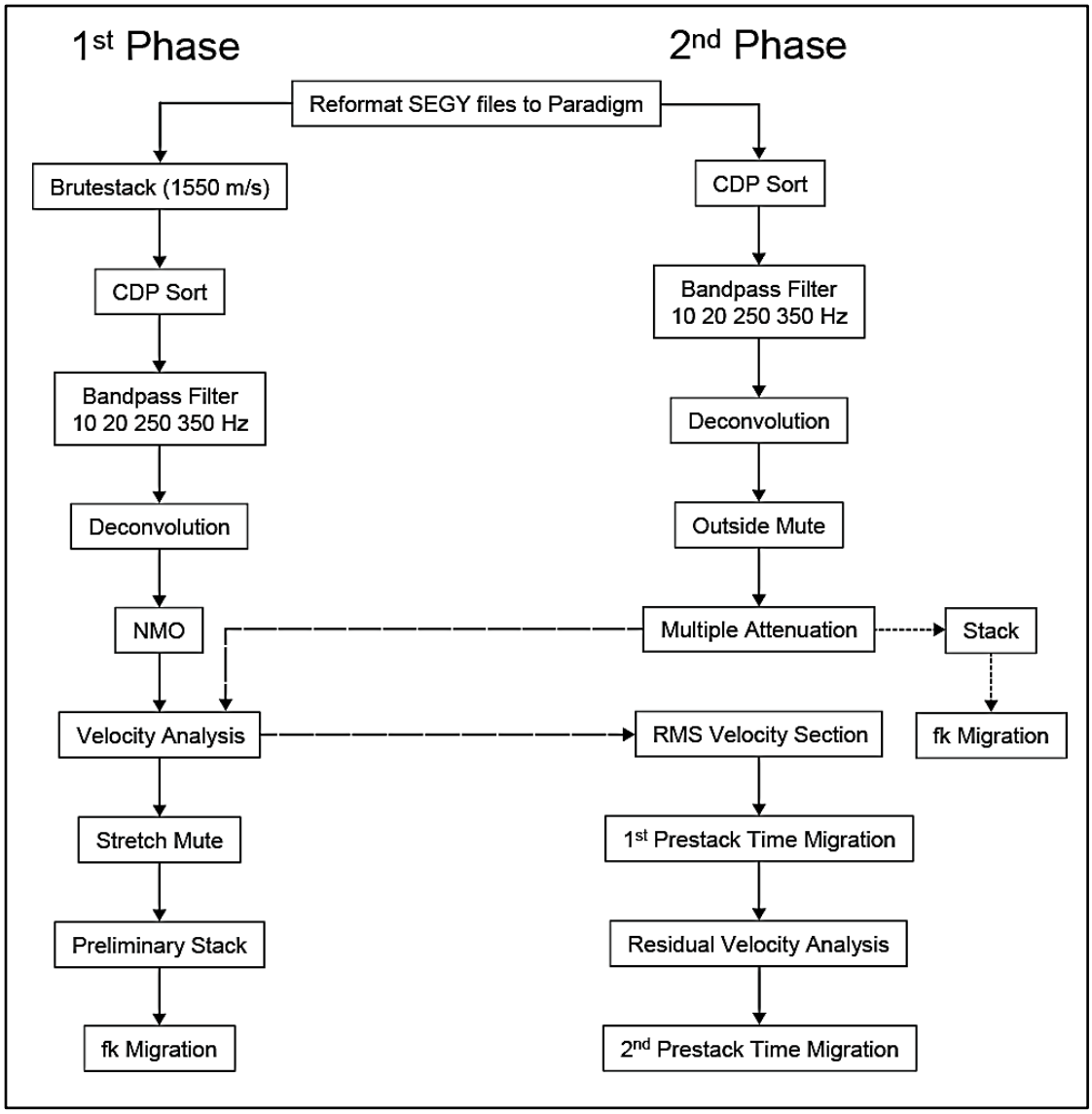

Figure 3.3: Two phase processing flow used for NicStrat MCS data. The second processing phase uses the velocity analysis of the first phase for its RMS velocity section. The initial fk migration from the second phase is used as quality control for the 1st prestack migration.

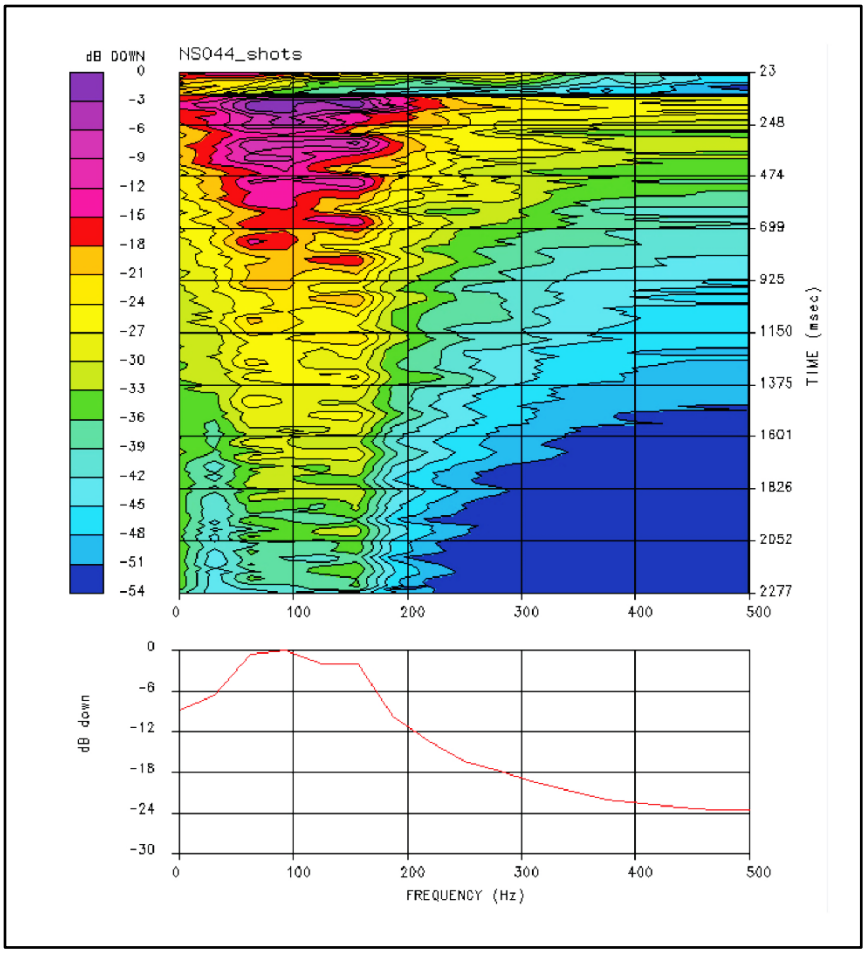

Figure 3.4: An example of a typical amplitude spectrum for a raw shot gather. The upper image is a plot of peak amplitude (coherency) as a function of frequency and time. Below is a plot of peak amplitude versus frequency. The amplitude spectrum exhibits a strong signal-to-noise ratio, though much of the periodic coherent signal is water bottom multiples. Dominant frequencies on the shelf are typically between ~30-180 Hz as exhibited on this shot gather. This shot gather is from the inner shelf at shot 1000 on line ns044 in the Salinas grid.

were then transformed into midpoint-offset coordinates and sorted into common midpoint (CMP) gathers before subsequently undergoing an iterative series of velocity analyses.

Velocity analysis was performed at least every 400 CMPs for each seismic profile. Areas that were more difficult to image (e.g. complex geologic structures) were analyzed every 100-200 CMPs. The procedure for velocity analysis entailed creating a root mean square (RMS) velocity function from CMP gathers by preferentially selecting high coherency velocity-time pairs from a cross-plot of velocity versus two-way travel (TWT) time (Fig. 3.5). Velocity analysis was conducted in conjunction with a normal moveout (NMO) correction which accounts for the difference in TWT of traces with horizontal offsets greater than zero, in effect flattening all velocity events to the zero-offset arrival time. A far-offset (outside) mute was also applied to CMP gathers during velocity analysis in order to remove distortions generated as artifacts of the NMO correction (Fig. 3.6). After RMS velocity functions were created for NMO-corrected and muted CDP gathers, a stacked section was created using the RMS velocity function created during velocity analysis. If necessary, velocity analysis was repeated or refined and another RMS velocity stack was created. The final stage of the first phase of processing was a post-stack migration. For this step, a frequency-wave number (f-k) migration, which uses a constant velocity to collapse diffraction hyperbolas by mapping in the frequency-wave number domain (Yilmaz, 2001), was performed.

The second processing phase was executed in order to better image high-angle strata and mitigate noise from multiple reflections. The first step in this second phase

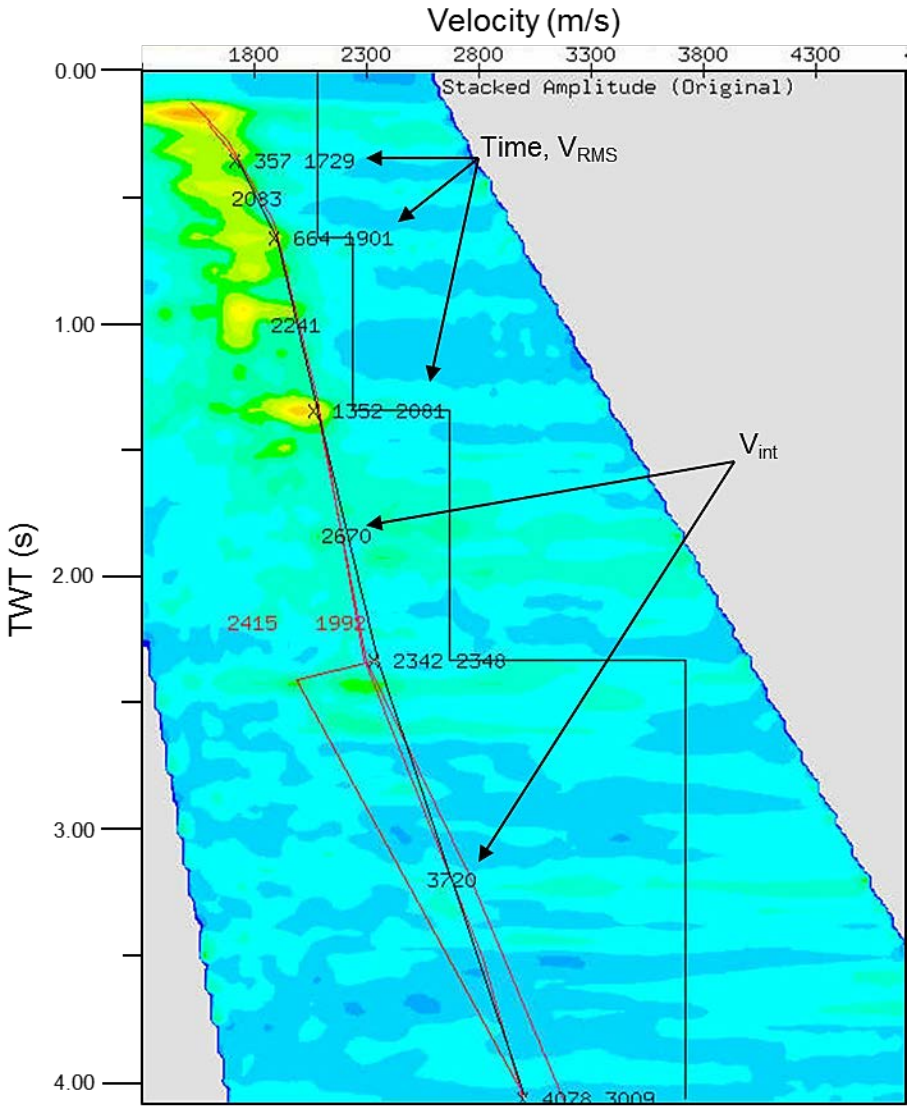

Figure 3.5: Example of velocity analysis from CMP 1330, line ns044. Each pick is represented by an X and is labeled by its time-RMS velocity (V_{RMS}) pair in units of milliseconds and meters per second, respectively. Curved black line is V_{RMS} function and red lines represent stacking velocity functions. Stepwise black line represents interval velocity (V_{int}) function.

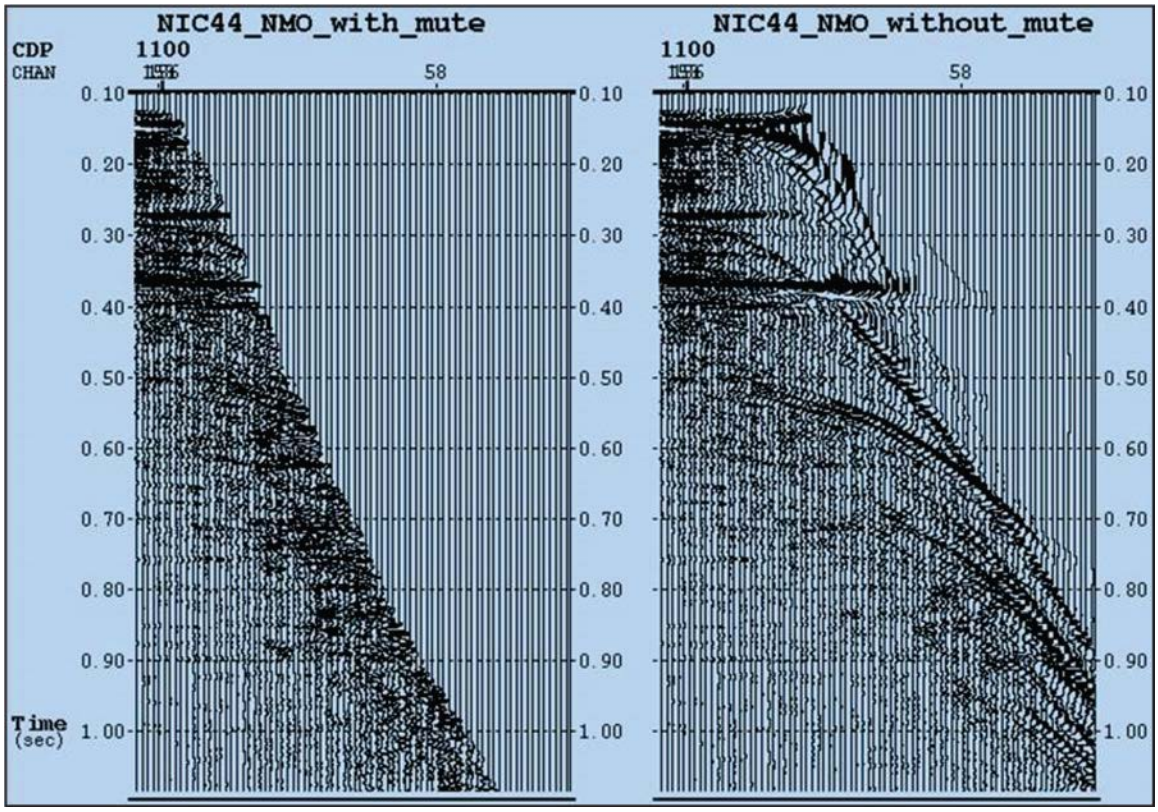

Figure 3.6: Example of normal moveout (NMO) correction of a common midpoint gather (CMP) with and without the far-offset mute applied. The left panel displays CMP 1100 from line ns044 and demonstrates the results of applying the far-offset (outside) mute in order to remove artifact distortions caused by the NMO correction. The right panel shows the same NMO-corrected CMP as it appears without the application of the far-offset mute. Note the distortions, or "stretching," to the far-offset high amplitude reflections in the shallow section (< 0.40 TWT) of the panel on the right.

was to apply an enhanced multiple attenuation routine to the shot gathers. This procedure involved applying the Surface Multiple Attenuation Calculation (SMAC) module in the Paradigm Focus© software which calculates a Taylor series approximation to identify and diminish multiple occurrences. Next the initial velocity analysis from the first phase was imported and used to create a RMS velocity section using Schlumberger GeoDepth© software. Using the RMS velocity section and the multiple-attenuated shot gathers, the first of two prestack Kirchoff time migration iterations was performed. At its conclusion, a residual RMS velocity analysis was conducted on the migrated shot gathers. Finally, a second prestack Kirchoff time migration was performed using the updated residual velocity analysis.

3.3 SUPPLEMENTAL MCS DATA FROM THE NICSEIS SURVEY

MCS data from the NicSeis survey, with coverage of the Sandino basin, Middle America Trench, and the adjacent Cocos plate, were available for integration with the 2004 NicStrat MCS data (Fig. 3.1). The NicSeis data were acquired during an earlier cruise aboard R/V *Maurice Ewing* (EW00-05; May 2000) with a 240 channel, 6 km hydrophone streamer and a 20 air gun source (total volume of 6817 in^3). The shot spacing was 50 m and the sampling rate was set to every 2 ms. This NicSeis MCS survey was designed for deeper subsurface penetration (16-20 s TWT) in order to image plate boundary processes associated with subduction. The NicSeis data were therefore acquired with a source with a lower mean frequency than that of the NicStrat data, resulting in lower vertical resolution (~15 m in the shallow section) than that of the NicStrat data (~5 m). In total, twelve NicSeis lines, comprising ten dip and two strike profiles, were incorporated into this study. The dip profiles provided added coverage on the shelf and slope, though with greater spacing between profiles than the NicStrat survey (Fig. 3.1).

Typically the dip profiles are separated by 20-30 km and, although several cross the shelf, the two strike lines only intersect dip profiles on the slope where correlation of reflections is particularly challenging (see Section 3.6).

3.4 INDUSTRY WELLS AND DATING OF UNCONFORMITIES

Six industry wells, four offshore and two onshore, have been drilled in the Sandino basin (INE, 1993) (Fig.3.6; Table 3.1). These offshore wells were used to provide age control for the seismic interpretations performed in this study. The locations of the offshore wells Corvina-1, Corvina-2, Argonaut, and Triton were deliberately crossed by two NicStrat seismic profiles (Fig. 3.1). The correlations between the seismic and well data were made using interval velocity models to convert the traveltimes to interpreted horizons to depth. The deepest of the four offshore wells, Corvina-2, was drilled by the exploration company Oceanic in 1974 near the crest of a margin-parallel anticline and reached a maximum depth of 3,628 m where it also penetrated the oldest sediments penetrated by any of these wells, from the Middle Eocene Rivas Formation (INE, 1993). Also drilled by Oceanic in 1974, Corvina-1 was located only ~800 m south of Corvina-2, but was abandoned due to drilling problems after only penetrating 1265 m. Argonoaut-1 and Triton-1 were drilled close by prior to the Oceanic wells in 1967 by Esso. Argonaut-1 lies approximately 11 km northeast of the Corvina wells penetrating the landward limb of another margin-parallel anticline while Triton-1 lies ~20 km southeast of Argonaut and drilled the northwest-dipping limb of an anticline with apparent NE-SW strike (Fig. 3.1).

Original well data were unavailable, but interpreted stratigraphic sections from these four offshore wells (Fig. 3.7) were correlated with intersecting seismic profiles ns054, ns067, and ns071 in order to provide age constraints on the mapped sequences.

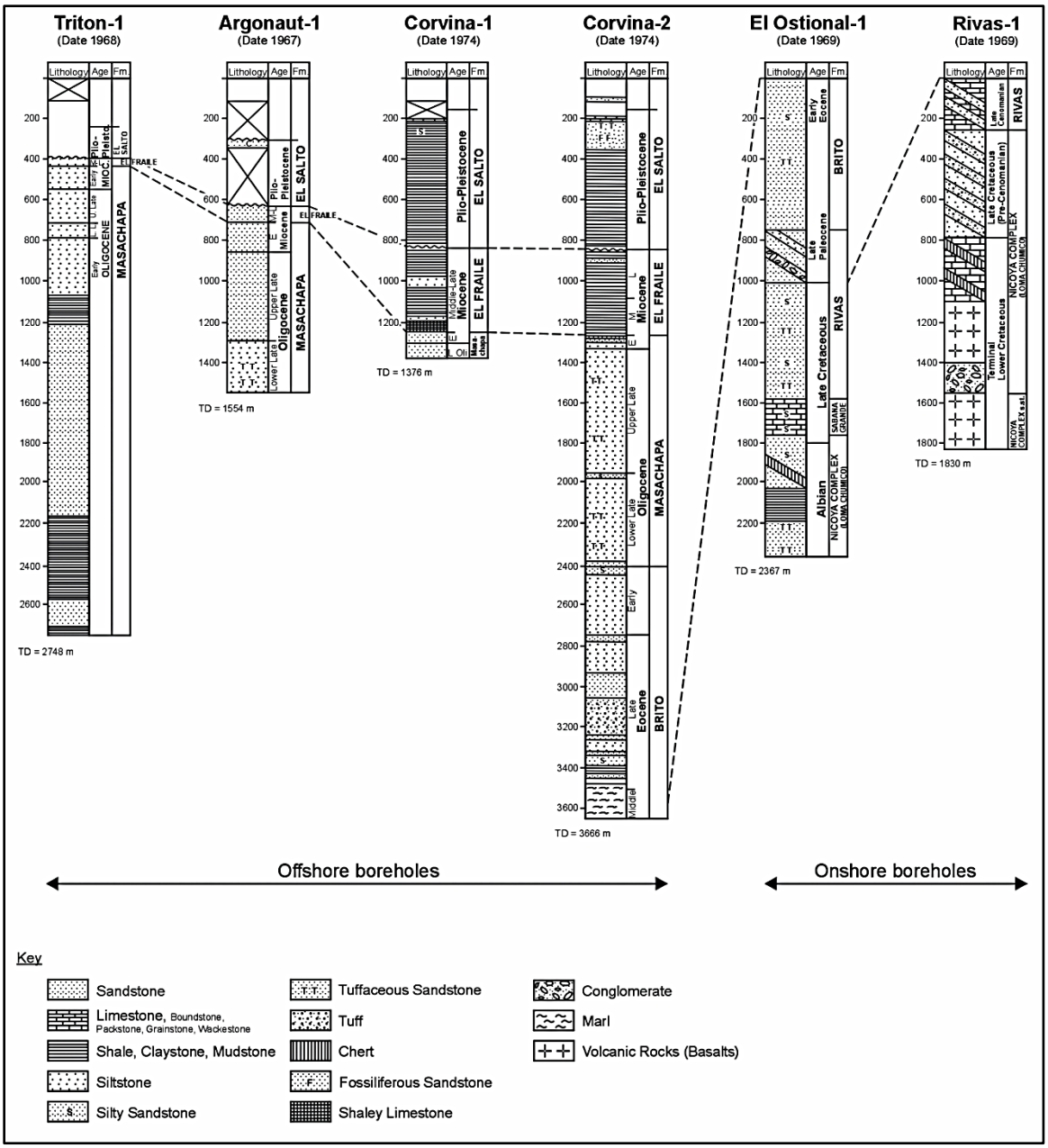

Figure 3.7: Exploration wells from the Sandino basin (from Struss et al., 2008). For locations, see Fig. 3.1.

The unconformities interpreted on profile ns054 were also compared to the interpretation of the colocated composite MCS profile from Ranero et al. (2000) and found to be in good agreement, providing support to our age assignments.

3.5 IDENTIFYING SEQUENCE BOUNDARIES AND SEQUENCES

Sequence boundaries were identified primarily by reflection terminations including truncation, downlap, toplap, and onlap (sensu Mitchum et al., 1977; Van Wagoner et al., 1988). Sequence boundaries were most commonly recognized as being onlap surfaces or by their truncation of underlying reflections (Table 3.1). In addition, sequence boundaries are typically of higher amplitude than surrounding reflections and occasionally separate distinct seismic facies.

Sixteen sequences and the acoustic basement were defined during seismic stratigraphic interpretation of the high-resolution NicStrat MCS data (Table 4.1). The top of each identified sequence is marked by its corresponding sequence boundary. For example, the upper boundary of sequence 2 is sequence boundary 2 (SB2). The youngest mapped sequence is sequence 16 and its upper boundary is the seafloor. The oldest mapped sequence boundary (SB1) caps a composite sequence (sequence 1) encompassing sediments of the Rivas and Brito Formations from Late Cretaceous to Middle Eocene (Table 3.2). Much of sequence 1 could not be imaged within the 4.0 s record of the NicStrat data and a lack of connecting strike-lines on the shelf for the deeper penetrating NicSeis survey prevented regional mapping of sequences that predate SB1. Therefore composite sequence 1 spans the majority of the time (~75-40 My) represented by the Sandino basin fill—nearly as long as all of the other interpreted sequences combined. Sequence 2 is also of long duration (~10 My) between Late Eocene and Early Oligocene

Seismic Sequence	Stratal Terminations	Internal Reflection Configurations	Stacking Pattern	Seismic Facies
13-16	toplap, concordant downlap, onlap, truncation	continuous parallel to divergent	progradational	hi amplitude, continuous, parallel to divergent
12	toplap, concordant downlap, onlap, truncation	continuous subparallel to divergent	progradational	hi amplitude, continuous, parallel to divergent
11	toplap, concordant, onlap, truncation	subparallel to divergent	aggradational, progradational	variable amplitude, continuous, parallel to divergent
10	toplap, concordant, downlap, onlap, truncation	subparallel to divergent	retrogradational	variable amplitude, continuous, parallel to divergent
9	toplap, concordant, downlap, onlap, truncation	subparallel to divergent	retrogradational	variable amplitude, continuous, parallel to divergent
8	toplap, concordant, downlap, onlap, truncation	subparallel to divergent	progradational	hi amplitude, continuous, parallel to divergent
7	toplap, downlap, truncation, onlap	subparallel to divergent	progradational	hi amplitude, continuous, parallel to divergent
6	toplap, downlap, truncation, onlap	subparallel to divergent	aggradational, progradational	hi amplitude, continuous, parallel to divergent
5	toplap, downlap, onlap	subparallel to divergent	aggradational	hi amplitude, continuous, parallel to divergent
4	toplap, downlap, truncation, onlap	subparallel to divergent	aggradational, retrogradational	variable amplitude, continuous, subparallel to divergent
3	toplap, truncation, onlap, downlap	hummocky, deformed, subparallel to divergent	progradational	hi amplitude, continuous, subparallel to divergent, mounded
2	toplap, onlap, downlap	deformed, subparallel to divergent	progradational	hi amplitude, discontinuous, subparallel to divergent, mounded
1	truncation, toplap, concordant, downlap, onlap	discontinuous, subparallel to divergent	aggradational, progradational	hi amplitude, chaotic to subparallel, mounded parallel to divergent

Table 3.1: Seismic characteristics of sequences. (Colors correspond to those displayed on interpreted seismic profiles in later chapters.)

Seismic Sequence	Age	Well-Correlated Formation	Lithology	Depositional Environment
13-16	Pleistocene to recent	N/A	Limestone, siltstone, and clay	marginal lagoon, shoreface
12	Pleistocene	El Salto	sandstone with siltstone layers	marginal lagoon, shoreface
11	Pliocene/Plio-Pleistocene	El Salto	sandstone with siltstone layers	marginal lagoon, shoreface
10	Pliocene/Plio-Pleistocene	El Salto	sandstone with siltstone layers	marginal lagoon, shoreface
9	Pliocene	El Salto	sandstone siltstone	marginal lagoon, shoreface
8	Late Miocene	El Fraile	sandstone siltstone	inner shelf
7	Middle Miocene	El Fraile	sandstone siltstone	inner shelf
6	Early Miocene-Late Oligocene	Masachapa	siltstone with sandstone layers	slope to neritic
5	Late Oligocene	Masachapa	siltstone with sandstone layers	slope to neritic
4	Late Oligocene	Masachapa	siltstone with sandstone layers	slope to neritic
3	Late Oligocene	Masachapa	siltstone with sandstone layers	slope to neritic
2	Early Oligocene	Brito	sandstone siltstone	slope to neritic
1	Upper: Middle to Late Eocene Lower: Late Cretaceous to Middle Eocene	Upper: Brito Lower: Brito, Rivas	Upper: limestone, sandstone Lower: turbiditic shales, sandstone	Upper: neritic, euphotic Lower: open marine, abyssal to bathyal

Table 3.2: Simplified age and lithology information for sequences based on correlations to commercial wells (INE, 1993) and onshore stratigraphic studies (Weyl, 1980). Lithology and depositional environment represent localized samples (i.e., wells, outcrops) and are not representative of entire sequences. (Colors correspond to those displayed on interpreted seismic profiles in later chapters.)

In contrast, sequences 3-12 represent higher frequency cycles that range in duration between 1-5 My, while the youngest sequences, 13-16, each likely represent only 100 ky-1 My of deposition.

3.6 STRUCTURE AND ISOCHRON MAPS

The interpreted MCS data were used to create structure and isochron maps in order to illustrate the structural and depositional evolution of the Sandino basin. Structure maps were created for each stratigraphic surface (SB1-16) as well as the acoustic basement and the top of the subducting Cocos plate. Structure maps represent the gridded interpretation data in two-way travel time (TWT) for each surface (e.g. SB1 structure map for the SB1 surface). Using pairs of structure maps, individual isochron maps were prepared for all but the youngest Pleistocene to recent sequences (13-16). For these sequences, a composite isochron map was generated using the base of sequence 13 (i.e., SB12) and the seafloor.

Isochron maps represent the gridded time difference, or time-thickness, between the structure maps of two successive surfaces. For example, the time-thickness of sequence 1 is calculated by subtracting the TWT values of the SB1 structure map from those of the structure map for the acoustic basement. Structural and isochron gridding were done using a convergent algorithm included in the GeoFrame® interpretation software. The gridding geometry was rotated 45 degrees in order to offer better coverage on the NW-SE trending shelf. Values less than zero were treated as null and a user-defined polygonal clipping boundary was used so that gridding extrapolations did not extend cross barriers such as the Middle America Trench or the Central American coast where no data are available.

3.7 MCS INTERPRETATION CHALLENGES

The active forearc setting of the Sandino basin is inherently subject to a high degree of vertical tectonics that shears and displaces strata, complicating stratigraphic interpretation, especially when limited to 2D time-migrated MCS data. Structures such as folds and faults are common within the Sandino basin and present challenging situations for stratigraphic interpretation. The area beneath the modern slope is particularly difficult to interpret because of the concentrated amount of deformation that occurs here due to subduction-related processes that rupture the margin wedge basement as well as propagate faults through the overlying sediments. Furthermore, the slope area is host to myriad slope channel incisions and mass wasting events which preclude continuous, mappable reflections. Therefore, sequence boundaries were initially identified beneath the shelf and eventually mapped throughout most of the shelf. These boundaries were extended to the slope where feasible.

Complex structure not only increases the difficulty of stratigraphic interpretation, it also makes processing and imaging more challenging for several reasons, such as high angle reflectors that do not permit normal incidence and sudden lateral velocity and impedance variations caused by the juxtaposition of steeply dipping units of varying lithology with one another as well as the heterogeneity of cementation across lithologic units (Yilmaz, 2001). Although time-migration helps to reconcile these complications, imaging malconformations remain in seismic data that attempt to image complex structure, even more so for those, such as the time domain NicStrat data, that have not been depth-migrated.

In select regions, such as in the northwestern part of the survey area and along the inner shelf in the central region, some interpreted surfaces extend to depths exceeding the record length (>4.0 s TWT) for the high-resolution NicStrat MCS data. In most cases,

this issue was resolved by using the accompanying NicSeis MCS data (16 s TWT) but due to the wider profile spacing of that survey, along-strike coverage was diminished.

Another issue affecting seismic data coverage was encountered during acquisition. In an effort to protect sensitive wildlife, such as sea turtles and whales, and in accordance with the federal Marine Mammal Protection Act (MMPA), acquisition of seismic data was paused in the event of a visual or acoustic detection of certain protected species. Encounters with marine animals that required such temporary shutdowns resulted in a total of nearly 32 hours of lost MCS data acquisition time. Due to time constraints, we were not able to resurvey parts of profiles that were not sampled due to MMPA compliance. Ultimately, this resulted in data discontinuities in several MCS profiles. In the most extreme cases, these discontinuities prevented interpretation and affected line-ties (Fig. 3.8).

Finally, dating precision is limited by several factors. Firstly, the commercial wells that were used to correlate with the seismic reflection data are over 40 years old and few of the drilling records are publicly available. The published data from these wells consist only of cutting descriptions and, though geophysical well log data were acquired (INE, 1993), they are not available and in some cases presumed lost. Further complicating the dating of seismic units, each of the exploration wells were drilled into anticlinal structural traps whose complex structures presents both processing and interpretative challenges. The presence of hydrocarbons in these structural traps introduces an additional source of error to the migrated seismic section through distortion caused by low velocity natural gas reservoirs, commonly referred to as “velocity pull-down.”

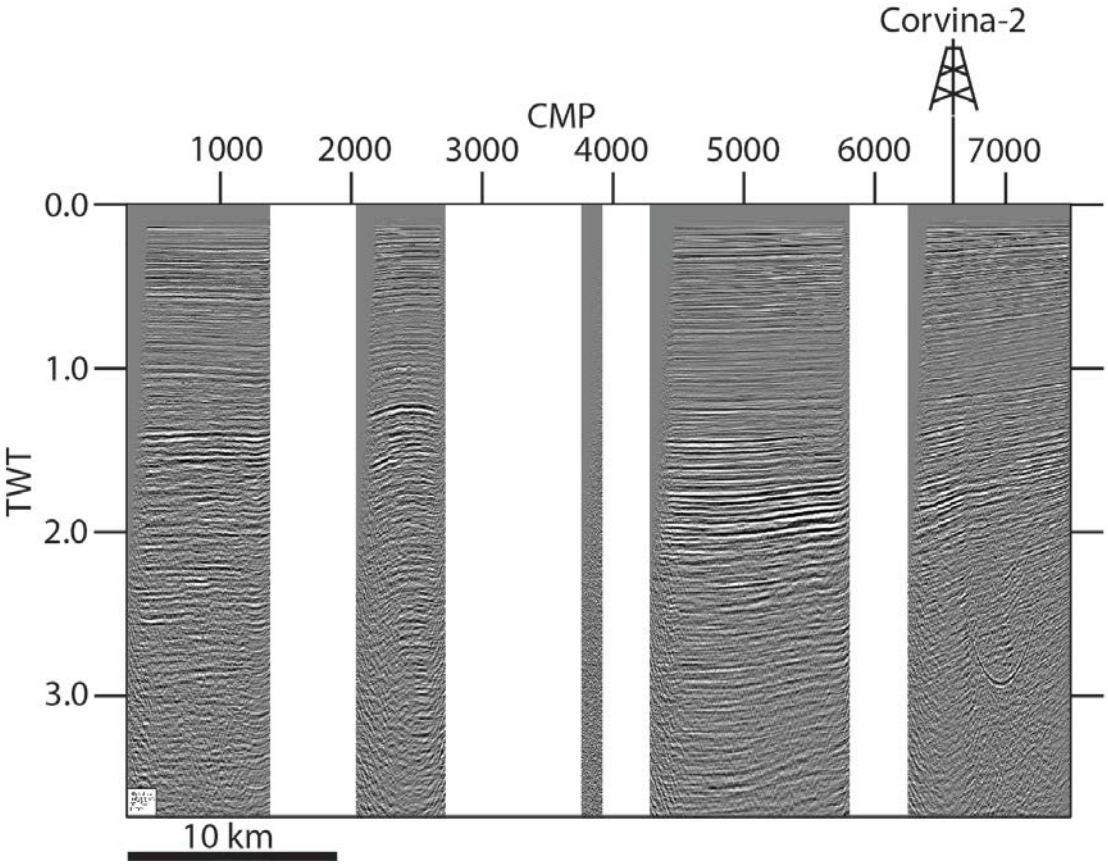

Figure 3.8: Example of a particularly severe set of data discontinuities created as a result of Marine Mammal Protection Act (MMPA) compliance. Pictured is line ns067, a well-tie, and gaps in data were due to encounters with numerous sea turtles during acquisition.

Chapter 4: Sandino Basin Interpretation

In this chapter, the morphology of the Sandino basin is described based upon the analysis of MCS data. The chapter is divided into two parts. The first part describes depositional sequences and structures from select MCS profiles that represent different regions of the Sandino basin. For organizational purposes, the Sandino basin is arbitrarily divided into the following geographical regions: Northern, Central, Southern, and Nicoya. Several profiles are featured in order to highlight the significant spatial variation in structure and deposition within the basin. The location for each of the MCS profiles referenced in this section is displayed on Figure 4.1. The second part of the chapter presents the structure and isochron maps for the acoustic basement and the depositional sequences.

4.1 OBSERVATIONS FROM MCS PROFILES

4.1.1 Northern Region

4.1.1.1 Line NS102

The NicStrat survey coverage in the northern region is limited to two strike profiles from the middle shelf that connect two dip profiles that enter the Gulf of Fonseca at their northeastern extent (Fig. 4.1). These MCS profiles reveal a basin that is characterized by relatively undeformed stratigraphy as shown on line ns102 (Fig.4.2). Line ns102 spans from the modern middle shelf at its southwestern limit, across the volcanic arc to the northeast, and into the Gulf of Fonseca, the northern limit of the Nicaraguan Depression (Fig. 4.1). Several normal faults are present along the entire profile and at least two right-lateral strike slip faults are found within the Nicaraguan

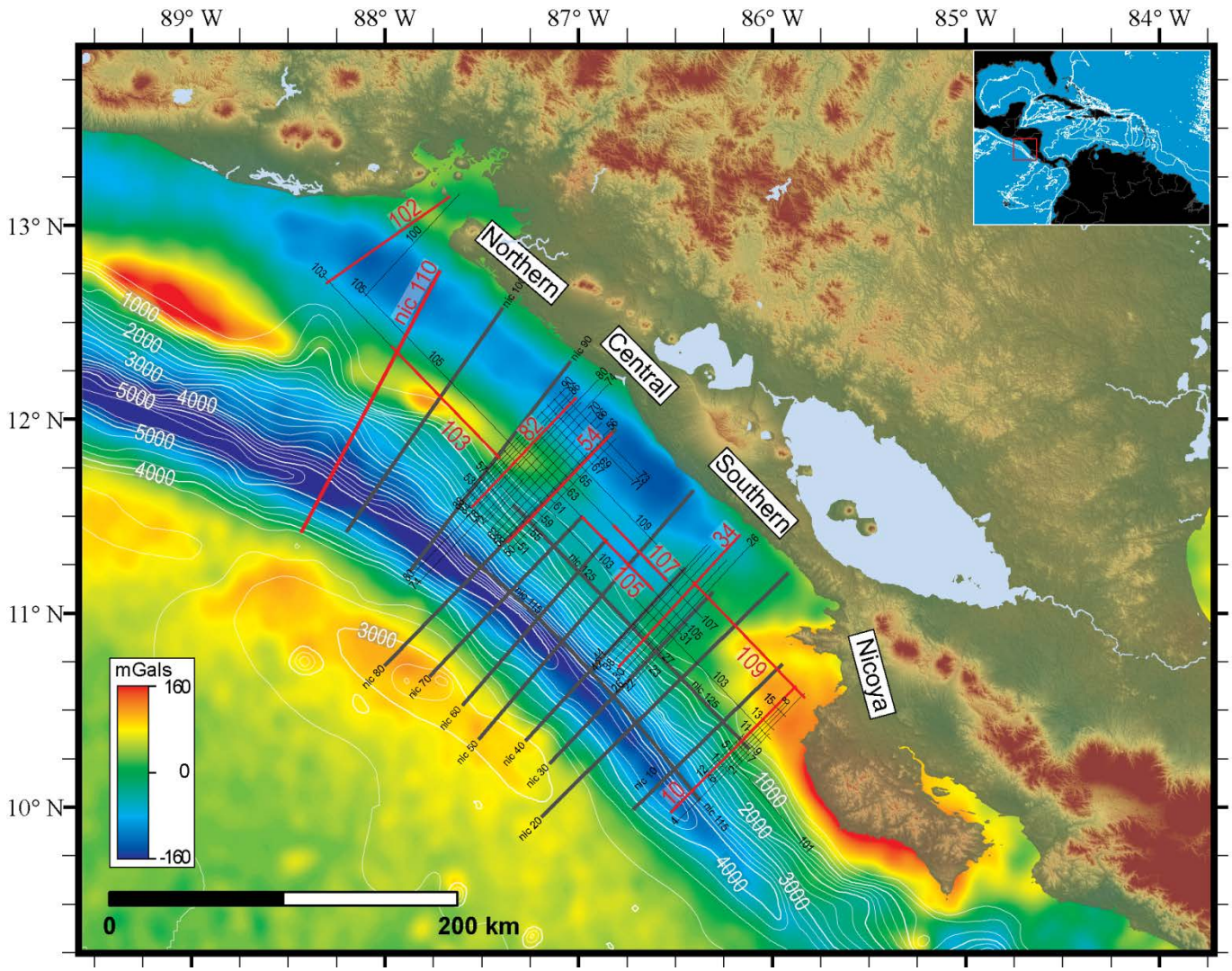

Figure 4.1: Map of Sandino basin with NicStrat (thin black lines) and NicSeis (thick dark gray) survey locations. Seismic data displayed in this section are indicated in red. Topography from SRTM data is shown onshore. Offshore, gravity data (Sandwell and Smith, 2009) is overlain by 250 m contour (white lines) bathymetry (GEBCO, 2008)

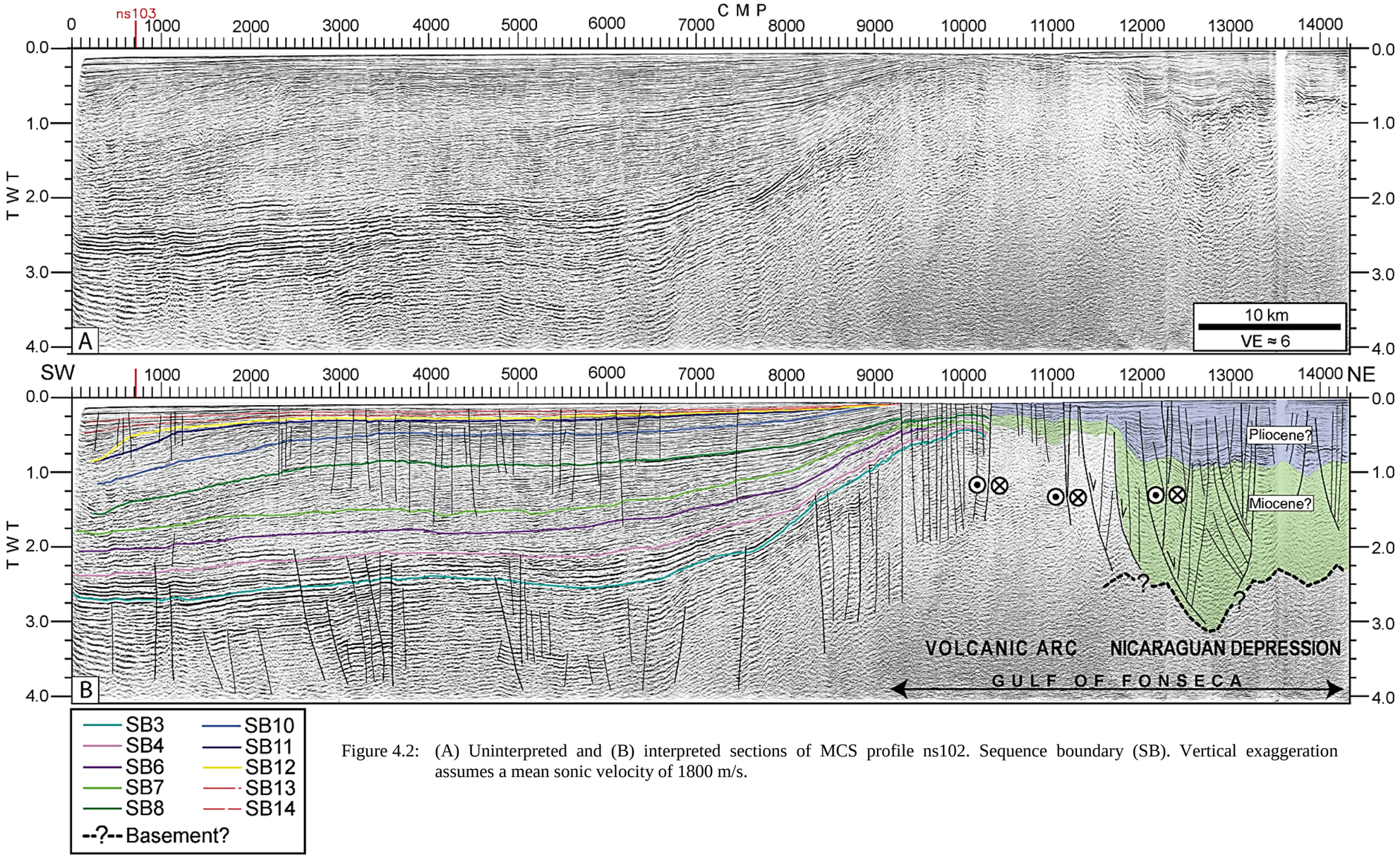

Figure 4.2: (A) Uninterpreted and (B) interpreted sections of MCS profile ns102. Sequence boundary (SB). Vertical exaggeration assumes a mean sonic velocity of 1800 m/s.

Depression and the volcanic arc. A few sequences are absent on this line including sequence 5, which terminates at an angular unconformity to the southeast, and the oldest sequences, sequences 1 and 2 which could not be tied because they exceed the 4.0 s record length on the connecting strike line. The acoustic basement is also below the 4.0 s record length for this line. Because older sequences are not able to be mapped here, the base of the Late Oligocene sequence 3 cannot be directly constrained by NicStrat MCS data.

The sequence boundaries dating to the Late Oligocene, SB3 and SB4, and the Early Miocene, SB6, lie conformably atop one another beneath the middle shelf in a relatively undeformed section of the forearc basin that features only near-vertical small offset faults that converge in a flower structure pattern. Beneath the middle shelf, the Late Oligocene sequences, sequences 3 and 4 have a tabular geometry with high amplitude, subparallel to hummocky (e.g. upper sequence 4, ~5000-6000 CMP) reflections, while the Early Miocene sequence 6 exhibits a tabular-shaped variable amplitude succession of reflections. To the northeast, SB3 and underlying reflections are uplifted, dipping trenchward at the volcanic arc. Sequence 4 maintains a thickness of ~0.25 s ΔTWT beneath the shelf before thinning considerably at ~8000 CMP and eventually terminates in the northwest as it onlaps seismic strata at the volcanic arc massif. Sequence 6 measures ~0.2 s ΔTWT in thickness across the shelf and decreases to ~0.1 ΔTWT at 8100 CMP before SB6 is truncated by SB7 at ~0.35 s TWT (Fig. 4.2).

The Mid-Miocene sequence 7 is thin (>0.2 s ΔTWT) and lens-shaped with internal reflections downlapping SB6 to the southwest beneath the middle shelf and onlapping SB6 to the northeast at the volcanic arc. The Early Miocene sequence 8 is thickest beneath the middle shelf with a thickness of ~ 0.5 s ΔTWT where the sequence progrades with internal reflections downlapping SB7 to the southwest. Sequence 8 thins

to > 0.1 s ΔTWT at the volcanic arc where internal reflections onlap SB7 (Fig. 4.2). At the northeastern extent of ns102, SB8 is tentatively mapped across the volcanic arc, traversing both dip slip and strike-slip faults and entering the Nicaraguan Depression where it reaches a depth of ~1.0 s TWT. Sequence 10 rests conformably above SB8 with a relatively constant thickness of ~0.5 s TWT across the shelf. Sequence 10 thins slightly to the northeast where SB10 is truncated seaward of the uplifted volcanic arc by SB12. Sequence 11 pinches out seaward of the volcanic arc where it onlaps SB10 at its base and is truncated by SB12 at its upper boundary. Sequence 11 progrades across the shelf and increases in thickness from ~0.25 s TWT to 0.5s TWT around CMP, 1200 where reflections downlap SB10.

Sequences younger than SB11 are markedly thinner beneath the shelf. The internal reflections of sequence 12 increase in dip angle abruptly at 700 CMP before downlapping and terminating on SB11. Across the shelf, sequence 12 is >0.1 s TWT and the upper boundary, SB12, truncates underlying reflections. Sequences 13 and 14 drape underlying reflections on the shelf gradually decreasing in thickness before pinching out landward of the volcanic arc.

At least 2.5 s TWT of sediment is observed in the heavily faulted Nicaraguan Depression. The age of the sediment is difficult to determine due to the truncation of younger sequences, the prevalence of strike-slip faulting, and poorly imaged strata across the volcanic arc. Therefore the age of the basin fill within the Nicaraguan Depression is tentatively determined to be Mid-Miocene to recent.

4.1.1.2 Line NIC 110

South of the Gulf of Fonseca, the deep penetration NIC 110 dip profile crosses the deepest section of the depositional forearc basin and the outer arc high feature, the

Corinto High, previously identified using gravity data (Fig. 4.1). The MCS data clearly reveal uplifted forearc basement beneath the slope and outer shelf (Fig. 4.3). Possible thrust faults within the outer arc high basement are marked by small dotted lines. The top of the subducting Cocos slab is shown beneath the margin wedge at 8.0 s TWT in the southwest and descends below the seismic record (15.0 s TWT) beneath the outer shelf. Thrust faults are inferred based on the morphology of the top of basement blocks (as mapped by horizon B) and by coherent reflections within the margin wedge. In the upper plate beneath the outer arc high, a region that corresponds with the seismogenic zone of the plate interface (McIntosh et al., 2007), parallel high amplitude reflections that dip landward, characteristic of underplated sediments, are imaged within the upper plate. Above this region (~6200 CMP), the basement reaches its shallowest point and the overlying strata form a horst bounded by active northeast- and southwest-dipping, normal faults that offset ~3.5 s TWT thick sediments that date to at least the Eocene epoch. Obvious compressional features are absent within the deep basin and the underlying acoustic basement. The Late Cretaceous to Mid-Eocene age sequence 1 reaches a maximum thickness of ~5.0 s TWT with the oldest units exhibiting divergent to subparallel internal reflection patterns and forming a wedge that onlaps the acoustic basement to the southwest. The sequence thins to < 0.5 s TWT at its shallowest point (6500 CMP) as it bypasses the basement high before terminating within an extensional sub-basin beneath the upper slope (6700-7700 CMP).

Sequences 2 and 3 of the Oligocene share similar seismic facies characteristics with sequence 1. Like sequence 1, both display continuous aggradational to progradational reflections with divergent to subparallel reflection patterns. SB3 appears as a high amplitude reflection from beneath the outer shelf to the graben above the

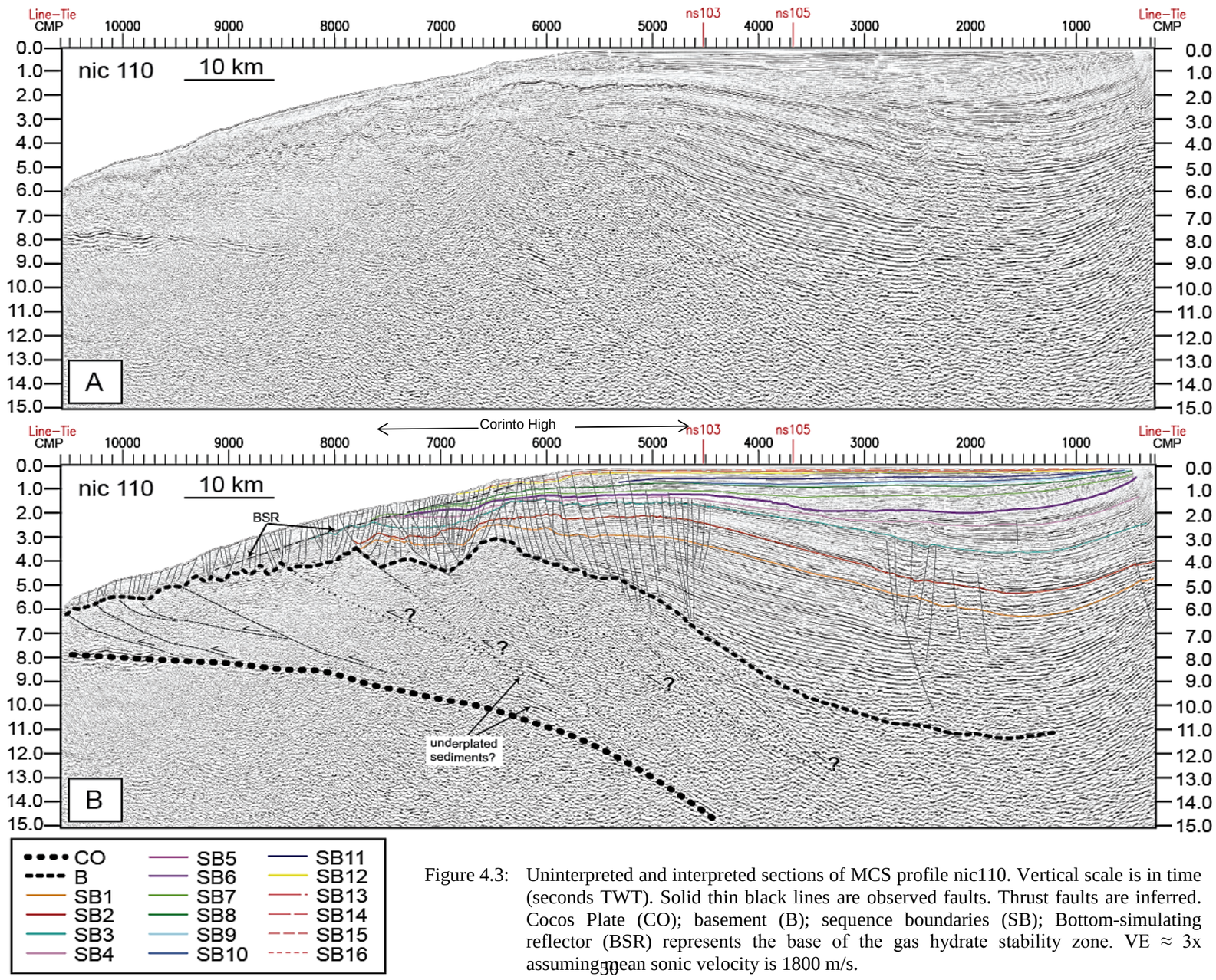

Figure 4.3: Uninterpreted and interpreted sections of MCS profile nic110. Vertical scale is in time (seconds TWT). Solid thin black lines are observed faults. Thrust faults are inferred. Cocos Plate (CO); basement (B); sequence boundaries (SB); Bottom-simulating reflector (BSR) represents the base of the gas hydrate stability zone. VE ≈ 3x assuming mean sonic velocity is 1800 m/s.

basement high of the outer arc. Representing the remainder of the Oligocene through the Miocene, sequences 4, 6, 7, and 8 infill the deep basin before thinning significantly towards the outer shelf and eventually terminating at the outer arc sub-basin beneath upper slope. Sequence 9 is retrogradational, downlapping SB8 near CMP 4400. Sequence 10 and 11 prograde but each terminate by downlapping SB8 on the shelf. Sequence 12 is marked by relatively thin deposition across the shelf that culminates in a prograding package of sigmoidal clinoforms beneath the shelf edge measuring ~0.5 s TWT in thickness.

4.1.1.3 Line NS103

In the strike direction, line ns103 obliquely intersects the axis of the Corinto structural high observed in gravity data (Fig. 4.1 and Fig. 4.4). The basement reflection is not imaged well on line ns103 at this location (Fig. 4.4) but correlation with line ties from the deep penetration NicSeis survey suggest that it follows the general trend of the overlying sediments. Sequence 1 is deposited over the basement, folded, and truncated beneath CMP 11300 by SB3 at a depth of ~1.25 s TWT. Sequence 2 is also truncated by SB3 at the Corinto High. Oligocene to Early Miocene strata onlap the southeastern Corinto high including sequence 5 which pinches out at CMP 10200. Internal reflections of sequence 6 downlap SB5 in the southeast as the sequence approaches the Corinto high (~CMP 7000-9000). Near the region above the basement high and to its southeast, sequence 7 contains discontinuous and chaotic facies that show evidence of truncation and channelization. Continuing to the northwest, the Mid-Miocene sequence 7 tapers with internal reflections downlapping SB6. The overlying sequence 8 exhibits continuous sub-parallel to divergent reflections that onlap the Corinto High. The Pliocene sequences 9-11, thicken upsection with sequence 9 being the thinnest and

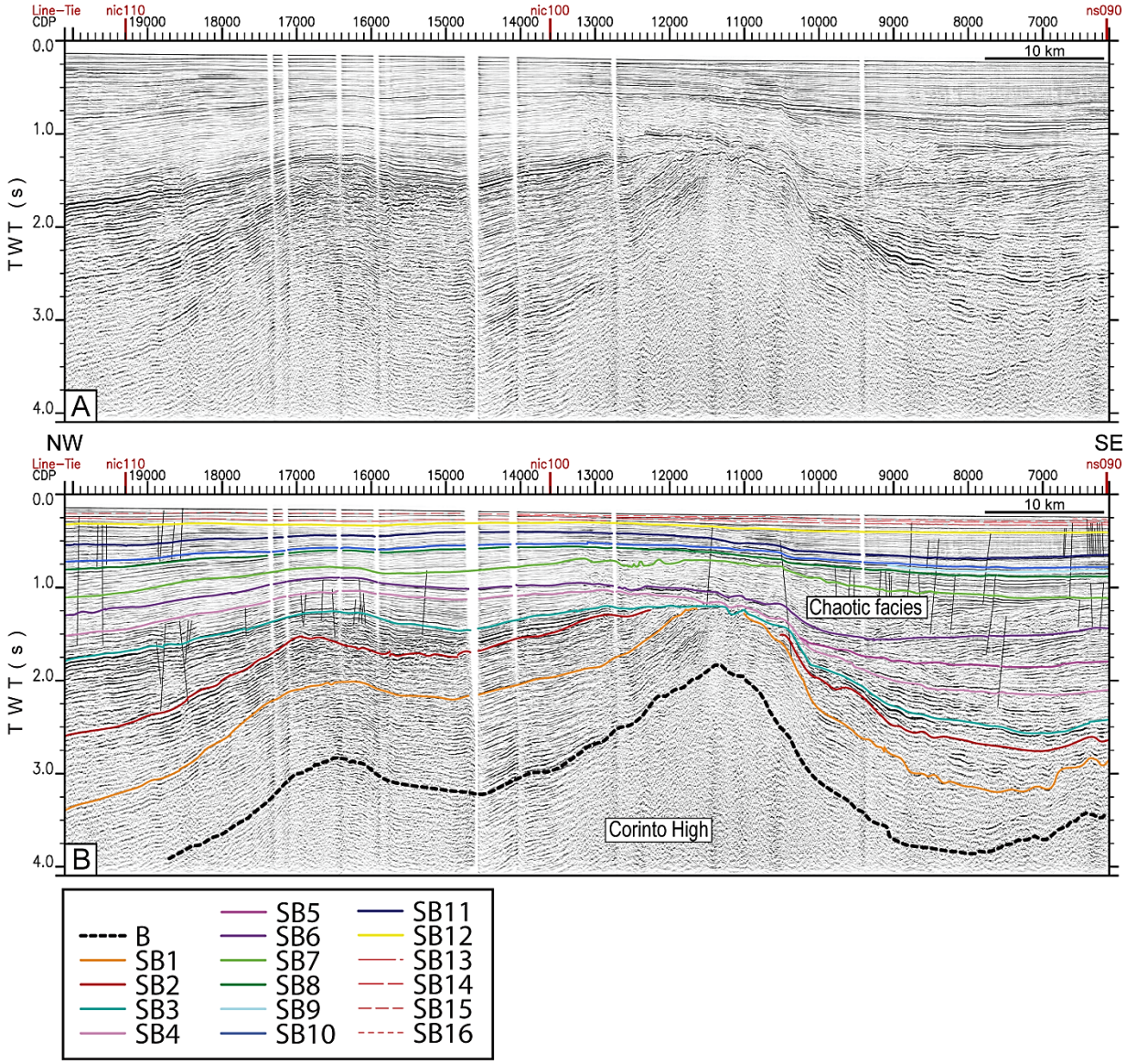

Figure 4.4: (A) Uninterpreted and (B) interpreted sections of MCS strike profile ns103. Vertical exaggeration is ~11:1 assuming a mean sonic velocity of 1800 m/s. Basement (B). Sequence boundary (SB).

terminating as an onlap on SB8, southeast of the basement high. The Plio-Pleistocene sequence 12 is thickest in the southeast (~0.25 s TWT) where earlier reflections onlap SB11 as they approach the Corinto High. Notably, SB12 is sub-horizontal to the seafloor across the Corinto High, displaying only a very slight change in depth relative to older sequence boundaries. The Pleistocene sequences (SB13-16) show divergent reflections which are deposited conformably over one another. Sequences 14 and 16 are restricted to the southeast terminating as onlaps on SB13 (~14000) and SB15 (CMP ~6600) respectively.

4.1.2 Central Region

4.1.2.1 Line NS082

Continuing to the southeast, the basement high responsible for the gravity expression of the Corinto High diminishes beneath the middle shelf (Fig. 4.1) but is still observed on seismic profiles in the region, including line ns082 (Fig. 4.5). Here, the basement reflection reaches a minimum depth of approximately 2.75 s TWT and is deformed beneath the upper slope by an active, large-offset (~1.0 s TWT), listric normal fault with an apparent landward dip and negative flower-structure morphology. Tilted, syndeformational growth strata deposited during sequence 4 are observed against an antithetic of the primary fault. Several other active normal faults with smaller offset appear beneath the outer shelf, past the shelf break, and beneath the upper to middle slope. With the exception of the large-offset normal fault at the outer arc, normal faults downdip of the shelfbreak predominantly dip trenchward. Landward of the shelfbreak, the majority of faults dip to the northeast including several active faults that affect basement (CMP 5500-7000). Inactive faults, affecting basement and strata at least as old as Mid Eocene (sequence 1) to Oligocene (sequences 2-3) overlie the basement of the

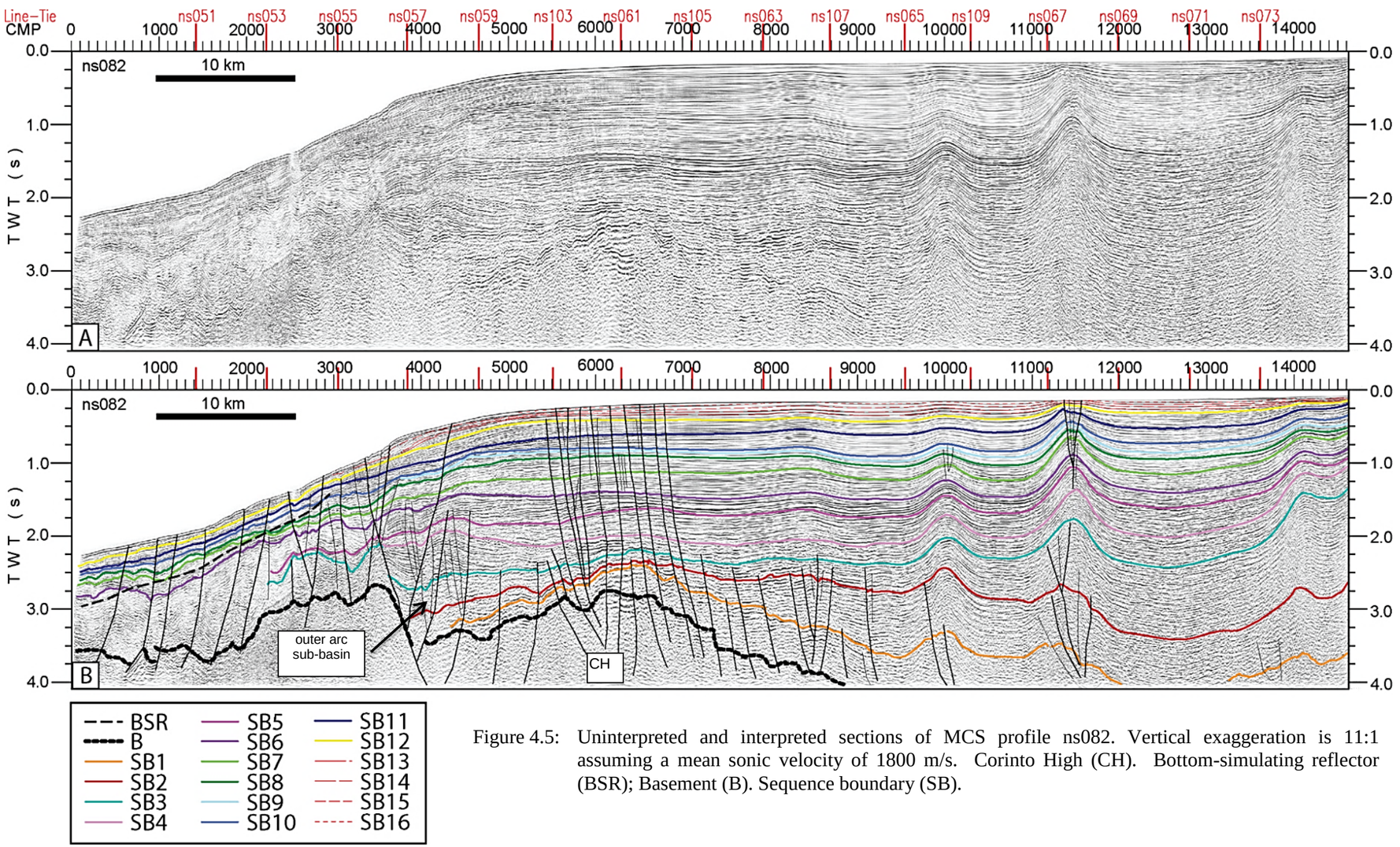

Figure 4.5: Uninterpreted and interpreted sections of MCS profile ns082. Vertical exaggeration is 11:1 assuming a mean sonic velocity of 1800 m/s. Corinto High (CH). Bottom-simulating reflector (BSR); Basement (B). Sequence boundary (SB).

projected Corinto High (CMP ~6300) form a horst with normal faults dipping away from the axis of the basement high. Sediments of the forearc basin are actively folded by four anticlines in this region. The most prominent these are two symmetrical upright anticlines (CMP 10000 and 11500) deforming all sixteen sequences with a crest-to-crest wavelength of ~9.7 km. The larger amplitude syncline (CMP 11500) is offset by a series of active normal faults. The third is less tightly folded and found seaward (CMP 8400). This open anticline affects only Oligocene (sequence 5) to recent sequences and, though symmetric to shallow depths (< ~0.6 s TWT), it is slightly asymmetric at depths greater depths with apparent vergence to the northeast. The fourth anticline is a northeast vergent asymmetric fold located near the landward extent of line ns082 (Fig. 4.4). Reflections from within sequences as old as Late Oligocene are observed onlapping the anticlines in this region of the basin and the crests of a few of these anticlines have been periodically eroded since Late Pliocene to recent.

Sequences 1 and 2 prograde across the shelf, decreasing in thickness as they approach the northeastern boundary of the outer arc high (Fig. 4.4). Above the basement high (CMP ~6000-6500), these sequences display a hummocky, high to variable amplitude seismic character. Sequence 3 reaches a thickness ~ 1.0 s in the deep basin but thins to < 0.3 s TWT seaward of the middle shelf anticlines. SB3 is a high amplitude reflection at the outer arc high where it truncates underlying reflections and is underlain by hummocky, variable amplitude reflections of strata deposited in the sub-basin beneath outer shelf to upper slope (CMP ~3800-6000).

Sequences 4-6 of the Late Oligocene to Early Miocene represent a shift in depocenter from the inner shelf to the middle (sequence 5) and outer shelf (sequences 4 and 6). On the shelf seaward of the folds and across the outer arc high to the sub-basin, the internal reflections of sequence 4 are hummocky and of variable amplitude. In

contrast to other sequences, the internal reflections of sequence 4 are dipping landward within the sub-basin southeast of the large offset outer arc fault. Overlying deposition from sequence 5 decreases in thickness at the outer arc sub-basin with variable amplitude and discontinuous to hummocky reflections while subsequent deposition from sequence 6 is continuous high amplitude and increases in thickness as clinoforms prograde and downlap SB5 at the outer arc sub-basin. Sequences 4-6 decrease slightly in thickness across the anticlines.

The Mid Miocene sequence 7 is retrogradational exhibiting continuous reflections seaward of the anticlines with deposition that decreases in thickness at the outer shelf as the amplitude becomes less coherent (Fig. 4.5). Sequence 8, capped by a continuous high amplitude SB8, is progradational with its thickest succession beneath the shelf edge and its thinnest on the inner shelf where base reflections onlap the anticlines.

The Early and Mid-Pliocene sequences 9 and 10 are relatively thin progradational to aggradational units that are thickest beneath the inner and middle shelf units that decrease in thickness towards the shelf edge (Fig. 4.5). Sequence 11 is relatively thick (~0.25 s TWT) on the shelf with a retrogradational wedge-shaped appearance that is heavily faulted across the larger amplitude anticline (CMP 11500) and SB11 possibly represents truncation there, as well. The landward extent of SB11 truncates the asymmetric anticline (CMP 14100). The Plio-Pleistocene SB12 shows clear truncation of older reflections across the two landward anticlines as well as the seaward anticline (CMP 8400). Sequence 12 is progradational and develops a succession of sigmoidal clinoforms beneath the shelf edge. The Pleistocene sequence boundaries, SB13-16, are continuous high amplitude reflections that are erosional beneath the inner shelf and prograde to the shelf break or upper slope.

4.1.2.2 Line NS054

Line ns054 is oriented parallel to ns082 and is positioned 28 km southeast in the Central region (Fig. 4.1). The structure observed on ns054 (Fig. 4.6) is relatively similar to that of ns082 (Fig. 4.5) however key differences exist. Strata in the deep basin are also folded on line ns054 but the analogous anticlines are positioned ~7.5 km farther landward from the shelf break. The anticlines on line ns054 are relatively upright with axial planes that dip slightly seaward but the reflections of Oligocene and earlier sequences are not continuous across the crest of the largest anticline (CMP 12700). The gravity high trend associated with the Corinto High is diminished and located beneath the middle shelf at line ns054 (Fig. 4.1) where a normally-faulted structural high is observed that correlates with the position of the gravity anomaly (CMP ~7700-9100).

Similar to ns082, an active landward-dipping normal fault that offsets basement and strata at least as old as Eocene is present at the outer arc high beneath the shelf break (CMP 5200). The acoustic basement and oldest units (Sequences 1-3) are folded on the downthrown side of the fault plane while the overlying younger sequences are offset by synthetic normal faults and dip towards the adjacent fault plane on the downthrown block. Slightly further landward, basement and sequences dip landward, away from the fault plane. The material beneath the slope is structurally complex due primarily to the presence of a multitude of faults that vary in age and orientation disrupting seismic reflections. Consequently, SB1-SB3 were unable to be mapped across much of the slope specifically as a result of discontinuities caused by rotated fault blocks (Fig. 4.6). These fault blocks appear to be rooted in the outer arc basement and feature fold and thrust morphology interpreted to be Late Oligocene in age. Slope sediments overlying the fault blocks are offset by an extensional fault system (CMP ~1200-5000) with normal faults that tend to converge towards the fault block boundaries.

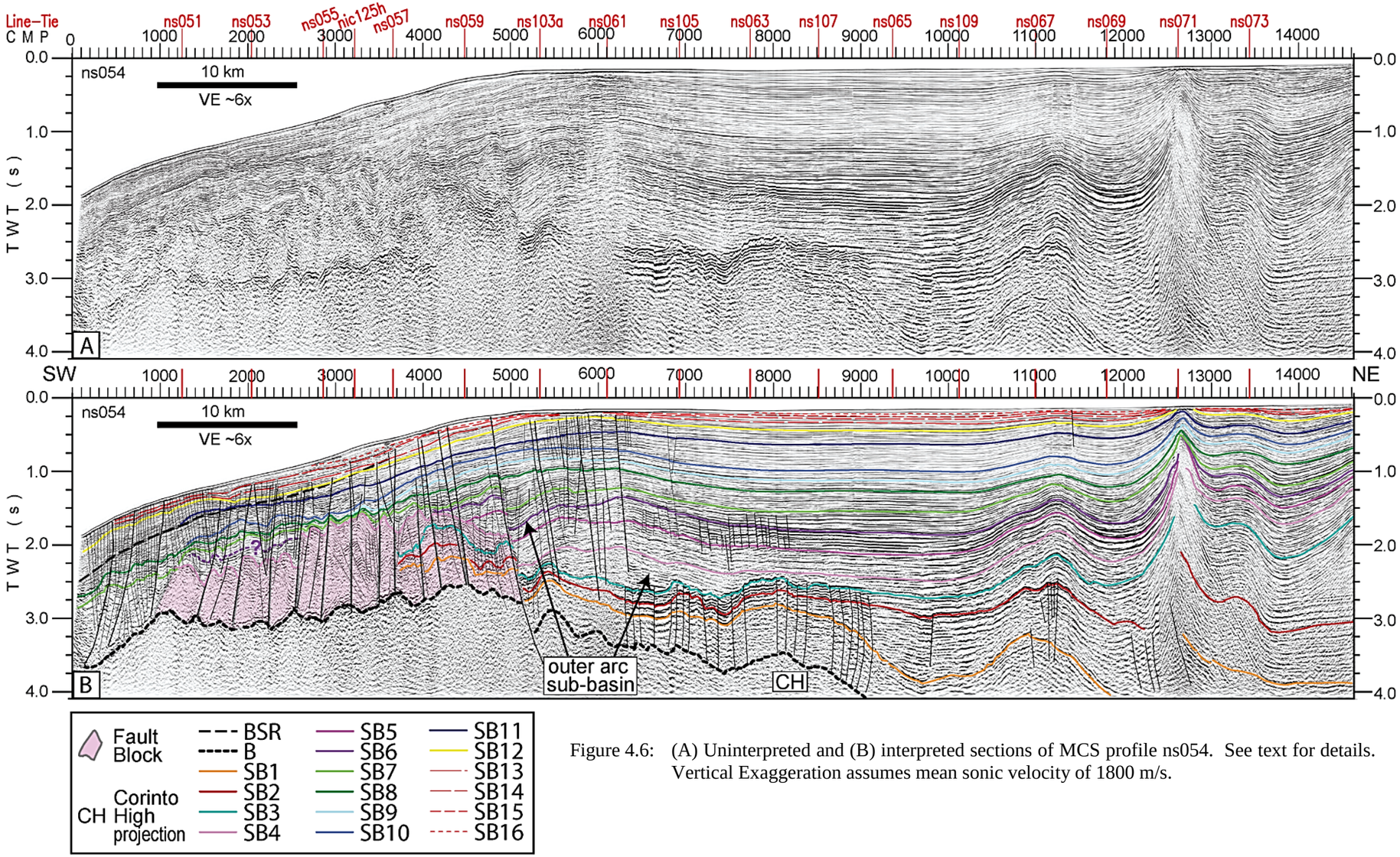

Figure 4.6: (A) Uninterpreted and (B) interpreted sections of MCS profile ns054. See text for details. Vertical Exaggeration assumes mean sonic velocity of 1800 m/s.

The seismic facies of sequence 1 observed on line ns054 is hummocky to semi-transparent with variable amplitude and onlaps the acoustic basement to the southwest beneath the outer shelf (Fig. 4.6). The upper boundary of SB1 is continuous and high amplitude across the shelf. Sequence 2 is thickest beneath the deformed inner shelf and thins substantially (< 0.25 s TWT) across the middle shelf basement high as the seismic facies changes from divergent and variable amplitude to hummocky and high amplitude. Base reflections onlap SB1 to the southwest within a sub-basin seaward of the anticlines where thickness reaches a ~1.0 s (CMP 9700). Sequence 3 is uplifted beneath the inner shelf, landward of the anticlines, then decreases in thickness to the southwest and remains relatively thin (< 0.2 s TWT) across the middle and outer shelf. At the middle shelf structural high, sequence 3 is mounded and SB3 marks the upper boundary of a hummocky, high amplitude succession which includes sequence 2 and upper sequence 1 locally (CMP 6400-9000).

Sequence 4 marks a transition to sediment storage that is more evenly distributed along the shelf in contrast to earlier sequences where storage is heavily concentrated in the inner shelf region, northeast of the gravity high (Fig. 4.6). The hummocky reflections of sequence 4 thin across the anticlines and the middle shelf gravity high while outer shelf deposition is focused within a landward-tilted outer arc sub-basin. The high degree of structural complexity beneath the slope hinders stratigraphic interpretation but based on fault-slide correlation of SB4 to the top of northeast dipping strata across the large-offset normal fault at the outer arc high (CMP 5100), SB4 is further interpreted across the landward-tilted fault blocks of the upper slope. Sequence 5 downlaps SB4 and terminates on the upthrown side of the large-offset normal fault at the outer arc high (CMP 4800). At the outer shelf, sequence 5 reflections are low amplitude and tilted landward. Continuing to the northeast, the seismic facies becomes continuous and subparallel to

divergent with high amplitude, low frequency reflections pinching out against each side of the larger fold. The Late Oligocene to Early Miocene sequence 6 is continuous, high amplitude, and terminates by downlapping SB4 at the fault blocks beneath the slope (CMP 4200).

The Mid Miocene SB7 and the Late Miocene SB8 surfaces are both continuous across the large fold at the northeast end of line ns054 (Fig. 4.6). While deposition of sequence 7 is relatively thin (< 0.15 s TWT) beneath the inner shelf, it is most pronounced on either side of the seaward anticline and thickness attenuates towards the outer shelf, coincident with the increasing dip angle of the underlying landward-tilted sequences. In contrast, the Late Miocene sequence 8 is more substantial landward of the large anticline (up to 0.25 s TWT), thins adjacent to the seaward anticline, and maintains a relatively constant thickness (~ 0.25 s TWT) across the middle and outer shelf. At CMP 6300, sequence 7 progrades and downlaps SB6 in an ~8 km wide sub-basin at the outer arc high. Growth strata within sequence 7 are observed at the shelf break against the footwall of the large-offset normal fault as well as beneath the slope as sediment drape onlaps SB4 above the fault blocks. Sequence 8 also increases in thickness at the outer arc sub-basin and exhibits syndeformational sedimentation against the normal fault. Sequence 8 downlaps SB7 on the footwall of the large normal fault (CMP 4400), where it is roughly half as thick (~0.25 s TWT) as it is on the hanging wall (~0.50 s TWT).

Early and Middle Pliocene sequences 9 and 10 are aggradational and generally concordant sequences that maintain a constant thickness across the shelf (~0.2 s TWT) and onlap the limbs of the larger anticline as well as truncate its crest. The Late Pliocene sequence 11 also onlaps and truncates the larger anticline. The seismic facies is identified as continuous and sub-parallel to divergent with depositional thickness that is approximately twice as much as the other Pliocene sequences across the shelf (~0.4 s

TWT thick). Just as on line ns082, sequence 11 is distinctly wedge-shaped at the outer shelf as it onlaps SB10 at the outer arc high progrades past the shelf break and delivers sediment to the slope. The Plio-Pleistocene sequence on line ns054 (Fig. 4.6) also resembles its profile on ns082 (Fig. 4.5). Here again, sequence 12 is progradational with sigmoidal clinoforms at the shelf edge, although on line ns054, SB12 is truncated at the seafloor across the larger anticline in the northeast (CMP 12700). SB12 is nearly exposed at the seafloor beneath the outer shelf (CMP 5800) where it is buried by approximately ~0.1 s TWT of sediment. Sequences 13-16 are truncated across the large anticline and are either truncated or pinch out at the outer shelf (CMP 5800). The seafloor also shallows slightly (~10 m) at this location near the shelf edge and, when contrasting the two MCS dip profiles presented from the Central region in this section, a difference in the relative depth of sequences across the shelf becomes apparent. Landward of the two largest folds on line ns082 (Fig. 4.5), sequence boundaries are nearly horizontal from beneath the outer to middle shelf, whereas the sequence boundaries from line ns054 (Fig. 4.6) display similar depths beneath the middle shelf but appear noticeably shallower beneath the outer shelf where the youngest sequences are not preserved (CMP 5800).

4.1.3 Southern Region

4.1.3.1 Lines NS105 and NS107

A portion from two regional strike lines, ns105 and ns107, are given in Figures 4.7 and 4.8 respectively which illustrate the transition from the Central to Southern region across the middle shelf. The featured sections are situated in between the prominent gravity anomalies of the Corinto High to the northwest and the approaching

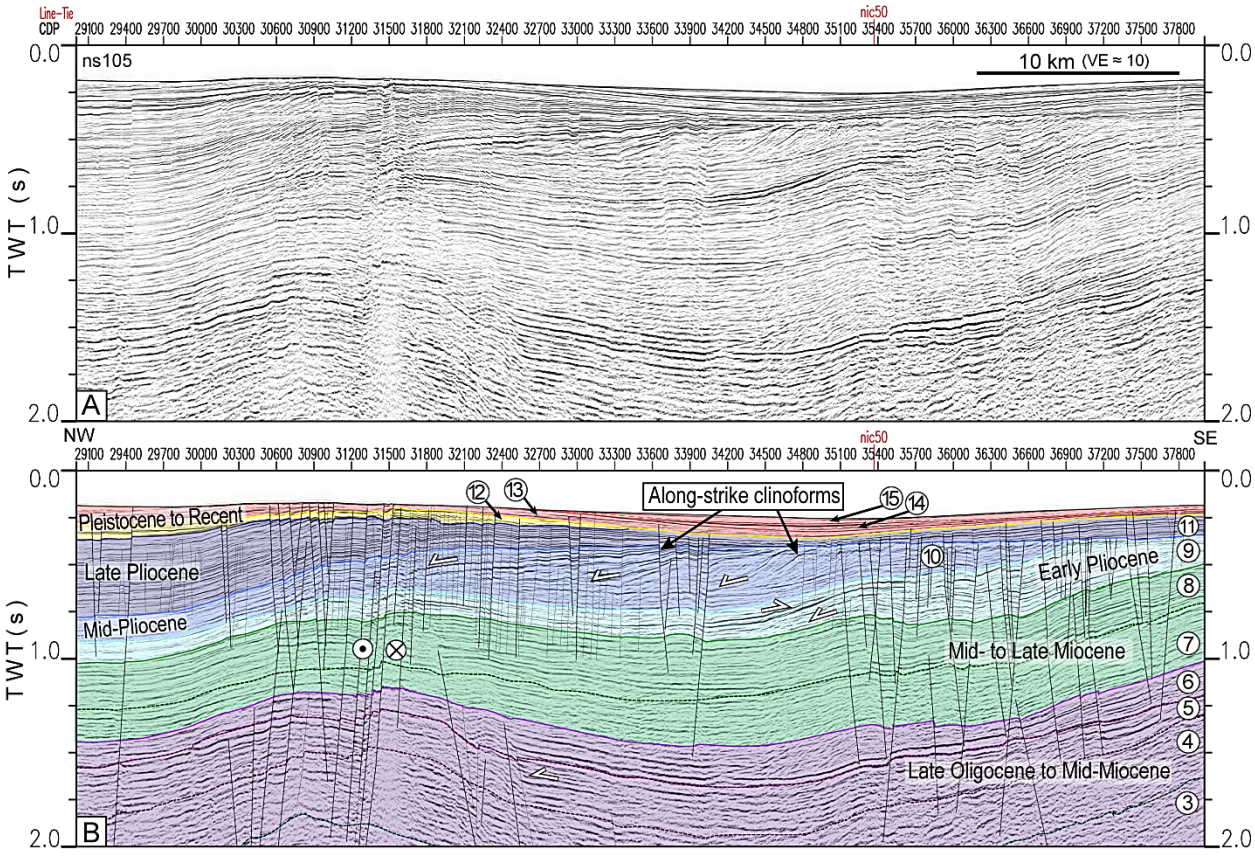

Figure 4.7: (A) Uninterpreted and (B) interpreted sections from line ns105. Circled numbers identify corresponding sequences and sequence boundaries. Sequence boundary numbers are defined as the top of the appropriate sequence. Select lap relations are represented by white arrows. Colored shading of sequences is for illustrative purposes only. Vertical exaggeration assumes a mean sonic velocity of 1800 m/s.

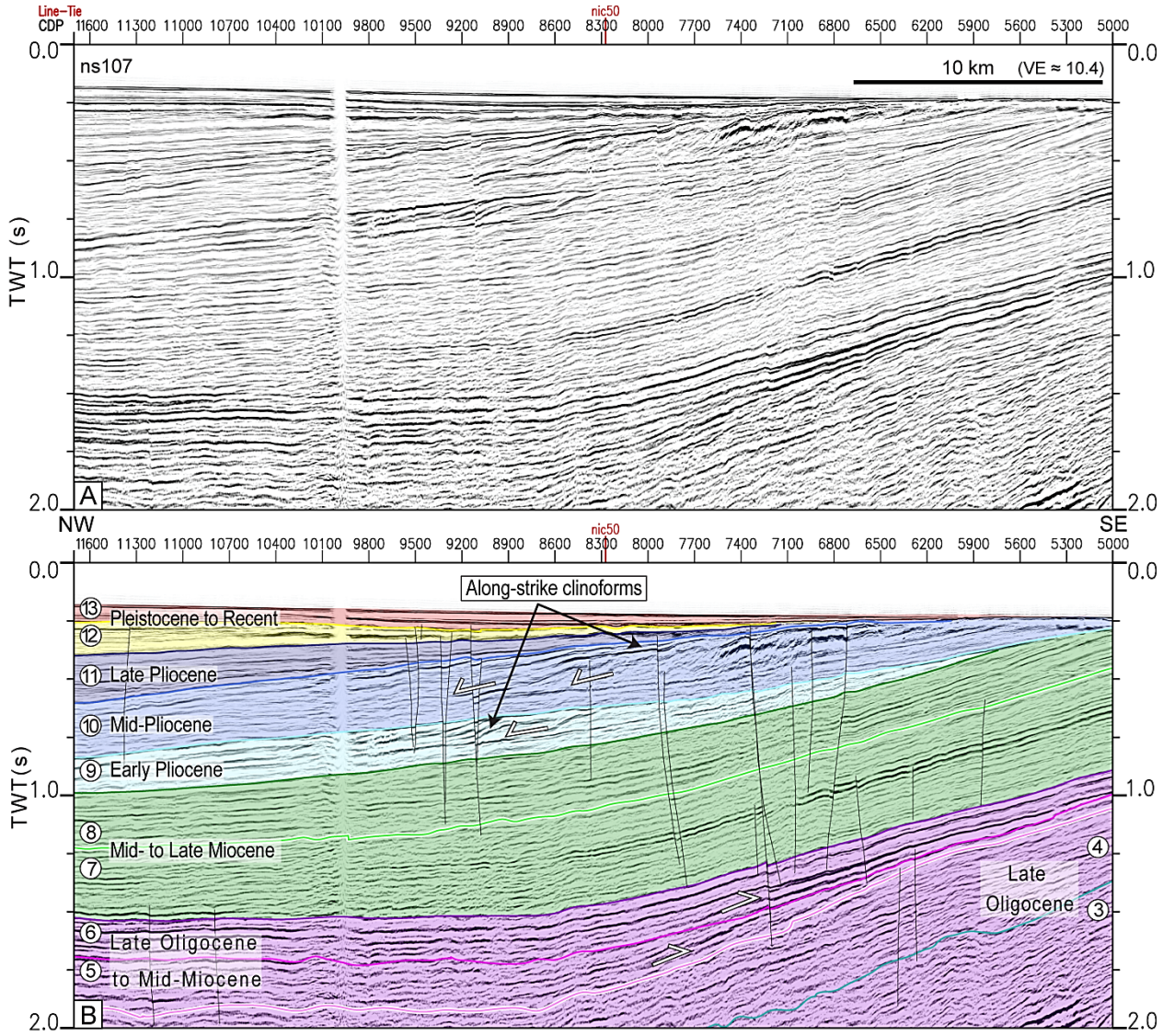

Figure 4.8: (A) Uninterpreted and (B) interpreted sections of line ns107. Circled numbers identify corresponding sequences and sequence boundaries. Sequence boundary numbers are defined as the top of the appropriate sequence. Select lap relations are represented by white arrows. Colored shading of sequences is for illustrative purposes only. Vertical exaggeration assumes a mean sonic velocity of 1800 m/s.

gravity high of the Nicoya region (Fig. 4.1). The dominant dip direction for strata on both profiles is to the northwest (Fig. 4.6 and Fig. 4.7).

Line ns105 shows continuous divergent seismic facies that are offset by numerous active faults with minor vertical displacement (i.e. 10s of meters). An active cluster of faults approximately 4-5 km wide at the crest of an anticline converge near CMP 31500. The seafloor is elevated locally and the southeastern blocks are upthrown relative to the northwestern blocks. This fault zone is identified as a transpressional strike-slip fault with left-lateral displacement.

The Mid-Miocene sequence 7 displays increasing thickness towards the southeast. Subsequently, the Early Miocene sequence 8 becomes thinner in that direction. Sequence 9 of the Early Pliocene is truncated by SB11 in the southeast but downlapping reflections within the sequence are preserved prograding towards a thinning sequence in the NW. Reflections from sequence 9 are elevated in the southeast and dip northwesterly. At CMP 34800, the upper reflections within sequence 9 onlap back toward the southeast before they are truncated by SB9. During the Mid-Miocene, sequence 10 develops a series of clinoforms that appear to prograde along-strike to the northwest. In the southeast (CMP 35000-37000) sequence 10 is truncated by SB11 which is downlapped by a thin wedge (>0.1 s TWT) of reflections from sequence 11. The Late Pliocene sequence 11 increases to 0.5s TWT at the northwest edge of the section. Sequences 12-15are deposited over erosional unconformities and drape sediment in the low lying regions on each side of the transpressional anticline.

The section of line ns107 displayed in Figure 4.8 is structurally less complicated than the adjacent section of ns105 shown in Figure 4.7. Sequences are observed to be uniformly elevated in the southeast with reflections dipping to the northwest. Sequences 3 and 4 of the Late Oligocene are discontinuous with variable amplitude. SB4 is

onlapped to the southeast by sequence. Subsequently, sequence 6 onlaps SB5 and represents a change from a hummocky variable amplitude seismic character to a continuous high amplitude facies. Sequence 7 is thickest in the southeast (~0.5 s TWT) and is characterized by a semi-transparent seismic facies interbedded with high amplitude reflections. The seismic facies of sequence 8 resembles sequence 7 but it is not as thick in at the elevated end of the section in the southeast (~0.25 s TWT). From CMP 5700 to the end of the section at CMP 5000, sequence 8 reflections are truncated by an angular unconformity corresponding with the top of the Early Pliocene sequence, SB9. Within sequence 9, a few downlapping reflections resembling clinoforms are preserved between two parallel high amplitude reflections. The Mid Pliocene sequence 10 contains a larger set of NW downlapping surfaces that appear to be clinoforms. This interval corresponds to that of the clinoforms observed previously on line ns105.

4.1.3.2 Line NS034

Transverse to the trench in the Southern region, the forearc basin is subdivided by a pronounced middle shelf high (CMP ~5000-9000) which contains active large offset (up to 0.5 s TWT) extensional faults dipping landward that deform the acoustic basement to the seafloor (Fig. 4.9). The offset along the primary faults affecting the middle shelf high increases with age reaching a maximum distance in the acoustic basement and sequences 1-2. Landward of the middle shelf high, a thick succession (> 4.0 s TWT) of compressionally deformed sediments of Late Cretaceous to Late Oligocene age is observed. The structures deforming the deep basin are not imaged well with these seismic data but a combination of folding and deep-rooted thrust faulting is inferred based on the observable morphologies. At the top of the deep basin, Late Oligocene sequences are tilted, dipping seaward and exposed at the seafloor and truncated by an

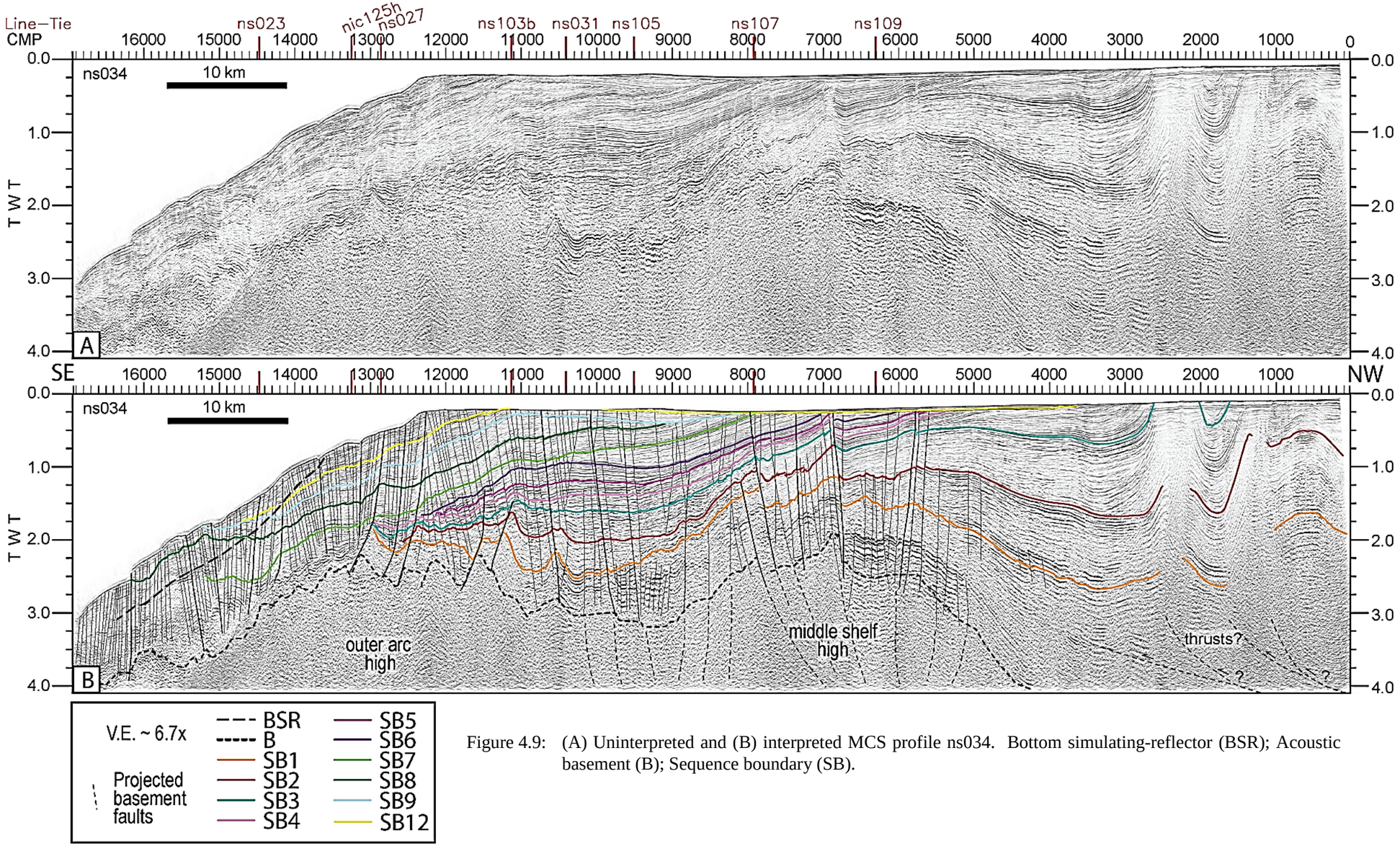

Figure 4.9: (A) Uninterpreted and (B) interpreted MCS profile ns034. Bottom simulating-reflector (BSR); Acoustic basement (B); Sequence boundary (SB).

angular unconformity (Fig.4.9). The angular unconformity in the northeast continues seaward to the southwest across the middle shelf high region. Continuing across the middle shelf high towards the outer shelf, several normal faults are observed with dips that converge toward the center of the relatively low basement region between the highs of the middle shelf and outer arc (CMP 9400) basement. Many of these extensional faults can be traced from the seafloor to near the basement. The normal faulting becomes more frequent beneath the outer shelf and the dominant dip direction of the faults in this region is landward. At the shelf edge, the dip direction switches orientation and the majority of faults beneath the slope are shown to dip trenchward.

Sequences 1-3 share similar morphologies on dip profiles in the Southern region (Fig. 4.9). The bulk of their deposition is northwest of the middle shelf high and each of these sequences decreases in thickness as they approach the middle shelf high, then prograde across a sub-basin toward the outer arc where they terminate before reaching the slope. Sequences 1 and 2 do not change thicknesses across the large offset fault at CMP 6800 but sequences 3 increases slightly (~0.2 s TWT) on the footwall.

Sequences 4-6 dip to the southeast beneath the middle shelf and are truncated at their landward limits by an angular unconformity. Above the middle shelf high, these sequences decrease in thickness and exhibit growth strata across the normal fault at CMP 6800. They are contained on the shelf and thickest where they downlap into the sub-basin between the middle shelf high and outer arc high.

Sequence 7 is truncated by the angular unconformity associated with SB12, while seaward sequence 8 is truncated by a younger angular unconformity associated with SB9. Sequence 7 downlaps SB8 across the outer shelf, thinning at the outer arc high, but continuing to deposit past the local basement high and down the heavily faulted slope. The preserved sequence 8 reflections prograde across the outer shelf with most of its

deposition beneath the slope. Reflections within sequence 9 toplap the SB9 angular unconformity beneath the outer shelf. The unit is progradational with oblique clinoforms at the paleo-shelf edge (CMP 11000). The mappable SB12 angular unconformity extends as far landward as CMP 3600 where it erodes a section of sequence 4. Sequence 12 is truncated at the outer shelf (CMP 9900-11100) in a region where horizontal reflections on the outer shelf become inclined reflections that dip trenchward and are located within a negative flower structure fault zone.

4.1.4 Nicoya Region

4.1.4.1 Line NS109

The Nicoya region of the Sandino basin includes an area where two distinct gravity anomalies extend offshore from northern Costa Rica (Fig. 4.1). On the strike profile ns109 (Fig. 4.10), the eastern edge of the gravity high projecting offshore from the Santa Elena peninsula correlates with a stark boundary at CMP 8700 between mappable sequences in the northwest and a transparent seismic facies to the southeast. This abrupt change in seismic character is inferred to be a right lateral strike-slip fault. Further to the southeast, the boundary between the gravity high trends projected from the Santa Elena and Nicoya peninsulas is not clearly indicated on the seismic data due to the low contrast between features in the transparent facies and further complicated by a data gap related to a marine mammal encounter. The upper boundary of the transparent seismic facies is a rough, high amplitude, low frequency reflection typical of the acoustic basement. This surface correlates with SB12 in the northwest, though it may represent a composite surface above the transparent seismic facies, and is overlain by Pleistocene sequences 13-16. Continuing to the northwest, SB12 truncates northwest dipping sequences 1-6 which

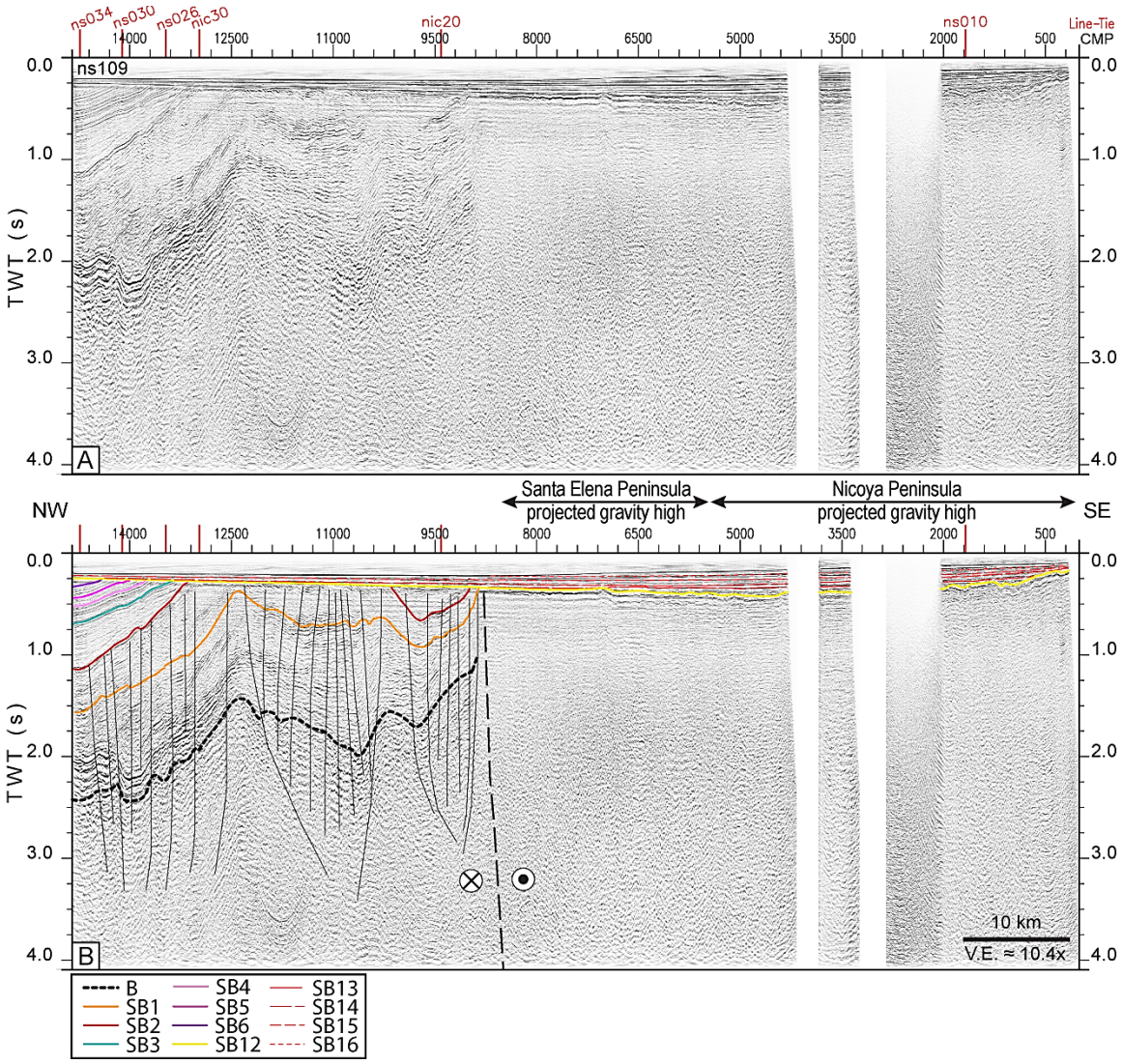

Figure 4.10: (A) Uninterpreted and (B) interpreted sections from MCS profile ns109. Acoustic basement (B); Sequence boundary (SB). Vertical exaggeration assumes a mean sonic velocity of 1800 m/s. This line intersects the offshore projections of gravity highs as observed on Fig. 4.1.

represent deposition from at least the Middle Eocene to the Late Oligocene. The acoustic basement, as well as sequences 1 and 2, is cut by several extensional faults that form negative flower structures.

4.1.4.2 Line NS010

In the dip direction, the Nicoya region is characterized by an elevated basement and lack of accommodation space beneath the middle and inner shelf (Fig. 4.11). The same transparent seismic facies capped by the rough, high amplitude reflection seen on line ns109 (Fig. 4.10), encompasses the first 25 km of the northeastern end of the profile. Beneath the outer shelf, the acoustic basement drops off sharply from ~0.5 s TWT at CMP 7800 to ~2.0 s TWT at CMP 6400 (~9 km horizontally, 1,350 m vertically). The basement descends at a more regular rate towards the trench after this initial drop off, finishing at a depth of ~3.8 s TWT for the remaining 40 km of the profile.

Sequence 1-5 represent deposition between the Late Cretaceous to Late Oligocene (orange and pink shading on Fig. 4.11) and appear chaotic to discontinuous and offset by numerous extensional faults that primarily dip trenchward. The larger offset faults affecting these sequences appear to be rooted in basement fault blocks. These sequences are concentrated at the outer shelf and upper slope. SB9 is an erosional unconformity preserved on the outer shelf and upper slope where underlying reflections terminate as toplaps. Reflections within this Late Oligocene to Early Pliocene interval (blue shading, Fig. 4.11) have a prograding wedge external form with a seismic facies that is discontinuous owing to the myriad extensional faults but reflections are less chaotic than the older units and can be traced more easily across faults. SB12 truncates underlying seaward dipping reflections of the Plio-Pleistocene beneath the outer shelf. The

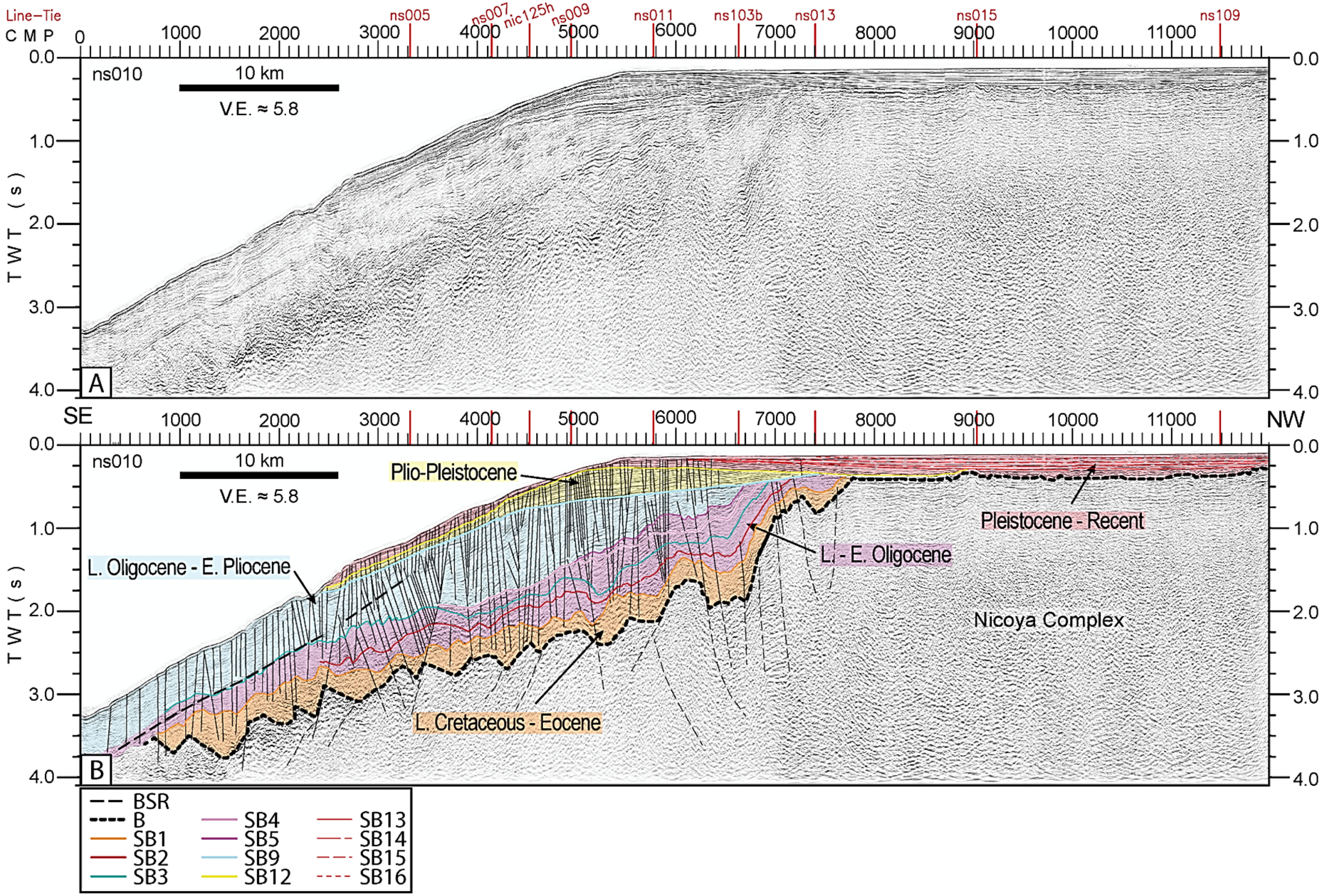
Line–Tie
CMP
ns005
ns007
nic125h
ns009
ns011
ns103b
ns013
ns015
ns109
ns010
10 km
V.E. ≈ 5.8
TWT (s)
A
SE
NW
Plio-Pleistocene
Pleistocene - Recent
L. - E. Oligocene
L. Oligocene - E. Pliocene
Nicoya Complex
L. Cretaceous - Eocene
B
BSR
B
SB1
SB2
SB3
SB4
SB5
SB9
SB12
SB13
SB14
SB15
SB16

composite sequence underlying SB12 exhibits sigmoidal clinoforms that prograde beyond the modern shelf break.

The Pleistocene to recent sequences (13-16) are contained mostly on the shelf overlying the rough basement unconformity though and truncate is also more orderly and continuous than the Late Oligocene and older sediments continuous also progrades, downlaps etc. making clinoforms. Sequences 13-16 are mostly contained on the shelf above the rough unconformity and onlap younger reflections at the shelf edge.

4.2 STRUCTURE AND ISOCHRON MAPS

4.2.1 The margin wedge and the acoustic basement of the offshore forearc

The margin wedge is defined here as the material between the top of the subducting Cocos plate and the top of the acoustic basement. The top of the Cocos slab was mapped on deeper penetration seismic profiles and a structure map was created in TWT to image this surface (Fig. 4.12A). On seismic reflection data, the Cocos slab shows a general shallowing trend to the southeast towards northern Costa Rica and the Nicoya peninsula.

A structure map was also created for the interpreted top of the acoustic basement (surface B) throughout survey region (Fig. 4.12B). Surface B represents the approximate top of the margin wedge and the depositional basement of the offshore Sandino basin (Fig. 4.12B). The structure map of the acoustic basement shows that the basement reaches its maximum depth in the northwest and shallows systematically to the southeast. The outer arc high is clearly visible as a shallow margin-parallel trend just landward of the trench. The trend of the middle shelf high diverges from the outer arc high in the Central region and projects towards the Santa Elena peninsula in the Southern and

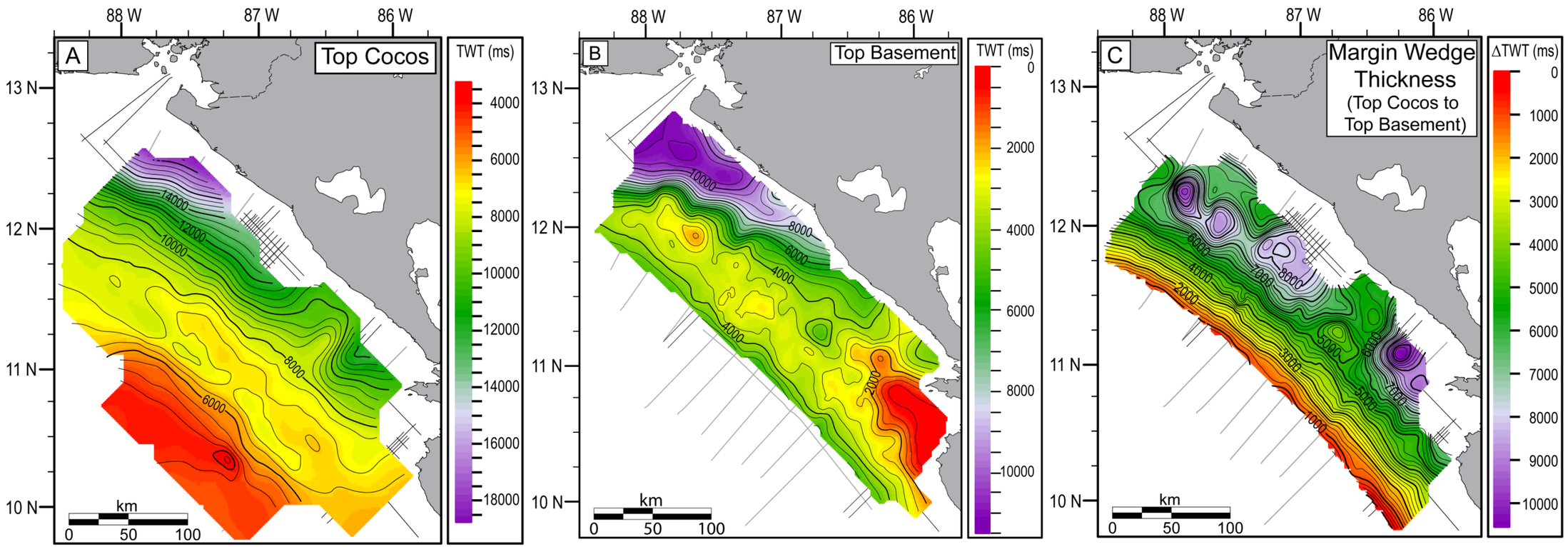

Figure 4.12: (A) Structure map of the mapped surface of the top of the Cocos slab. (B) Structure map of the top of the acoustic basement. (C) Isochron map of the margin wedge with time thickness determined from measuring from the top of the subducting Cocos slab to the acoustic basement of the upper plate (Note: Scales are not equal.)

Nicoya regions. The depth to the outer high forearc basement varies between ~2.0-3.0 s TWT in the central and northern regions of the Sandino basin.

An isochron map of the margin wedge was created by subtracting the TWT values for the structure grid of the top of the Cocos plate by the structure grid TWT values for the top of the acoustic basement (Fig. 4.12C). The thickness of the margin wedge beneath the slope increases updip uniformly along the margin and appears thickest landward of the outer arc high with an anomalously thin region (<6.0s TWT).

4.2.2 Late Cretaceous to early Late Oligocene structure and deposition

Structure and isochron maps for the oldest mapped sequence boundaries (SB1-SB3) and their underlying sequences (sequences 1-3) in this study are described together in this section due to their similar morphologies. The structure maps for sequence boundaries SB1-SB3and the isochron maps for their underlying sequences, sequences 1-3, share many general characteristics (Fig. 4.13A-F). In the Northern region of the Sandino basin, the structure maps for the sequence boundaries reveal the Corinto High at the outer shelf and a northwest- striking trough basinward measuring ~50 km wide along the middle and inner shelf. The trough shallows to the southeast in the Central region where local highs coinciding with folds observed on seismic profiles (Fig. 4.5 and Fig. 4.6) appear offset to the southwest. Other local highs located beneath the outer shelf of the Central region, are aligned NNE with the folds and roughly along strike with each other. Each of these structure maps displays a shallow ridge in the middle shelf area of the Southern region that correlates to the middle shelf high observed on seismic profiles (Fig. 4.9). SB1-3 reach their minimum depths north of the Nicoya peninsula in the Nicoya region where the sequence boundaries are observed to be truncated by erosional unconformities on seismic profiles (Fig. 4.10 and Fig. 4.11).

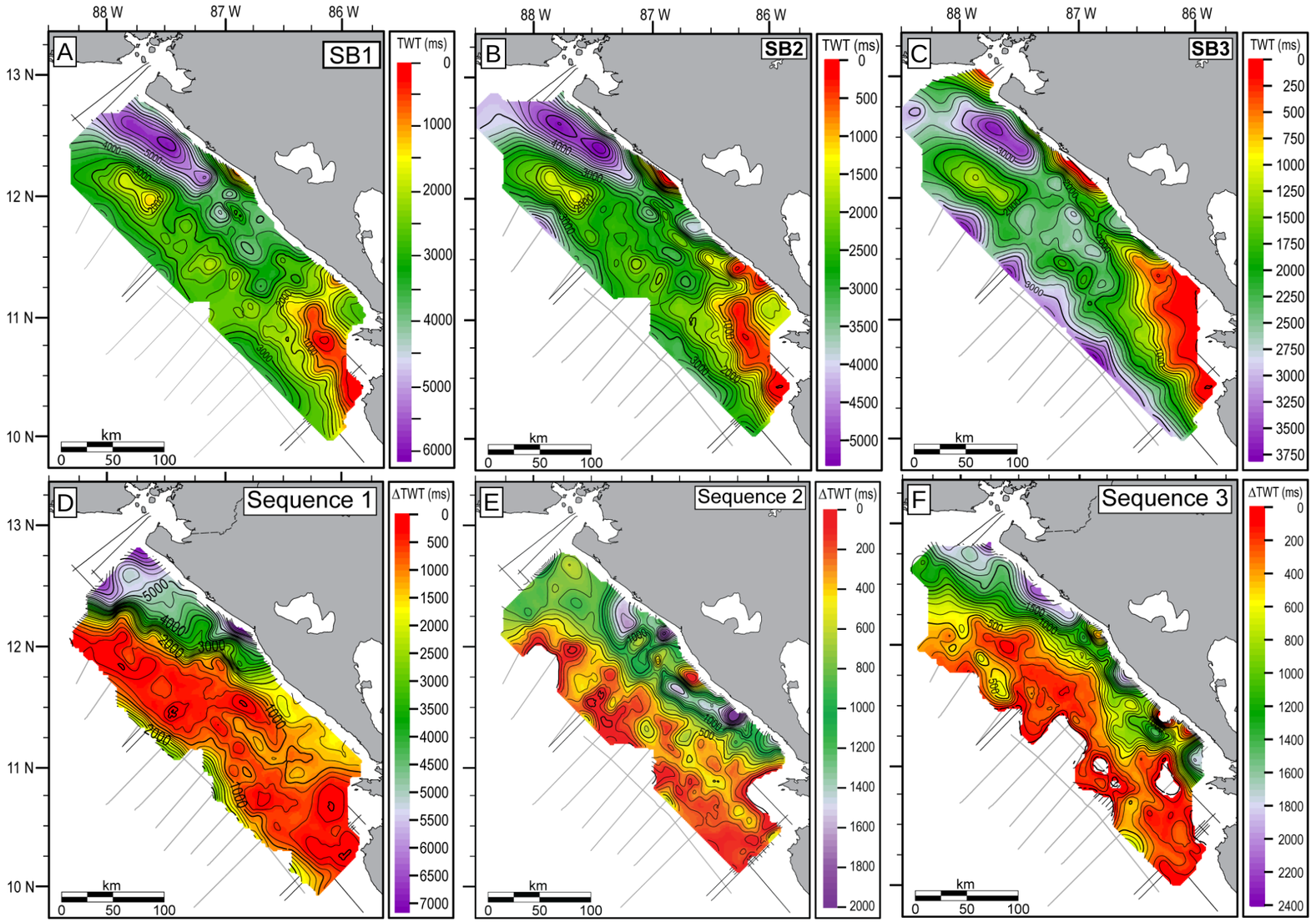

Figure 4.13: Late Cretaceous to early Late Oligocene sequences boundaries and sequences. Top row panels are structure maps for sequence boundaries SB1 (A), SB2 (B), and SB3 (C). Bottom row panels are isochron maps for sequence 1 (D), sequence 2 (E), and sequence 3 (F). Note that contours and color bar scales may vary for each map.

The isochron maps for sequences 1-3 (Fig. 4.13D-F) show that the primary depocenter for each sequence is landward of the outer arc high in the north and landward of the middle shelf high in from the Central to southern regions. Thickness decreases to the southeast for each sequence and very limited in much of the Nicoya region.

Deposition for sequence 1 is focused in the Northern region with a maximum thickness > 6.0 s TWT making it the thickest interpreted sequence in the basin (Figure 4.13D). The axis of the large depocenter of sequence 1 in the Northern region strikes sub-parallel to the margin and projects beneath the coast in the Central region. The sub-basin seaward of the middle shelf high of the Central region observed on seismic profiles (Fig. 4.9) is prominent on the sequence 1 isochron map (Fig. 4.13A).

The isochron map for sequence 2 shows a pattern of deposition that strikes northwesterly behind the middle shelf high (Fig. 4.13E). Several isolated areas of > 0.3 s TWT thick strata strike transverse to the margin across the middle shelf high and the outer arc high. The linear margin-parallel trend of the sub-basin southwest of the middle shelf in the Southern region is prominent here, as well.

A broad region extending landward of the basement highs in the Northern and Central regions (Fig. 4.13F) of < 0.5 s TWT thick strata is observed on the sequence 3 isochron map. In the Southern region, the depocenter extends farther southwest and across the middle shelf high than for the older sequences.

The isochron map, between the top of the Nicoya Complex and the top of sequence 3, shows a depositional trend subparallel to the modern trench (Fig. 4.14). The depocenter is located just landward of the outer arc high in the northwest and strikes ESE towards the coast. In the northwest of the basin, the combined thickness of both sequences, between the top of the Nicoya Complex basement and the top of sequence 3,

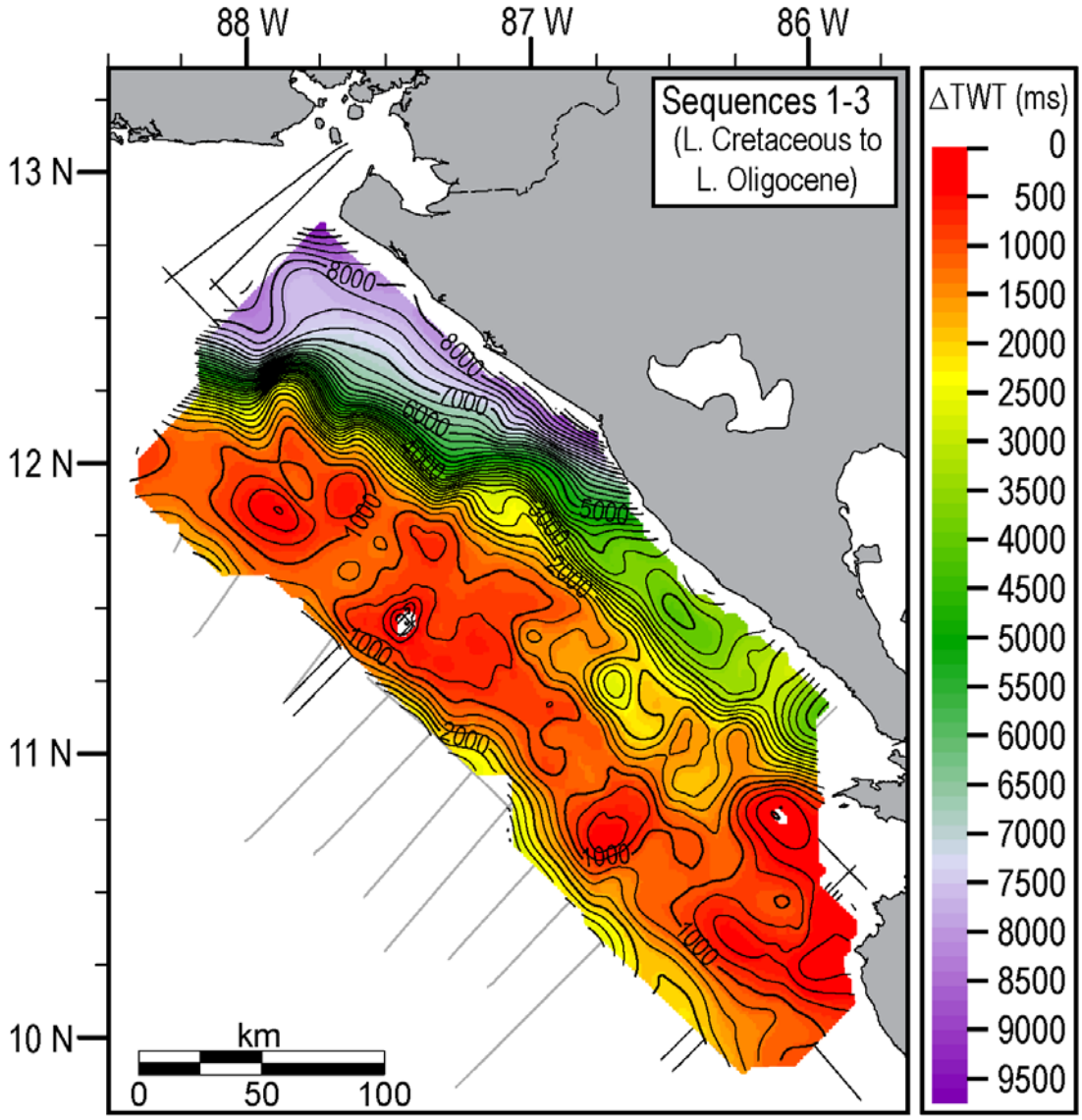

Figure 4.14: Late Cretaceous to early Late Oligocene deposition. The isochron map represents the total sediment thicknesses between the base of sequence 1 (B) to the top of sequence 3 (SB3).

exceeds 8.0 s TWT. The geometry of this primary offshore depocenter roughly follows the trend of the Top Nicoya structure (Fig. 4.12B).

4.2.3 Late Oligocene to Early Miocene structure and deposition

Sequence boundaries SB4-SB6 and deposition within sequences 4-6 are coeval with the latter Masachapa Formation from Late Oligocene to Early Miocene. The structure maps of SB4-SB6 (Fig. 4.15A-C) show that SB4 and SB6 are basinwide while SB5 is limited south of the Northern region. SB5 terminates to the north, and is observed onlapping the Corinto High (Fig. 4.4). With the exception of a more limited extent for SB5 in the northwest, the morphology of each sequence boundary within this succession is generally similar. The deep basin in the Northern region is apparent on both SB4 and SB6, as is the ridge of the Corinto High (Fig. 4.15). All three sequence boundaries rise rapidly in a parallel trend along the coast. A basin is observed in the Central region between the folded sediments of the inner shelf and the outer arc high. A second ridge on the outer arc, less elevated than the Corinto High, is also revealed directly trenchward of the deepest region of the Central region basin (Fig. 4.15). In the southern region a broad ridge coinciding with an anticline on line ns034 (Fig.4.9) has the same strike as the folds in the Central region but appears dextrally offset. Each of these sequence boundaries decrease in depth steadily to the south until reaching a depth of ~0.6 s TWT where the depth of the sequence boundaries flattens in the Southern and Nicoya regions where truncation is observed on seismic profiles (e.g. Fig. 4.10).

The isochrons show that the depocenter of sequence 4 is located along-strike beneath the inner shelf in the Northern region landward of the gravity high that corresponds to the Corinto High and the middle shelf high that are observed on the

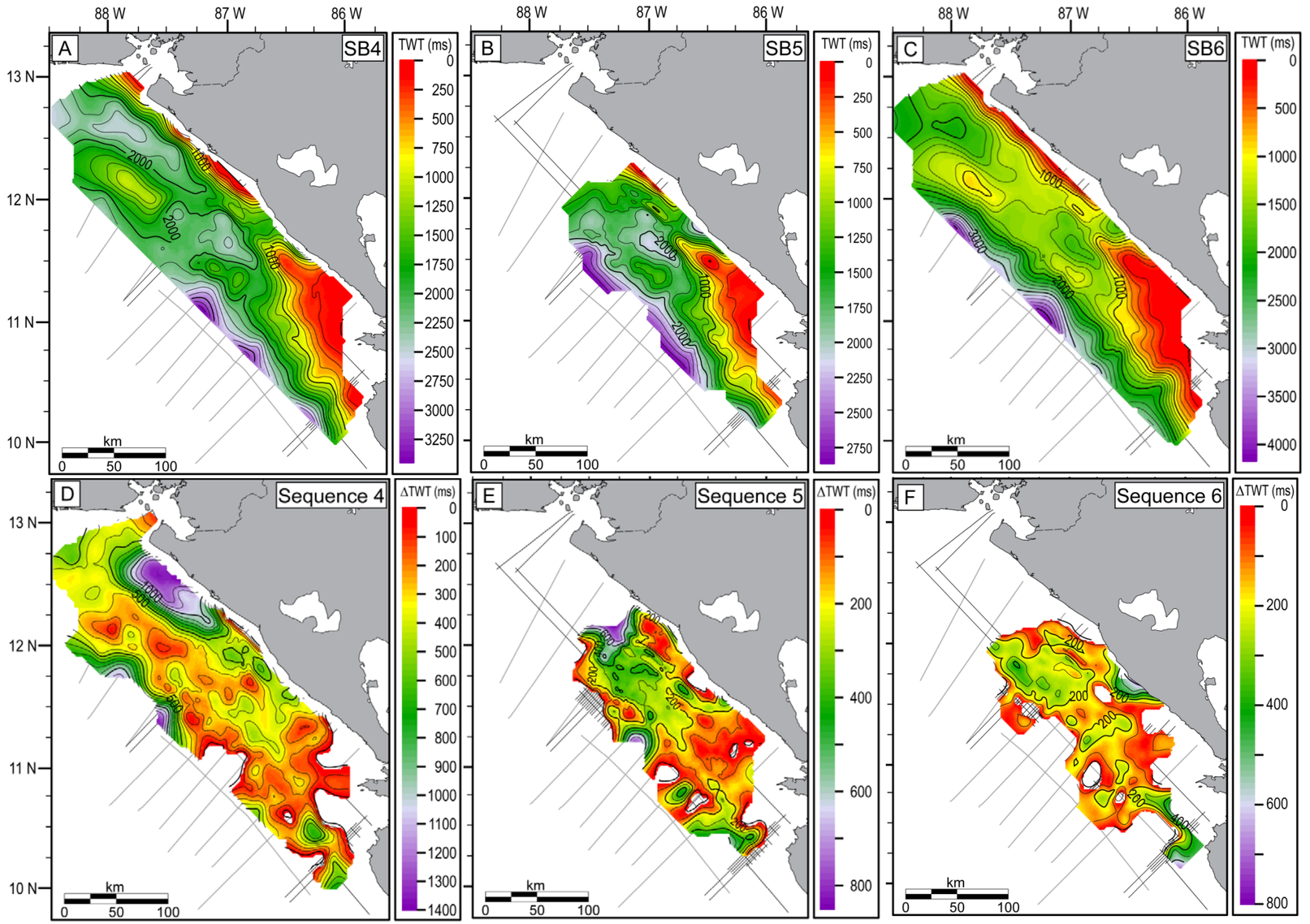

Figure 4.15: Late Oligocene to Early Miocene sequences and sequence boundaries. Top row panels are structure maps for sequence boundaries SB4 (A), SB5 (B), and SB6 (C). Bottom row panels are isochron maps for sequence 3 (D), sequence 4 (E), and sequence 5 (F). Note that contours and color bar scales vary for each map.

seismic profiles (Fig. 4.15D). Deposition of > 0.5 s TWT is observed beneath the slope in the Northern region of sequence 4 and the deposition in the outer arc sub-basin can be traced along the middle to outer shelf in the Central and Southern regions (Fig. 4.15D). Sequences 5 and 6 both show a distinct linear sub-basin in the outer arc region which connects southern depocenters beneath the outer shelf and slope to shelfal depocenters in the Central region. Within this Central region depocenter, sequences 5 and 6 display changes in thickness across the folds (Fig. 4.15E-F).

The isochron of the total deposition of sequences 4-6 (Fig. 4.16) reveals > 0.2 s TWT thick deposition in the narrow (~50 km wide) inner shelf basin of the Northern region which thins to the southwest across the Corinto High. A sharp transition is observed east of the Corinto High where thin sediments (< 0.3 s TWT) increase to ~ 1.0 s TWT thick in the span of ~20 km. The broad Central region depocenter is ~80 km wide and contains local structural highs with margin-parallel orientation. The outer arc sub-basin trends parallel to the trench east of the outer arc high.

4.2.4 Mid- to Late Miocene structure and deposition

The deposition of sequences 7 and 8 and the creation of SB7 and SB8 represent the Mid- to Late Miocene interval which is coincident with the El Fraile Formation. In general terms, the structure maps of SB7 and SB8 (Fig. 4.17A-B) do not depart significantly from the morphology of the structure maps for the Late Oligocene to Early Miocene sequence boundaries of the previous section (Fig.16A-C). The depression in the Northern region is diminished on the SB7 structure map (Fig. 4.17A) and indistinct on the SB8 map (Fig. 4.16B). A ridge appears on both maps at the Corinto High as does rapid shallowing along the nearshore area. A depression in the middle shelf of the Central region is observed to the north of a local high at the outer shelf in each structure

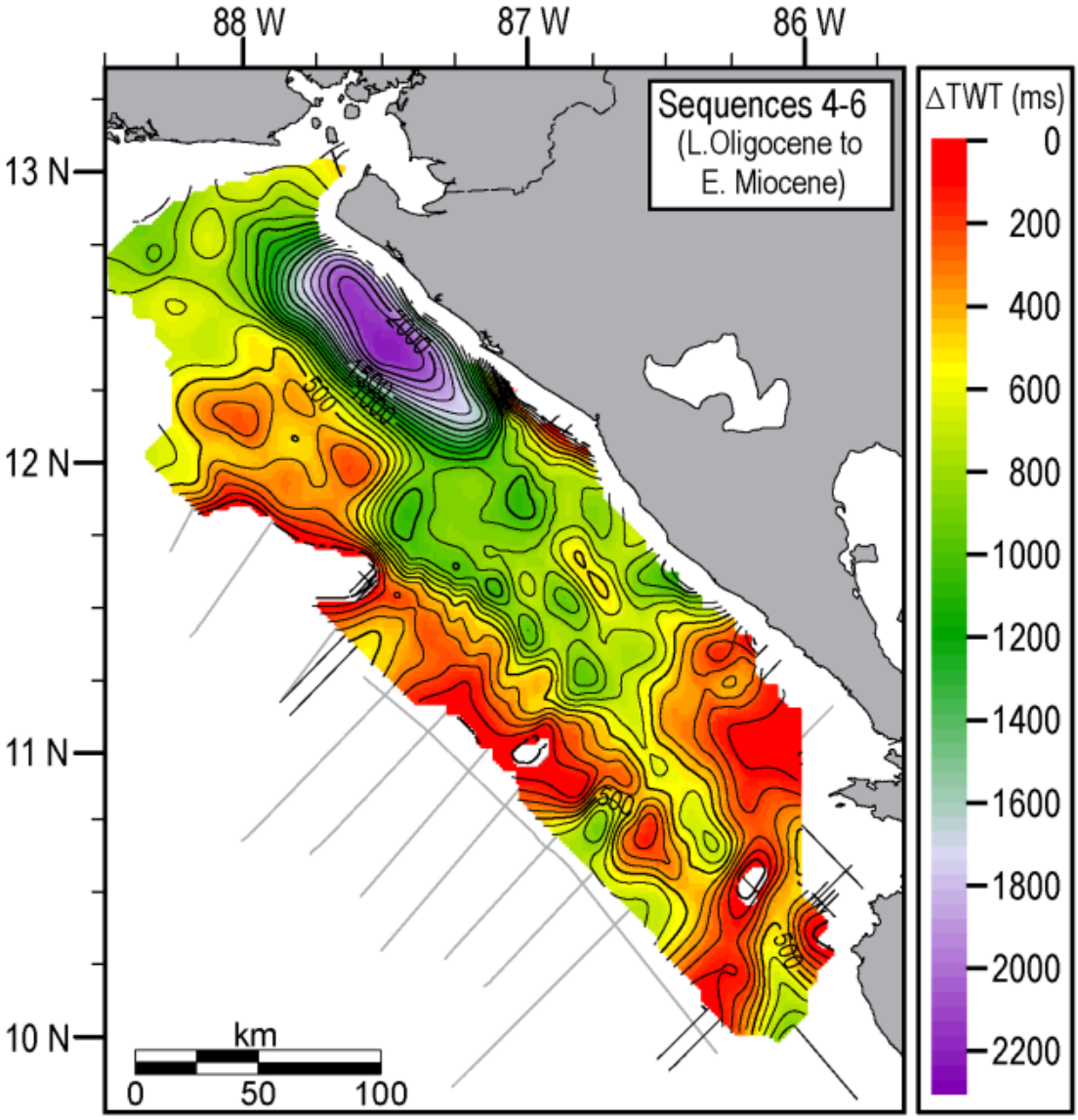

Figure 4.16: Late Oligocene to Early Miocene deposition. The isochron map represents the total sediment thicknesses between the base of sequence 4 (SB3) to the top of sequence 6 (SB6).

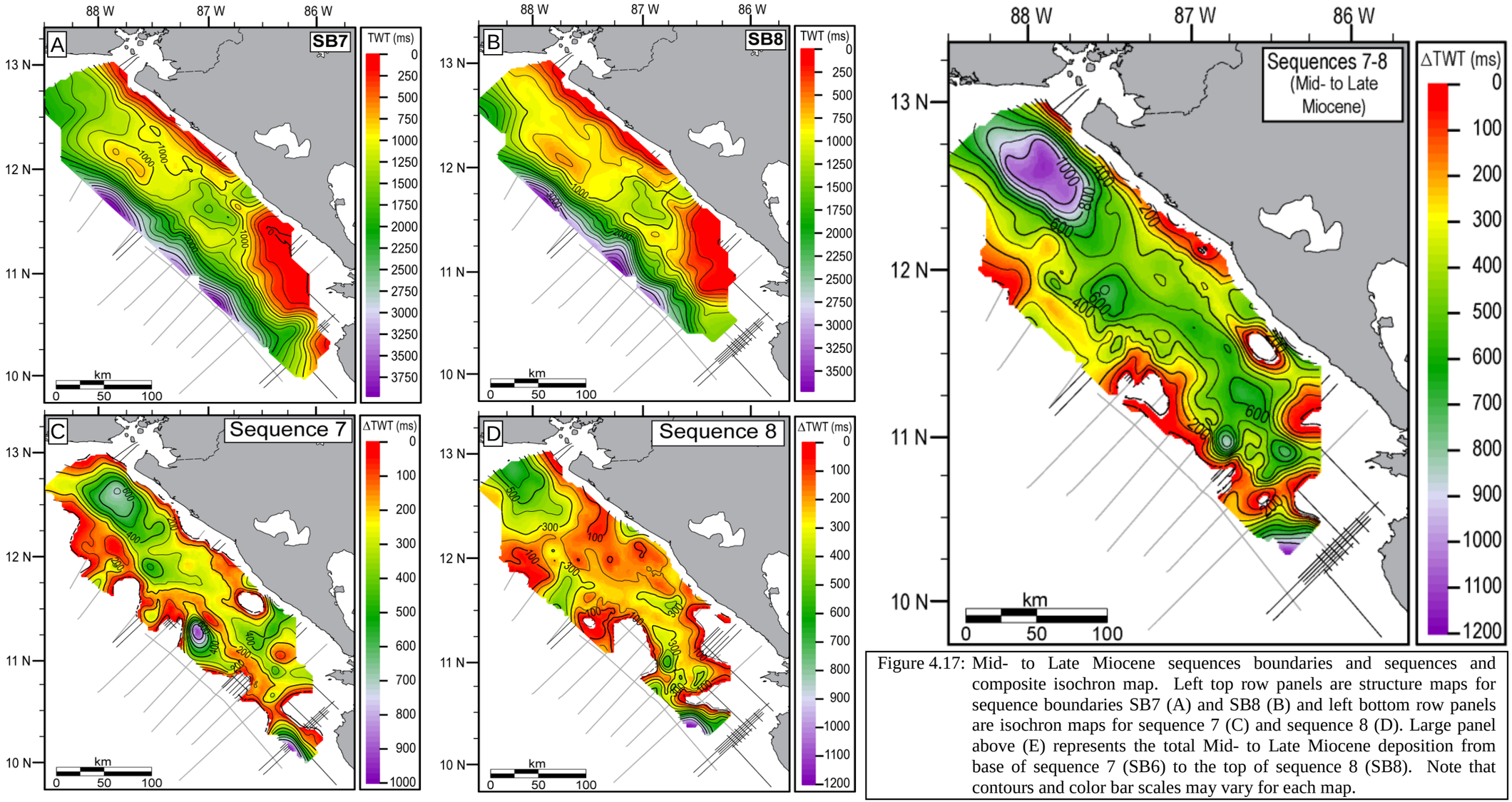

Figure 4.17: Mid- to Late Miocene sequences boundaries and sequences and composite isochron map. Left top row panels are structure maps for sequence boundaries SB7 (A) and SB8 (B) and left bottom row panels are isochron maps for sequence 7 (C) and sequence 8 (D). Large panel above (E) represents the total Mid- to Late Miocene deposition from base of sequence 7 (SB6) to the top of sequence 8 (SB8). Note that contours and color bar scales may vary for each map.

map and the two sequence boundaries decrease in depth along the shelf in the Southern region in an area mapped beneath the shelf along the entire margin. The isochron map for sequence 7 displays a depocenter to the north and east of the Corinto High (Fig. 17C). The depocenter in the Central region is connected by southeast-striking outer arc sub-basin to a northeast-striking zone of preserved deposition in the Southern region. Deposition for sequence 8 is predominantly in the northern basin and beneath the outer shelf and slope (Fig. 4.17D). On the slope, isolated lobe-shaped patterns of deposition are observed for both sequences. Lobes observed on the slope in the Central and Northern regions of sequence 7 become areas of low accumulation in sequence 8. Similarly, zones of low accumulation on the slope for sequence 7 transition to lobe-shaped deposition in sequence 8.

The composite isochron for sequences 7 and 8 reveals the thickest deposition to be in the Northern region and a depocenter that is parallel to the margin with much of the preserved deposition of the Central and Southern region occurring beneath the middle shelf (Fig. 4.17E). Trends in thickness appear to be offset along a roughly N-S boundary between the Central and Southern regions.

4.2.5 Pliocene to Early Pleistocene structure and deposition

The structure maps for sequence boundaries SB9-SB12 (Fig. 4.18A-D), individual isochron maps for the sequences 9-12 (Fig. 4.18E-H), and a composite isochron map of the total thickness of sequences 9-12 (Fig. 4.19) are presented in this section. These sequences and sequence boundaries are approximately coeval with the deposition of the El Salto Formation.

The structure maps of the sequence boundaries for each of the four sequence boundaries display a shallow basin in the Central region and a decrease in depth to the

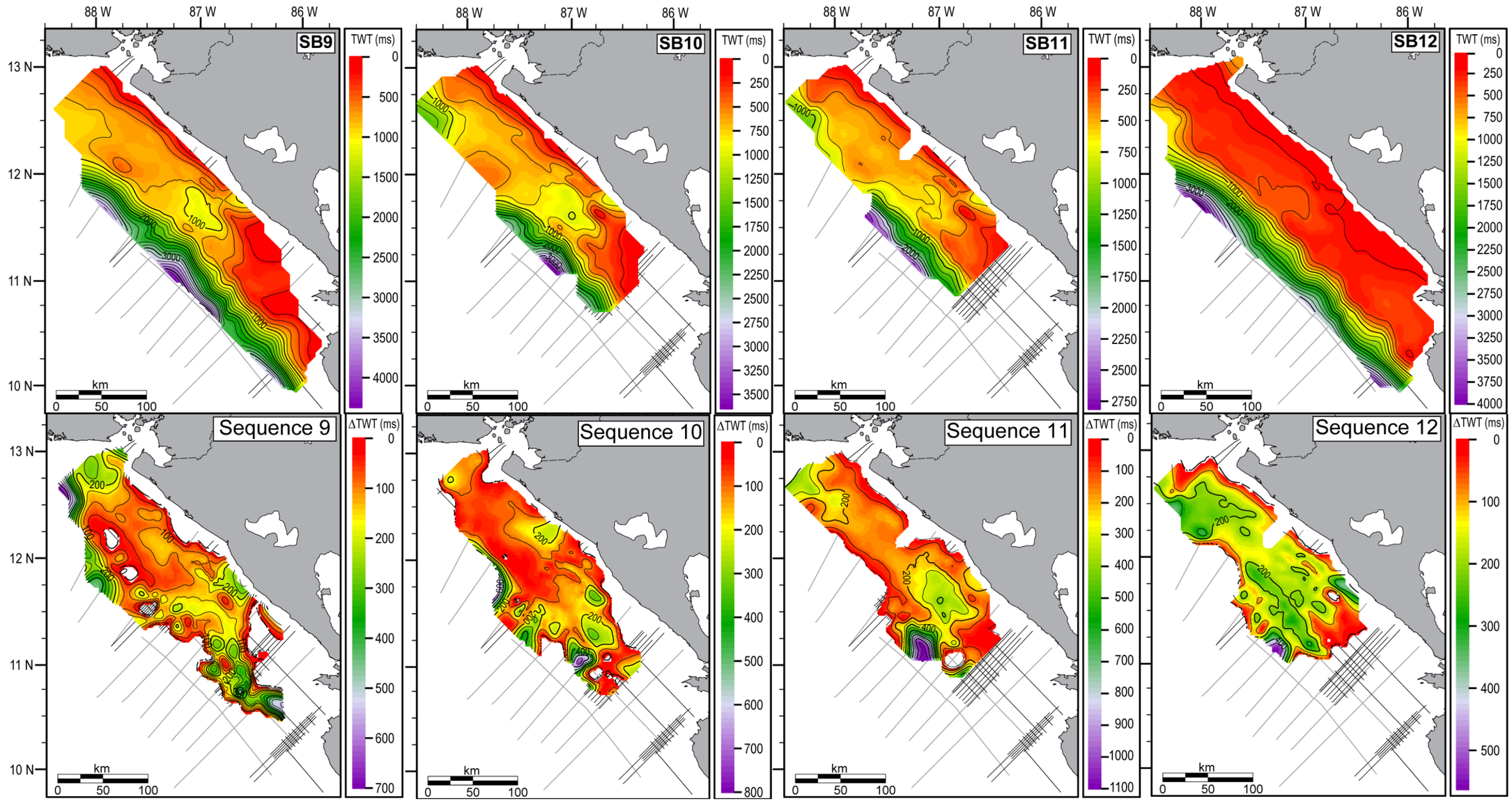

Figure 4.18: Pliocene to Early Pleistocene sequences and sequence boundaries. Top row panels are structure maps for sequence boundaries SB9 (A), SB10 (B), SB11 (C), and SB12 (D). Bottom row panels are isochron maps for sequence 93 (E), sequence 10 (F), and sequence 11 (G), and sequence 12 (H). Note that contours and color bar scales may vary for each map.

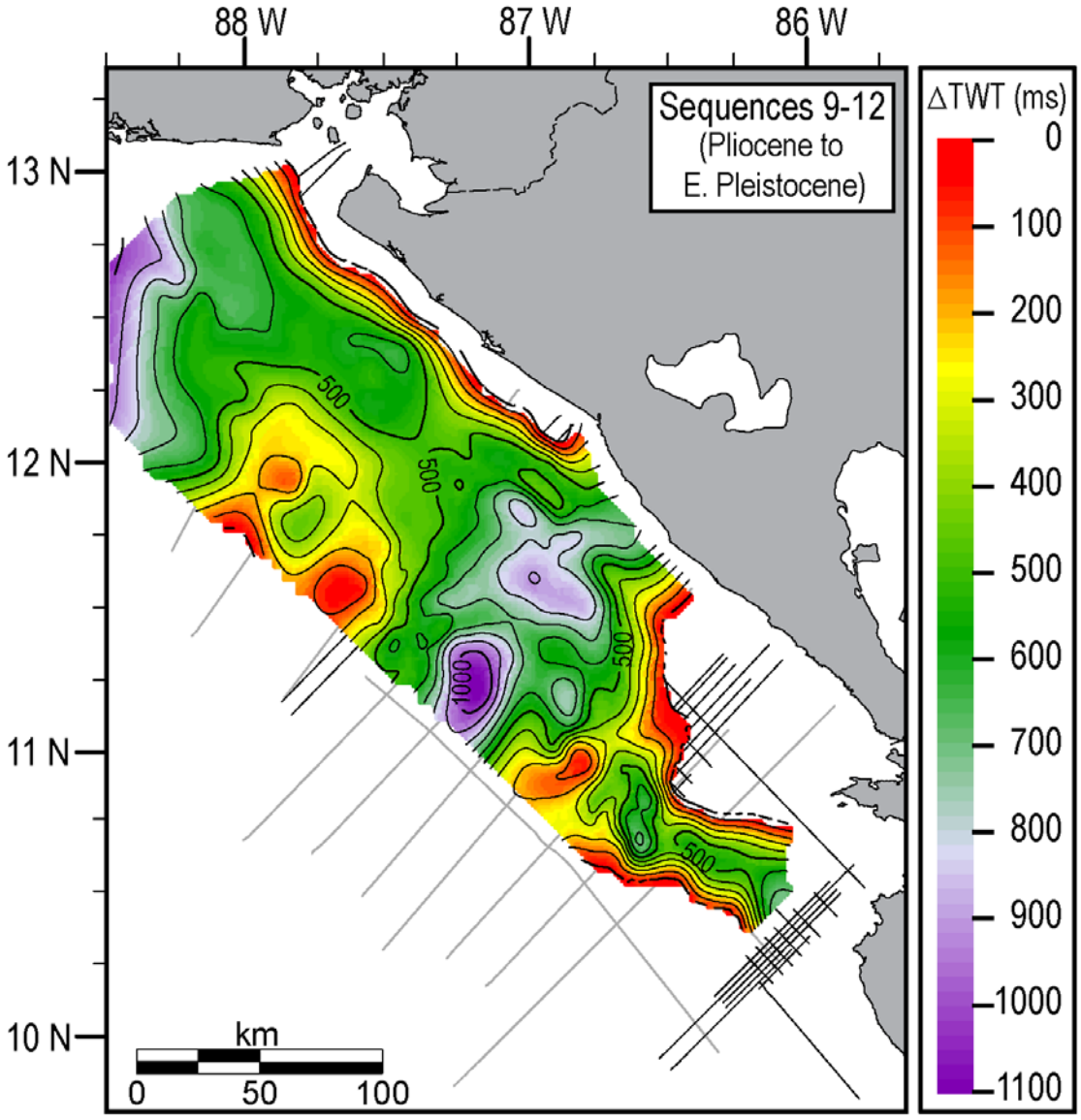

Figure 4.19: Pliocene to Early Pleistocene deposition. The isochron map represents the total sediment thicknesses between the base of sequence 9 (SB8) to the top of sequence 12 (SB12).

southeast (Fig. 4.18A-D). SB9 and SB12 are mapped on the majority of the slope whereas SB10 and SB11 do not cross the shelf break in the Northern region seaward of the Corinto High. The folds of the Central region are observed to be discontinuous, with folds in the south offset to the west from analogous folds in the north.

The isochron maps for each of the individual sequences reveal depocenters in the Central and Northern regions. The Central region depocenter develops in the same region as the basin observed on structure maps. The isochron map for sequence 9 (Fig. 4.18E) shows relatively high deposition in the south beneath the outer shelf which corresponds to prograding outer shelf clinoforms identified on seismic profiles (Fig. 4.9 and Fig. 4.11). The map for sequence 10 (Fig. 4.18F) shows a lobe-shaped depositional feature beneath the inner shelf of the Northern region. The sequence 11 isochron reveals the return of a depocenter in the Northern region after a hiatus in sequence 10 but landward of the Corinto High, deposition is thin across the shelf. The sequence is thickest beneath the slope and shelf of the Central region (Fig. 4.18G). Sequence 12 displays distinct margin-parallel trends of deposition across the shelf. The linear trend of accumulation on the outer shelf correlates with prograding clinoforms wedges observed on seismic profiles (Fig. 4.5 and Fig.4.6). Landward, the linear trends of the inner shelf are located within the folded region of the basin where truncation is observed on the crests of anticlines and small basins develop between them.

The main depocenter for the combined sequences 9-12 is beneath the shelf and slope of the Central region with a secondary depocenter in the Northern region (Fig. 4.19). Significant stratigraphic thickness is related to the clinoforms in the south as well. The Shelf of the Southern region shows either no accumulation or no preservation of strata and the Corinto High region continues to show relatively thin deposition.

4.2.6 Pleistocene to Recent structure and deposition

The most recent sequence boundaries (SB13-SB16) and sequences (13-16) are inferred to be from the Pleistocene to recent and their structure maps (Fig. 4.20A-D) are presented in this section along with a composite isochron of their combined (Fig. 4.20E). Each of the individual structure maps are relatively low relief and featureless (Fig. 4.20A-D). A shallow basin beneath the shelf in the Central region, in the same location as structure maps of older sequence boundaries (e.g. Fig. 4.19A-D) is apparent on each of the four structure maps. SB13 and SB16 are truncated in the Southern region but were able to be correlated with analogous reflections in the Nicoya region. The isochron map showing the total thickness of all sediments above the base of Sequence 13 shows depocenters on the shelf for the Northern, Central, and Nicoya regions. Deposition in the Southern region is limited to the outer shelf. The depocenter in the Nicoya region is associated with an incised valley that is observed on seismic profiles.

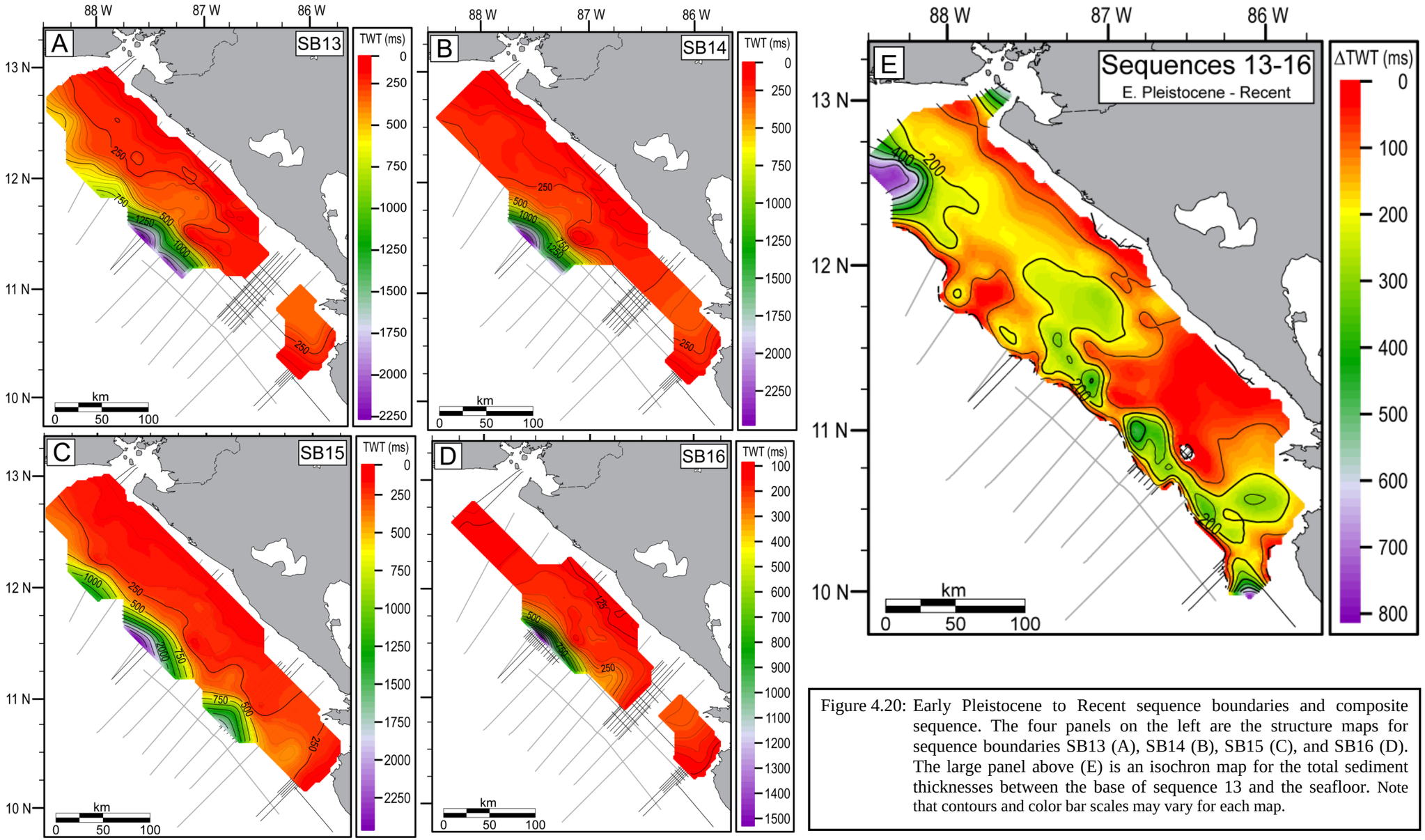

Figure 4.20: Early Pleistocene to Recent sequence boundaries and composite sequence. The four panels on the left are the structure maps for sequence boundaries SB13 (A), SB14 (B), SB15 (C), and SB16 (D). The large panel above (E) is an isochron map for the total sediment thicknesses between the base of sequence 13 and the seafloor. Note that contours and color bar scales may vary for each map.

Chapter 5: Tectonostratigraphic Evolution of the Offshore Sandino Forearc Basin Based on Regional Interpretation of 2D Multi-Channel Seismic Reflection Data

5.1 STAGE 1: LATE CRETACEOUS TO EARLY EOCENE

5.1.1 Incipient forearc basement structure

The structure of the acoustic basement shows a 25 km wide outer arc high in the Northern region (Fig. 4.12B) which correlates to the Corinto High gravity anomaly (Fig. 4.1). While the gravity high projects towards the middle shelf (Fig. 4.1), the outer arc high on the acoustic basement bifurcates southward into a trench-parallel outer-arc high trend and a middle-shelf high trend (Fig. 4.12B) that seismic profiles show to be distinct features (Fig. 4.5, Fig. 4.6, and Fig. 4.9). When these two basement high trends are compared to the isochron of sequence 1 (Fig. 4.13D), the main depocenter is bounded by the eastern basement trend so that the southwestern boundary of the depocenter is at the Corinto High and its continuation along the middle shelf high. Based on this evidence, I propose that the nascent outer arc high of the Sandino basin is the basement high that follows this Corinto High to middle shelf high trend with the seaward portion representing the early slope. This configuration is consistent with the proposed island arc origin of the Late Cretaceous forearc basement running continuously from the Santa Elena peninsula to at least as far north as Guatemala (Geldmacher et al., 2008; Kominz et al., 2008) and resulting from island arc accretion and the reversal of subduction direction from southwest to northeast at the western margin of the Chortis block (Fig. 2.1A; (Mann, 2007). In the southern and Nicoya regions, ophiolitic accretionary slices of the Nicoya complex were emplaced beneath the island arc material contemporaneously with the basement material that outcrops at the Nicoya Peninsula sometime soon after the

island arc terrane was accreted. Since the Nicoya Complex is not found beneath the toe of the slope in Guatemala (Geldmacher et al., 2008), whereas depleted tholeiites similar to the Santa Elena Complex are, the northern geographic extent of the Nicoya Complex is likely constrained to within the Sandino basin region. Based on observations from MCS data, the Nicoya Complex terrane is thought to reach at least as far north as line nic50 but may possibly extend beneath the Corinto High in the Northern region.

5.1.2 Late Cretaceous to Early Eocene deposition

Although a direct age correlation with well-ties to the MCS data is not possible for the deepest seismic horizons (Fig. 3.7), seaward dipping beds of the Brito Formation outcrop onshore in southern Nicaragua (Fig. 2.2) (McBirney and Williams, 1965; Weyl, 1980 *and references therein*) coincident with the projected trend of folded sequence 1 strata imaged on the dip-oriented seismic profiles that extend nearest to the coast in the Southern region (Fig. 4.9). The reflections of sequence 1 overlying basement in the deep basin are characterized by continuous to divergent seismic facies and confined to the northeast of the paleo-outer arc high, (Fig. 4.12). These reflections are imaged infilling the deep basin while onlapping the northeast flank of the acoustic basement beneath the middle shelf (Fig. 4.3 and Fig. 4.9). These units are interpreted as turbidites deposited in an underfilled, submerged ridge forearc basin (*sensu* Dickinson, 1995) which experienced uplift at the outer arc and subsidence in the forearc as a result of the newly formed subduction zone (Fig. 5.1A). The presence of thick, continuous, and relatively undeformed reflections of lower sequence 1 in the Northern region (Fig. 4.3) and the correlative thick units in the Central (Fig. 4.5, 4.6) and Southern regions (Fig. 4.9), which precede deformation, indicate that during this stage the forearc was likely dominated by subsidence as a result of sediment loading from clastic and volcanic material entering the

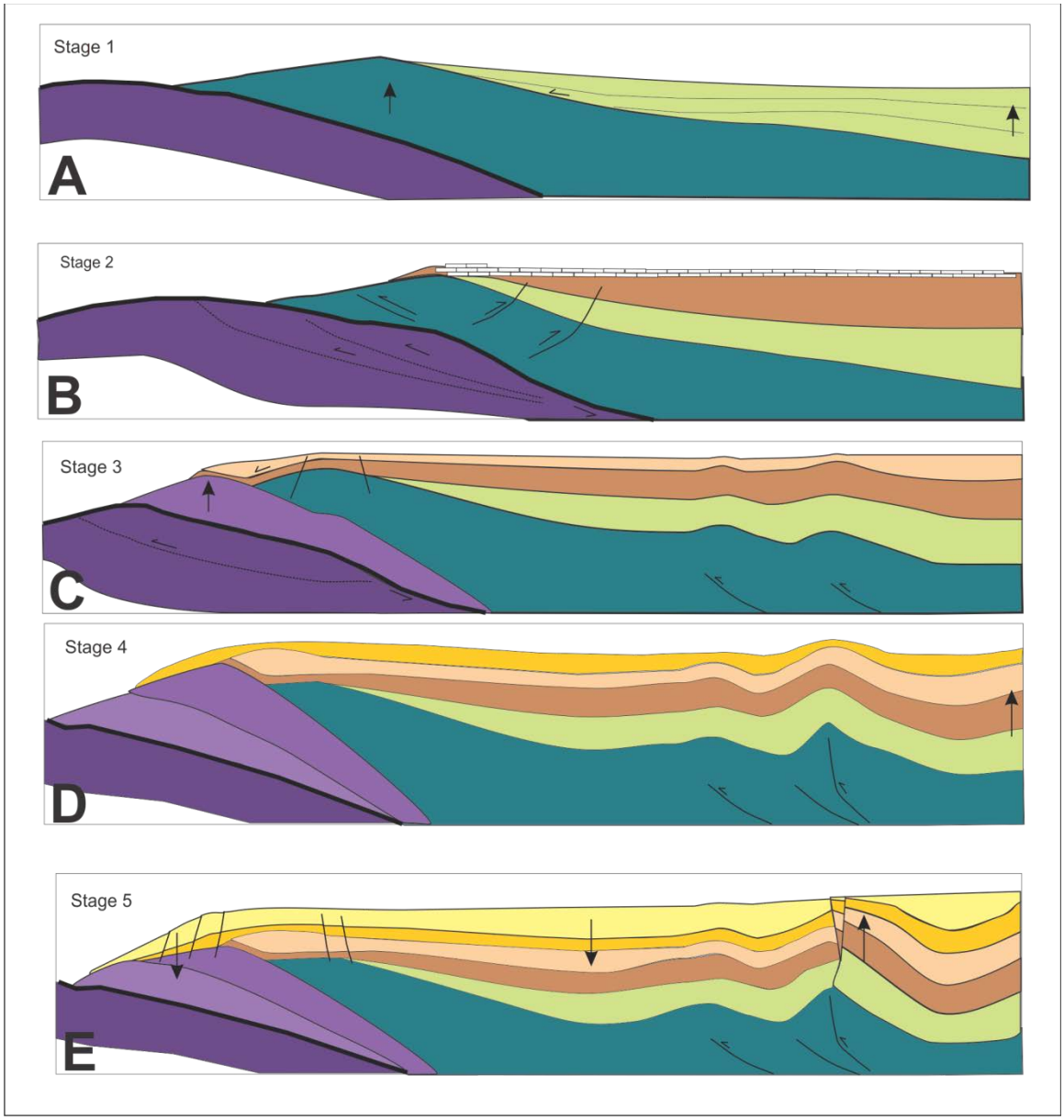

Fig. 5.1

Figure 5.1 Cartoon depicting the generalized tectonic and depositional evolution of the Sandino basin. (A) Stage 1 represents the configuration of the forearc basin at the following subduction initiation. (B) Stage 2 of the forearc development features collision with and delamination of an allochthonous terrane resulting in uplift of the outer arc and forearc basin facilitating deposition of shallow water carbonates. (C) Stage 3 shows basal accretion of the delaminated subducting terrane and involves (continued?) collision and accretion of bathymetric highs on the subducting ocean crust. The outer arc sub-basin develops as a piggy-back basin between the original forearc basement and the newly accreted material. The compressional strain begins to manifest as fault propagation folds in the deep basin. (D) Stage 4 displays trench retreat (i.e. slab roll back as the result of further basal accretion of the subducting plate. Coastal flexure initiates likely as a result of the volcanic front migrating trenchward. (E) Stage 5 shows subsidence occurring beneath the outer arc and middle shelf and local uplift at the fault propagation folds in the forearc basin accompanied by an influx of sediment. See text for further details. (No scale intended.)

basin. Subsidence was potentially enhanced by synclinal downwarping driven by horizontal tectonic stresses that were also related to subduction. The submerged ridge configuration is interpreted to have persisted along the entire study area throughout the Late Cretaceous to Late Eocene.

5.2 STAGE 2: MID-EOCENE TO EARLY LATE OLIGOCENE

Following the previous stage of prolonged structural stability, the second stage of forearc development involves key tectonic and depositional changes. Although the main depocenter remains in the trough landward of the middle shelf high, the rate of deposition outpaces the subsidence-driven rate of accommodation and sequences prograde across the middle shelf and outer arc highs allowing deposition to begin at the outer arc sub-basin (Fig. 4.3, Fig. 4.5, and Fig. 4.9). The hummocky high amplitude reflection of SB1 at the middle shelf high (Fig. 4.5 and Fig. 4.6) is characteristic of a carbonate facies in seismic reflection data, and is tied to the Corvina-2 where it intersects limestone lithology of the Brito Formation (Fig. 3.7). Above the outer arc high, the semi-transparent seismic facies of the lower strata found within the rotated fault blocks beneath the upper and middle slope is also characteristic of carbonate deposition. According to plate reconstructions (Mann, 2007) (Fig. 2.1), the Sandino basin was subtropical during the Eocene (~15° N) and a significant long-term decrease in sea-level occurs during the Mid-Eocene (Miller et al., 2005). Considering these factors, the upper sequence 1 is interpreted to have developed within a shoaling shelf with water depths eventually decreasing to the photic zone thereby allowing development of a carbonate platform on the middle to outer shelf with local patch reefs above both the outer arc and middle shelf basement highs. Carbonate-dominated deposition continued into the Oligocene with the primary depocenter during the Late Eocene to Late Oligocene sequences 2 and 3 located within

the trough of the deep basin landward of the combined Corinto High and middle shelf high trend (Fig. 4.13E and F). Sequence 2 features small (>25 km wide) lobe-shaped depocenters trenchward of the middle shelf basement high which are interpreted as slope fans that were in part due to a forced regression during the eustatic fall of the Eocene-Oligocene transition (Miller et al., 2005).

The shallowing of the slope and outer shelf is likely to have been affected by tectonism because multiple episodes of uplift are observed during this stage. Uplift in the Late Eocene is recorded at the middle shelf high in the Central region by the prekinematic sequence 1 strata that have been tilted landward with reflections dipping to the northeast and are subsequently onlapped by reflections of sequence 2 (Fig. 4.6; CMP 8800-10500). The middle shelf high in the Southern region was uplifted during this stage producing fault-controlled channel incisions with northwest strike (Fig. 4.9; CMP 7000-8000). Uplift at the outer arc during Early to Late Oligocene is clearly documented along-strike at the Corinto High (Fig. 4.4) where sequences 2 and 3 onlap the antiform from the southeast and SB3 truncates sequences 1-3 as a subaerial angular unconformity (CMP 11000) (Fig. 4.4). SB3 is expressed throughout the Sandino basin as an angular unconformity and is interpreted to be driven primarily by vertical tectonism during this stage. Early to Late Oligocene compression is documented by southwest-directed fold and thrust features which are found above the outer arc basement high in the Southern (Fig. 4.9) and Central regions (Fig. 4.6).

The cause of uplift during this stage is interpreted as accretion and underplating of allochthonous terrane, possibly an oceanic plateau (Walther et al., 2000), that originated from the subducting Farallon plate (Fig. 5.1B). Similar uplift that began in the latest

Oligocene has been observed in outcrop to the southeast in Costa Rica (Lundberg, 1982; Seyfried et al., 1991).

5.3 STAGE 3: LATEST OLIGOCENE TO EARLY MIOCENE

Deposition in the Latest Oligocene was strongly affected by the accretionary episodes of the previous stage. Following the major uplift and unconformity of SB3, the seismic facies shift abruptly to continuous and variable amplitude reflections (Fig. 4.5 and 4.6) signaling a general cessation of carbonate production. This was likely due to increased clastic input across the shelf as accommodation in the deep forearc basin decreased. Subsidence and nearshore flexure as a result of the major accretionary event beneath the Corinto High can be seen affecting the composite depocenter of sequences 4-6 (Fig. 4.16) in the Northern region which is narrower and shifted slightly landward from that of the previous stage. The uplift near the present coastline is demonstrated to have initiated after the major unconformity of SB3 and during the Late Oligocene sequence 4 by the landward thinning of this sequence observed on dip profiles (Fig. 4.2, 4.3, and 4.4). The amount of uplift beneath the modern nearshore increases to the southeast which created a more evenly distributed depocenter in the Central region (Fig. 4.16). Folding of the deep basin within the Central and Southern regions is initiated during this stage and is clearly shown on the isochron maps of sequences 5 and 6 to have affected deposition (Fig. 4.13E and F). Folding of the middle to inner shelf and nearshore uplift during this period may be a result of the transition to a superfast seafloor spreading rate in the Early Miocene (Wilson, 1996). The thin to absent deposition of the inner shelf in the Southern and Nicoya regions is a result of pronounced shortening and uplift during this stage and is expressed as onlapping sequences pinching out on strike lines approaching the southeast (Fig. 4.7). Uplift in the Southern region is shown on strike lines. Beneath the outer shelf

and slope, this stage marks a transition from a compressional to extensional stress regime as a result of portions of the accreted terrane being further subducted. The trench-parallel outer arc sub-basin (Fig. 5.1C) experienced subsidence during previous collisional events, behaving as a piggy-back basin, and during this stage was infilled as the continued uplift nearshore provided an influx of sediment that was able to reach the outer shelf and slope (Fig. 4.4, 4.5, and 4.9).

5.4 STAGE 4: MID-MIOCENE TO LATE MIOCENE

During this stage, the effect of tectonism on deposition in the Sandino basin varies dramatically along-strike. Tectonism in the Northern region was expressed entirely as subsidence as the deep basin continued to subside at a rate that was now nearly equal to that of sedimentation. The Central region is a zone of transition where both extensional and compressional horizontal stresses were at work. Beneath the middle to inner shelf in the Central region, the offshore region underwent shortening as folding of the deep basin and uplift of the nearshore continued (Fig. 4.5 and 4.6). Seaward of the folding, the northern Central region underwent steady subsidence during this stage (Fig. 4.5) while the southern Central region experienced an initial episode of rapid uplift at the outer arc, inverting the sub-basin infilled during the previous stage, before relenting to an extensional phase developing growth strata at a major landward dipping fault beneath the outer shelf (Fig. 4.6),

The initial uplift at the outer arc during this stage is likely related to a later stage collision with a subducting allochthonous terrane which shifted the outer arc vertically as it passed underneath (Fig. 5.1D). Another possibility is that the localized uplift, which appears to have begun during the Early Miocene, was an effect of the super-fast Miocene spreading rate that occurred from 19-10 Ma (Wilson, 1996). However, it is unclear why

this would not be expressed more regionally. The extensional phase at the outer arc high is interpreted to result from trench retreat (i.e. slab rollback) subsequent to terrane accretion. In the Southern region, and presumably in the Nicoya region as well, the middle shelf to nearshore have experienced an extreme amount of uplift since the Late Oligocene exhuming and eroding the majority of the Neogene record. Uplift in the Southern region during this stage provided sediment for the southeastern part of the depocenter for the Mid- to Late Miocene sequence 5 (Fig. 4.15E). The degree of uplift experienced in the Southern region during this stage was likely related to the proximity to the thickened Cocos plate subducting to the south along the MAT which may have featured the Panama Fracture Zone (PFZ) ~9 Ma off the coast of the present-day Nicoya Peninsula (McIntosh et al., 1993) (Fig. 5.2).

A eustatic fall in the Mid-Miocene resulted in a forced regression during deposition of sequence 7 which is supported by the angular unconformity of SB7 nearshore (Fig. 4.2) and the lobe-shaped slope fans that developed on the slope (Fig. 4.15A). Fans also develop around the exhumed middle shelf of the Southern region (Fig. 4.15D).

5.5 STAGE 5: PLIOCENE TO RECENT

During the Plio-Pleistocene, the offshore Sandino basin begins its current tectonic stage which is characterized by regional subsidence beneath the middle to outer shelf as a result of E-W extension and local uplift at the folded sediments of the forearc basin (Fig. 5.1E). The localized uplift of anticlines in the Central region may be a product of northwesterly forearc sliver transport. The composite isochron for sequences 9-12 (Fig. 4.19) reveals a depocenter in the Central region that is interpreted to be bounded by a pair of right-lateral strike-slip faults that strike roughly NNE-SSW and can be seen offsetting

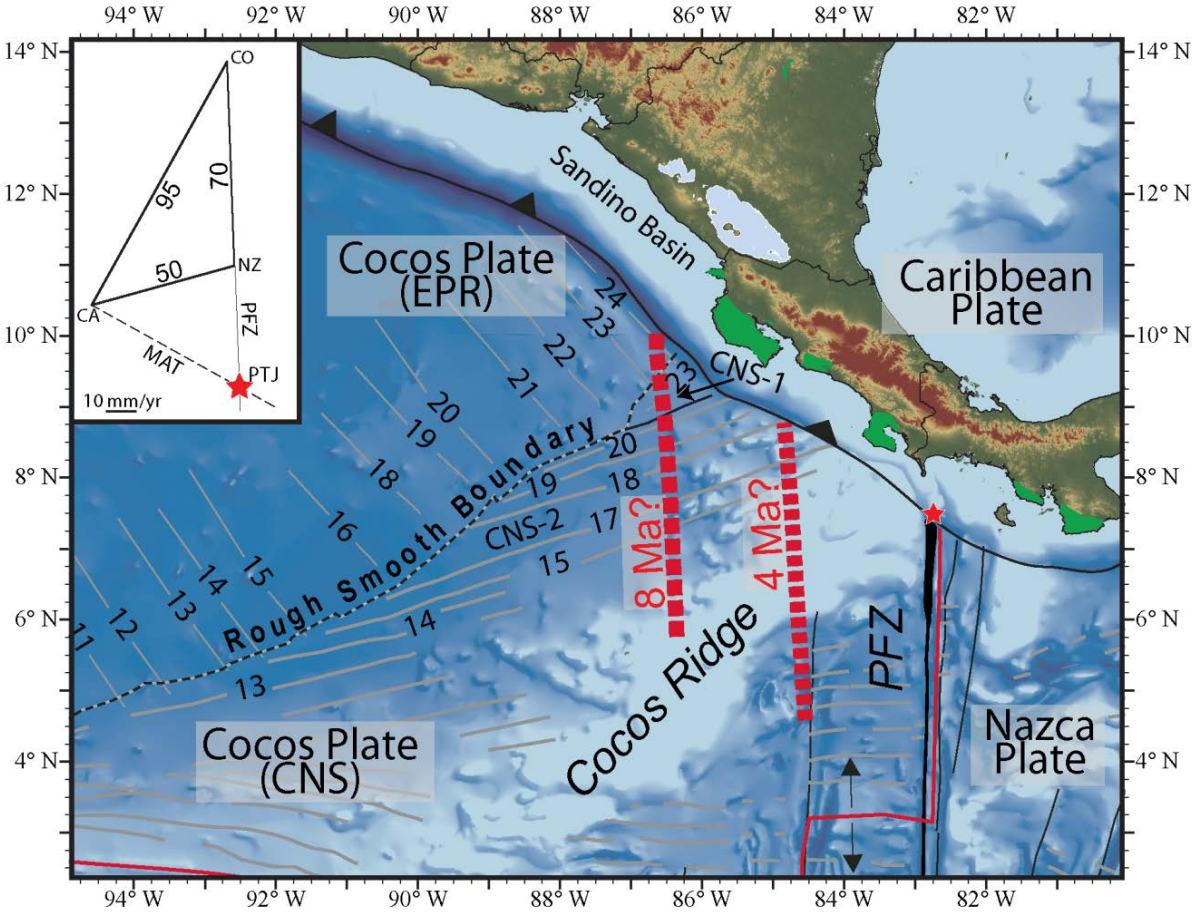

Fig. 5.2 Map of the Panama triple junction (PTJ, red star). Heavy red dashed lines indicate inferred location of the Panama Fracture Zone (PFZ, thin red line) 8 Ma and 4 Ma (McIntosh et al., 1993). Seafloor magnetic anomalies are shown as gray lines with ages in black, where labelled (Barckhausen et al., 2001). CNS-1 and CNS-2 refers to oceanic crust derived from previous orientations of the Cocos-Nazca spreading center. Ophiolitic outcrops are denoted by kelly green fill. Inset is a vector plot of plate motions related to the Panama triple junction. CA, Caribbean plate; MAT, Middle America trench, NZ, Nazca plate; CO, Cocos plate. Values are in mm/yr.

the nearshore trench-parallel folds of the forearc basin (e.g. Fig. 4.18H). The E-W extension at the offshore graben marked by the depocenter in the central region of the composite isochron for sequences 9-12 (Fig. 4.19) is interpreted to be the result of counterclockwise transtensional block rotation of this strike-slip bounded basin. These strike-slip faults may have formed during accretionary events where gaps in the incoming terrane or rheology contrasts differentially sheared the margin wedge. The Nicoya and Southern regions of the MAT are zones that experience a higher degree of coupling at the plate interface than the MAT of the Central region (Correa-Mora et al., 2009) which may be related to the block boundaries discovered offshore (Fig. 5.3).

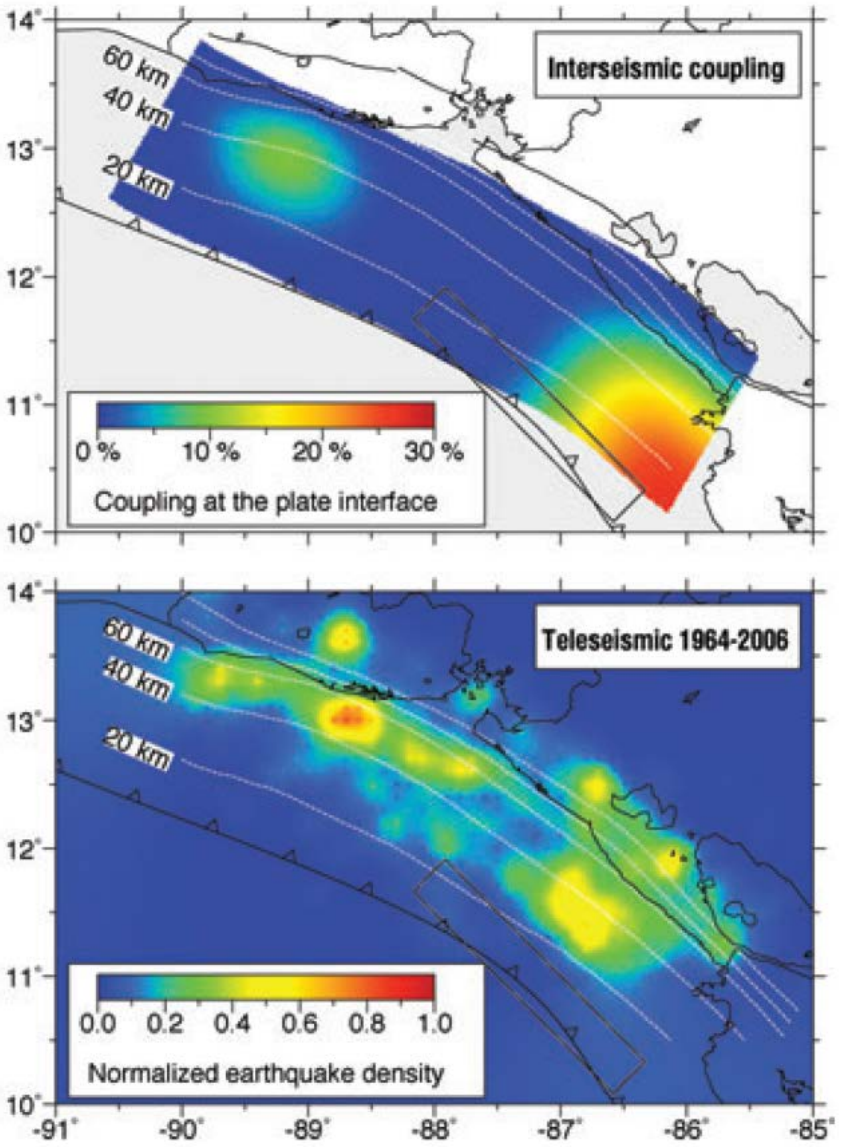

Figure 5.3 (A) Interseismic coupling of the plate interface based on inverted GPS velocities. (B) Normalized earthquake location density for all events from 1964-2006. Dotted white lines represent depth contours of subducting slab. Gray box represents rupture area of the tsunamigenic 1992 Mw 7.6 event offshore Nicaragua (Satake, 1994) (*modified from* Correa-Mora et al., 2009).

Chapter 6: The Subduction Setting of the Sandino Forearc Basin: Subduction Erosion, Sediment Subduction, and Terrane Accretion

6.1 INTRODUCTION

Two models have previously been proposed to describe the evolution of the Nicaraguan convergent margin. Both models were based on offshore seismic data that were limited to a single transect in the Central region of the Sandino basin were therefore necessarily simplified. The first model proposed that subduction initiation was responsible for an early outer arc high which formed a barrier to slope deposition with early deposition focused in the subsiding forearc basin. Later deposition filled the basin and the outer arc began to subside due to subduction erosion. Local uplift was attributed to transpressional deformation along margin-parallel strike-slip faults (Ranero et al., 2000). The second model suggested that an outer arc high was created in the Eocene as the buoyant lithosphere of an oceanic plateau arrived at the subduction zone and resisted subduction. The upper part of this plateau accreted to the margin wedge while the lower part delaminated and descended farther down the subduction zone. This jamming of the subduction zone created a deceleration in plate convergence which tore the downgoing slab and allowed asthenospheric material to upwell into the resulting void creating a high velocity body beneath the Sandino basin which correlates to the Corinto High location on gravity maps (Walther et al., 2000). Each model contains points that remain valid, but disagreement as to whether the observed extensional features are best described by a model of subduction erosion or subduction accretion remains.

6.2 EROSIVE AND ACCRETIONARY MARGINS

Active margins are often categorized as accretionary or erosive margins based on the dominant long-term subduction zone processes, especially those that manifest at the

subduction front (Fig. 6.1). Accretionary margins form thick wedges of thrusted sediment which were off-scraped from the downgoing plate at the frontal zone of subduction and/or underplated at depth at the plate interface, *e.g., Barbados* (Brown and Westbrook, 1988); *Nankai* (Gulick et al., 2004). In contrast, erosive margins lack such a substantial sedimentary wedge extending the upper plate basinward, *e.g., Costa Rica* (Ranero and von Huene, 2000). Without steady accretion of sediments at the trench, subduction erosion is thought to be the dominant process in erosive margins. This process involves basal erosion of the upper plate (Fig. 6.1B) that is theorized to result from a variety of causes including hydrofracturing by overpressured fluids in the subduction zone, abrasion by seamounts and oceanic ridges, and fault-bend half-grabens on the downgoing plate (Lallemand et al., 1994; Von Huene et al., 2004). However, an apparently erosive margin, that is one without a substantial frontal accretionary wedge of sediment, may still be referred to as accretionary so long as the long-term process results in a net transfer of crustal material from the subducting plate to the overriding plate, including by the mechanism of underplating (Clift and Vannucchi, 2004). In each type of margin, the long-term position of the trench will behave according to the nature of the subduction zone. In accretionary systems, the trench axis will migrate seaward as sediment accumulates at the frontal wedge whereas at erosive margins, the position of the trench will generally advance landward as the upper plate is consumed by tectonic erosion. Likewise, in generic cases where the dip of the subducting slab is not drastically altered, the position of the volcanic front will migrate away from the trench in erosive margins and towards the trench in an accretionary margin.

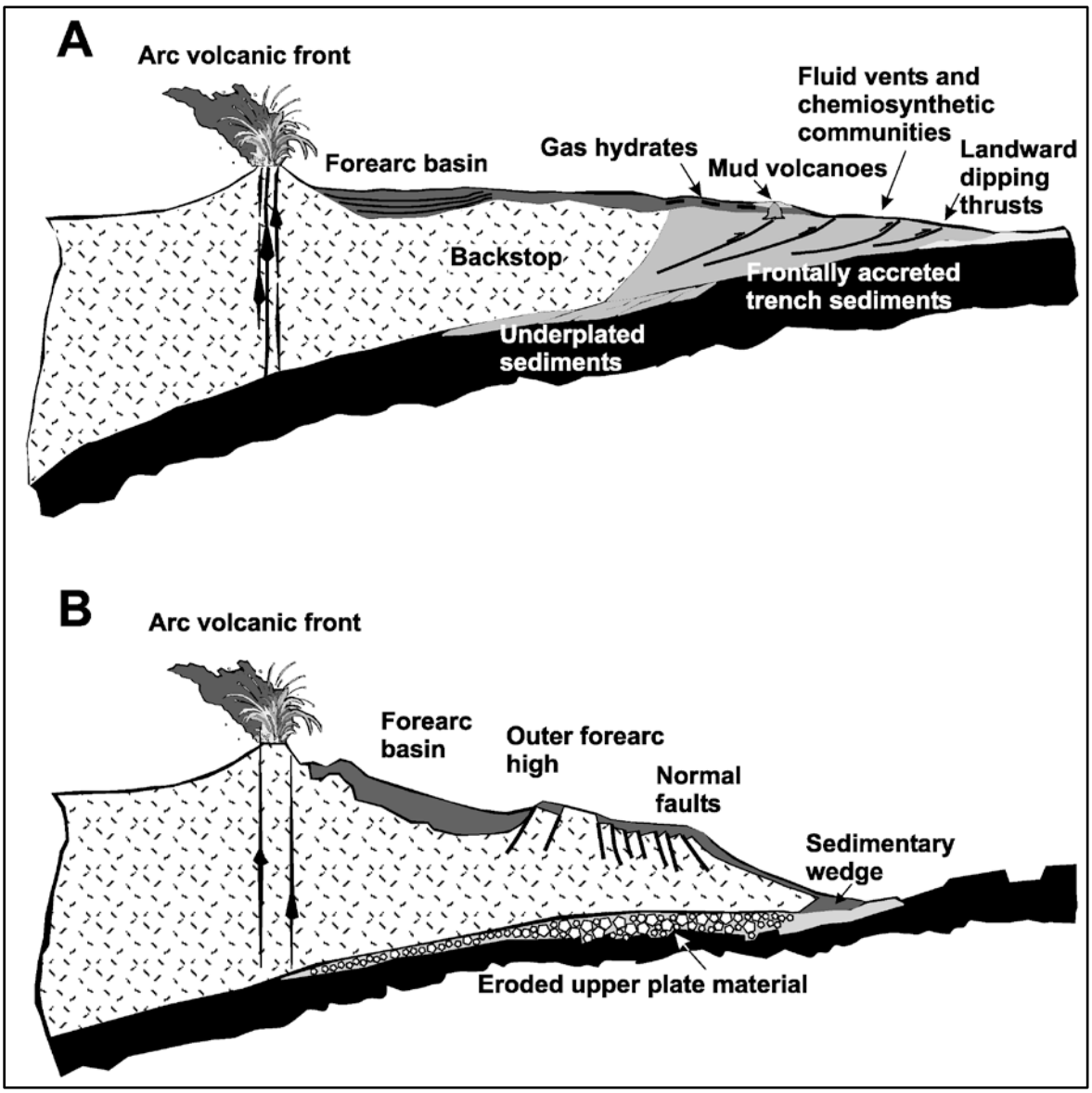

Figure 6.1: Illustrations of common characteristics of (A) an accretionary margin, and (B) an erosive margin. Accretionary margins are fronted by a broad accretionary wedge of thrusted sediments derived from both the upper plate forearc and trench-slope as well as from off-scraped sediments atop the downgoing slab. Erosive margins lack a substantial sedimentary wedge and instead are fronted by sediment-draped igneous basement rocks of the upper plate. Extension is expressed by a horst at the outer forearc high with seaward-dipping normal faults on the trench-slope (Clift and Vannucchi, 2004).

6.2 CLASSIFYING THE CONVERGENT MARGIN OF NICARAGUA

Previous studies have characterized the Nicaraguan convergent margin as erosive due primarily to its lack of an accretionary wedge as well as the existence of trenchward dipping normal faults on the slope, as seen on seismic reflection profiles and indicating a sustained extensional strain regime above the margin wedge (Clift and Vannucchi, 2004; Ranero et al., 2000). Based on comparisons with other similar margins, the trench retreat rate for Nicaragua has been inferred to be 2.0 km m.y.$^{-1}$ which is comparable to calculations made for Costa Rica and Guatemala with values of 3.0 km m.y.$^{-1}$ and 0.9 km m.y.$^{-1}$ respectively (Clift and Vannucchi, 2004). However other information suggests that the Nicaragua margin is not substantially erosive. For example, the volcanic front in Nicaragua has migrated trenchward ~50 km since Late Oligocene while the dip of the subducting slab has likely been unchanged since at least the Miocene (Ehrenborg, 1996; Jordan et al., 2006). Thus, one can infer that the trench has not advanced landward but rather retreated seaward at a rate of ~2.0 km m.y.$^{-1}$.

The Nicaraguan convergent margin does not appear to be a typical erosive or accretionary margin (Fig. 6.1). The margin has the outward appearance of an erosive margin in that it lacks an accretionary wedge but shows little evidence of being consumed at the plate interface other than the pervasive extensional structures found on the outer slope. The extraordinary thickness of forearc basin strata does not support the theory that Nicaragua is a margin where subduction erosion has been the dominant process during the Cenozoic. Previous workers observed progradation of Early Miocene sequences that would not have been preserved if significant coeval tectonic erosion had been occurring (McIntosh et al., 2007).

6.3 EVIDENCE FROM 2D MCS DATA

The results of this study confirm that the seaward progradation of sequences has persisted since well before the Early Miocene (McIntosh et al., 2007) and very likely since the inception of the forearc basin in the Late Cretaceous as evidenced by the preservation of the seaward extent of lower sequence 1 seismic strata. This study also shows that the Northern region has maintained a relatively stable configuration for the duration of the Sandino basin including a pronounced outer arc high that does not show significant frontal degradation of the margin wedge (Fig. 4.3). Furthermore, in the Southern and Central regions where the depocenter has experienced shortening and the paleo-outer arc high associated with the middle shelf high is fronted by the modern outer arc high (Fig. 4.12), the margin wedge appears to have increased its mass due to what is interpreted as multiple episodes of terrane accretion. Fault blocks above the outer arc high in the Central (Fig. 4.5) and Southern (Fig. 4.6) regions during the Mid-Eocene to Late Oligocene display evidence of thrusting prior to extension and are interpreted to have formed during collisional events above a pre-thickened margin wedge as an allochthonous terrane converged with the upper plate.

6.4 COMPARISON TO NUMERICAL MODEL STUDIES

Comparisons of data to numerical modelling results provide key insights into the complex processes taking place during accretionary events. Recent studies show that the age of the subducting terrane plays a key role in its behavior at the subduction zone. Numerical models suggest that the age of the embedded lithosphere and strength of the upper crust are primary factors in determining whether an oceanic plateau is accreted or subducted (Vogt and Gerya, 2012). The convergent margin of Nicaragua shares some similarities with modelled plateau subduction depicting basal plateau accretion (Fig. 6.2)

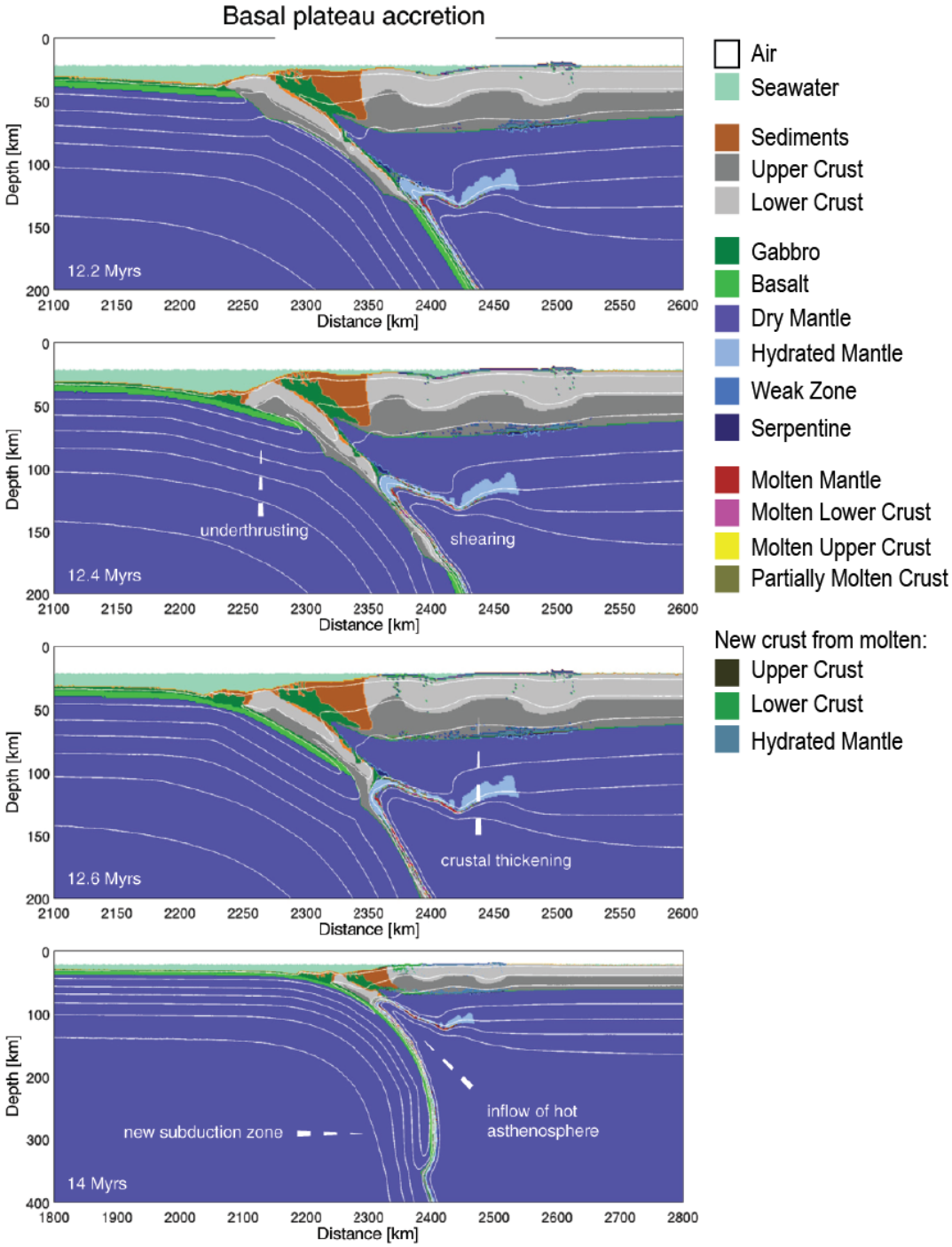

Figure 6.2: Geodynamic model of basal accretion of oceanic plateau. The slab age is 40 Ma with a weak upper crust of wet quartzite. The model resembles the structure of dip profiles in the Northern region (modified from Vogt and Gerya, 2012).

in the Northern region and underplating accretion in the Central and Southern regions (Fig. 6.3). The basal accretion model involves the oceanic plateau being delaminated and accreted in slices to the upper plate. Localized zones of strong shear develop in the upper plate and extension of the margin wedge occurs due to slab roll-back following the detachment of the slab. The underplating plateau model predicts that an oceanic plateau will subduct to mantle depths at which point slab tear occurs and the heated buoyant plateau uplifts and assimilates with the crust above.

6.5 OTHER MECHANISMS FOR TRENCH SLOPE EXTENSION

Trenchward dipping normal faults are not unique to subduction erosion and may have formed as the result of processes other than subduction erosion. Trench-normal tensional strain at the slope may be the result of slab roll-back following terrane accretion. MCS data offer strong support for terrane accretion as multiple instances have been documented of uplift at the outer where seismic strata are tilted landward and basins are inverted. Slab-roll back (due to change in the dip angle of the subducting slab) has been proposed as a possible explanation for the opening of the Nicaraguan Depression. Walther et al. (2000) proposed that the subduction zone migrated westward after the accretion of an oceanic plateau. The subduction retreat postulate is supported by geodynamic modelling results that suggest the interbasinal folds may have initiated while the trench was 50 km farther landward than its present location and therefore the subsequent southwestern retreat of the trench would have been a result of terrane accretion in accordance with the Walther model (Cailleau and Oncken, 2008).

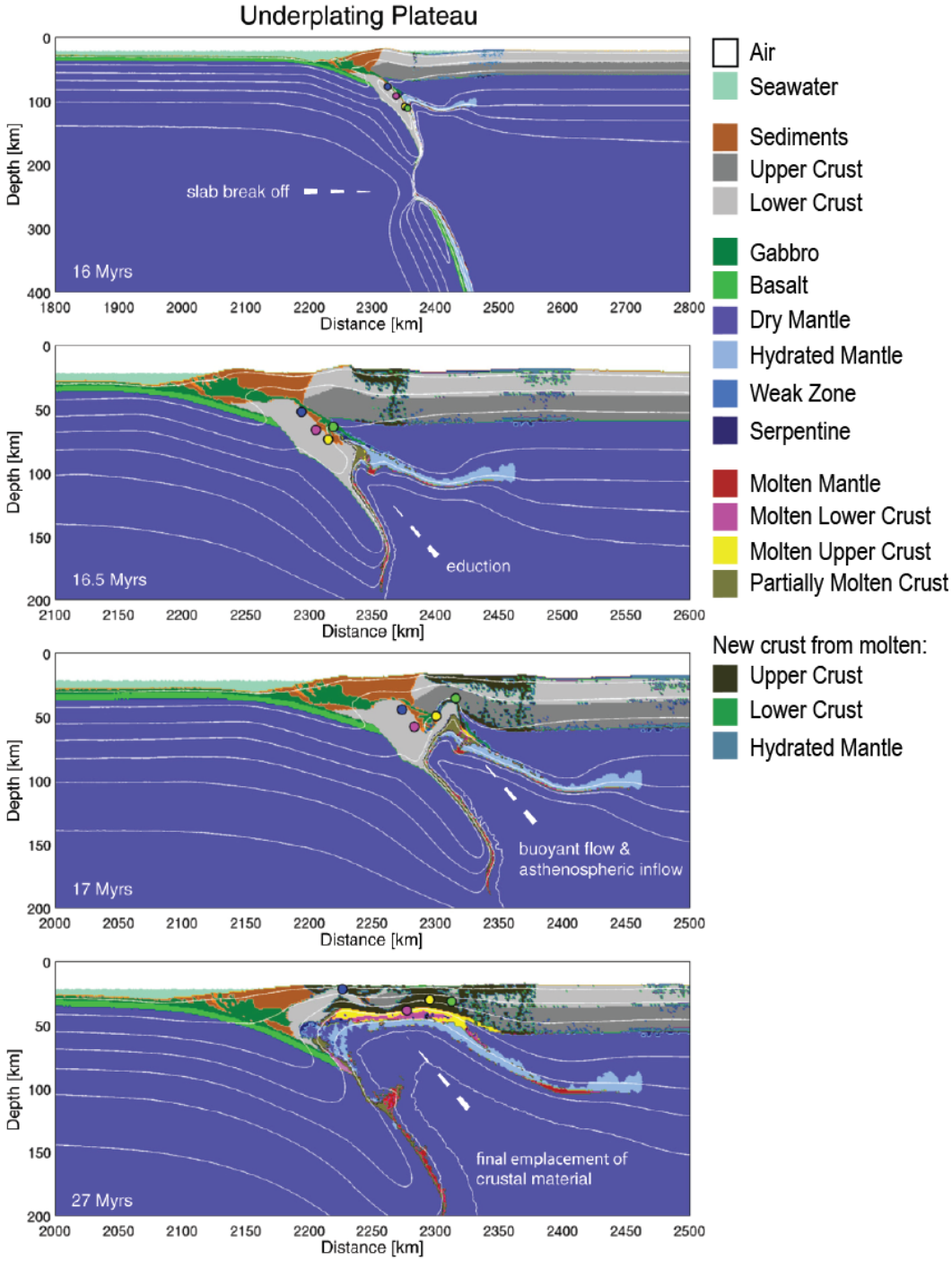

Figure 6.3: Geodynamic model of an underplating oceanic plateau. The age of the slab is 40 Ma and the lower crust rheology is a weak wet quartzite. Yellow, pink, blue, and green dots represent individual crustal "rocks." Note general similarities in uplift pattern with the Southern region (modified from Vogt and Gerya, 2012).

Sediment underplating is another process by which extensional features can be created within the slope. An example where seismic reflection data may depict this is the nic110 dip profile in the Northern region (Fig. 4.3). On this profile, a horst is imaged beneath the shelf break. Below that are the outer arc high and the subducting slab. Above the subducting slab, a series of high amplitude parallel reflections that resemble the downgoing plate are observed. These reflections may be evidence for a past downstepping of the décollement resulting in the underplating of sediments from the subducting slab. The region beneath the outer arc high also coincides with the updip limit of the seismogenic zone (McIntosh et al., 2007), a region where underplating is generally favored to occur (e.g. Matsumura et al., 2003).

The Hikurangi subduction zone offshore northeastern New Zealand is a convergent margin where an oceanic plate is actively subducting (Reyners et al., 2011). The northern New Zealand margin is thought to be dominantly erosive (Clift and Vannucchi, 2004) but some studies suggest that the process of underplating is equally as, or even more important to the subduction process in this region (Scherwath et al., 2010; Sutherland et al., 2009). The Raukumara forearc basin associated with the Hikurangi subduction zone is similar to the Sandino basin in that it contains an extraordinary stratigraphic thickness for a forearc basin with a maximum of ~10 km (Scherwath et al., 2010). Collision of a thickened subducting plate is hypothesized to be a dominant factor in the development of anomalously thick forearc strata (Sutherland et al., 2009).

6.6 CONCLUSIONS

While evidence for subduction erosion does exist on the Nicaragua margin, it is unlikely to be a process that has dominated the subduction zone for prolonged periods in the Cenozoic. In fact, despite the lack of a substantial accretionary wedge of sedimentary

material at its subduction front, the Nicaraguan margin appears to have been affected by accretionary processes in the form of multiple events of crustal terrane obduction that added significantly to the volume of the upper plate. The basement beneath the slope offshore Nicaraguan remains unsampled so the origin of accreted terrane remains unclear.

Chapter 7: Discussion on the Potential for Isolating a Eustatic Signal in Depositional Sequences of the Sandino Basin

7.1 Challenges of Sequence Stratigraphy on an Active Margin

The complexities inherent in the stratigraphic record of active margins have led to sequence stratigraphy being applied more frequently to passive margin sections. Convergent margins are subject to numerous interactions between fluctuating global sea-level (eustasy), active tectonics, and variation in sediment supply introduced to the basin. There are two principal mechanisms for eustatic change: 1) fluctuations in polar ice cap volume controlled by climate change (i.e. glacioeustasy), and 2) variations in the volume of the world's ocean basins in response to changes in the volume of mid-ocean ridges (Donovan and Jones, 1979). However, active tectonic processes obfuscate the eustatic signal since the relative position of the shoreline is also dependent on vertical tectonics that operate at time variant rates. Furthermore, by altering the relief of the basin, tectonic deformation also introduces changes to sediment transport which consequently affects the local rate of sedimentation, a key factor in the development of sequences (Van Wagoner et al., 1988).

Despite the myriad obstacles presented by convergent margins to isolating a eustatic signal within depositional sequences, previous studies such as Burger et al. (2001; 2002) have found that forearc basins may not only preserve a record of global sea level, but the unconformities could be distinguishable from those of tectonic origin.

7.2 Potential Advantages of the Sandino Basin

Special circumstances afforded by the Sandino basin may one day help overcome the challenge of identifying and distinguishing a eustatic signal on a convergent margin. Although tectonism is interpreted as the dominant component of sequence development

in the Sandino basin, its effect diminishes across the forearc basin to the northwest. The northern Sandino basin is a unique location in that it has experienced a prolonged period of deposition, amassing >16 km of strata since the Late Cretaceous, while simultaneously undergoing relatively mild structural deformation. If better age control were acquired using modern drilling techniques in the Northern region, then those depositional sequences could be compared to global sea level records and sea level proxies to test for a eustatic signal.

When compared to global sea level curves and oxygen isotope data, sequence boundaries do not generally agree with major sea level fluctuations (Fig. 8.1). However, the majority of sequences mapped during the course of this study extend across multiple regions suggesting that factors other than tectonism played a large role in their development. The relative quiescence in tectonism during the Pliocene to recent suggests that these youngest sequences may have been largely affected by changes in base level. For example, sequence 12 appears throughout the study area as a progradational wedge with clinoforms downlapping past the modern shelf edge (*see* Figs. 4.2, 4.3, 4.5, 4.9). The upper boundary for sequence 12 (SB12) is interpreted to coincide with the top of El Salto Formation, or ~1 My, near the time of the Mid-Pleistocene Climate Shift. Without proper age constraints on these youngest sequences, correlations with eustasy remain tenuous.

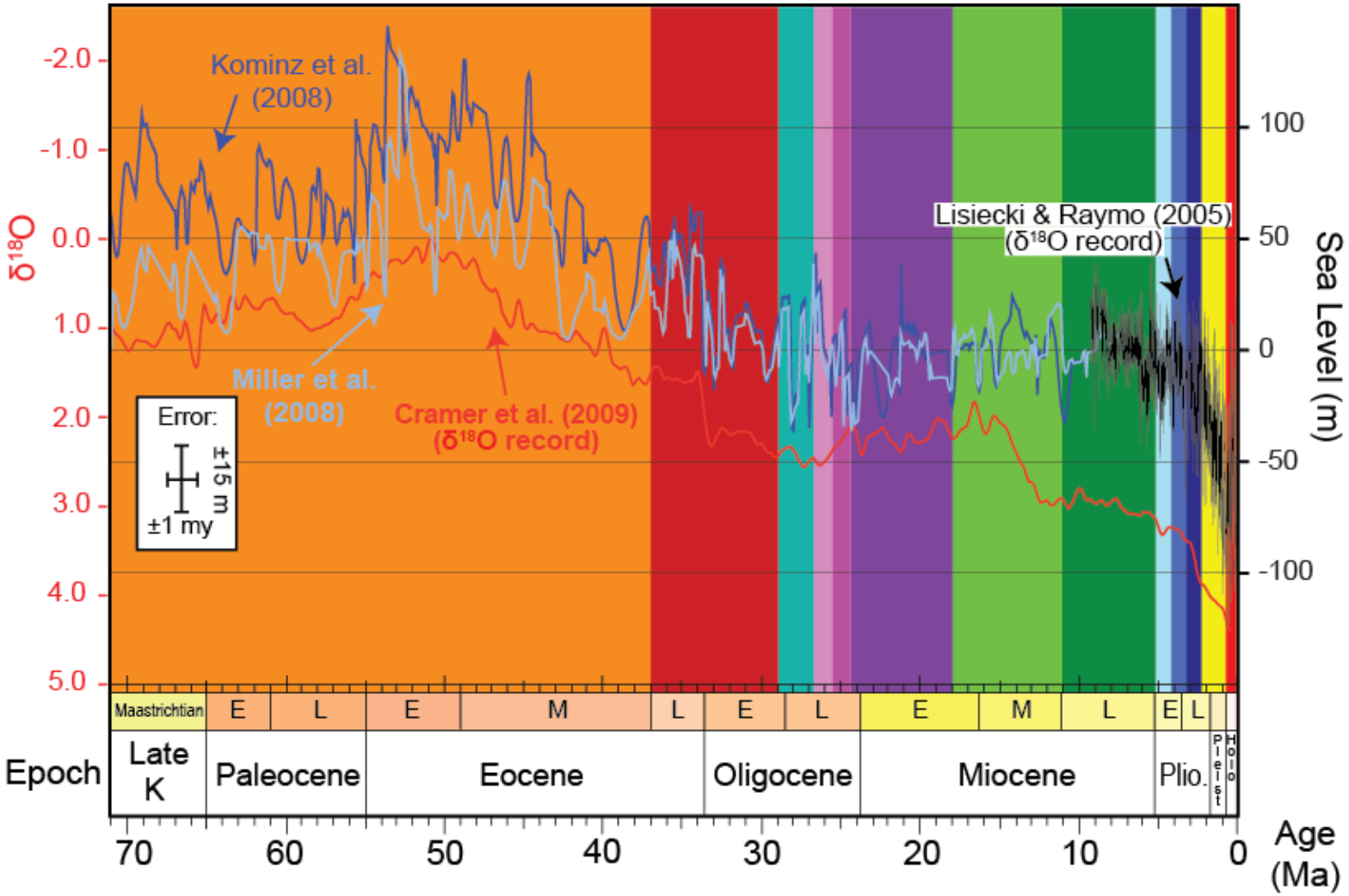

Figure 7.1 Comparison of sea level and oxygen isotope curves to age of sequences and sequence boundaries. Background shading color corresponds to the respective sequence from Table 3.1. Ages of sequences are approximately based on the well-tie at Corvina-2. Sea level and proxy curve data modified from Miller et al. (2011).

Chapter 8: Conclusions

8.1 SUMMARY

The goal of this study was to interpret 2D multichannel seismic (MCS) reflection profiles acquired from the offshore Sandino basin in order to further understand the tectonic and depositional history in this unique active forearc basin setting. The high resolution MCS data set acquired in 2004 (EW04-12) in conjunction with the deep penetration MCS profiles acquired in 2000 (cruise EW00-05) facilitated the first academically published attempt of a regional interpretation of both the depositional sequences within the forearc basin and the structural deformation of the upper plate brought about by tectonism affecting the convergent margin. This chapter represents a summary of the results and conclusions for this thesis.

8.2 SUMMARY OF CHAPTER 4 RESULTS

Using industry well data to constrain age estimates, sixteen sequences boundaries were identified based upon reflection terminations and the geometry of each corresponding sequence was determined by mapping these sequence boundaries throughout the survey region, beneath the entire shelf and portions of the upper slope. Observations and analysis of seismic profiles from the Sandino forearc basin reveal a systematic along-strike variation with regard to deposition, structure, and stratigraphic preservation. The region with maximum sediment thickness is in the north where evidence for compressional horizontal strain is least and stratigraphic preservation appears greatest. The extensional downwarped basin in the northwest is continuous and unfolded from the outer high to the inner shelf in the northwest and here the total thickness of Sandino basin deposits reaches >11.0 s TWT (Fig. 4.1). Total sediment thickness is generally greatest within this NW-SE striking trend that converges with the

Nicaraguan coast. The maximum thickness of this trend decreases towards Costa Rica from the basin maximum in the northwest to ~4.0-6.0 s TWT in the central basin, and to <3.0 s TWT in the southeast. In the dip direction, the total sediment thickness typically decreases as it approaches the outer high and the trench-slope. From northwest to southeast, the forearc basin displays an increasing amount of evidence for compressional deformation. Trench-parallel folding begins to appear beneath the inner shelf ~80 km southeast of the northernmost Pacific coast of Nicaragua and continues to the southeast with tighter hinges that are beveled at the seafloor. The decreasing stratigraphic thickness in the southeast is accompanied by the shallowing of sequences and an increase in erosional contacts. Several sequences from the northern parts of the basin are not preserved in the south whereas all sequences are represented in the north. In addition to the outer shelf structural high, the southeastern region of the forearc features a margin-parallel structural high in the middle shelf that subdivides the forearc into two sub-basins: an inner basin between the nearshore and the middle shelf high and an outer basin between the middle shelf high and the outer arc high. From this middle shelf high to the coast, beds at the seafloor are truncated by an angular unconformity. In the southern most Sandino basin, the sediment cover is extremely thin (< 0.25 s ΔTWT) on the shelf and the majority of preserved deposition resides in the region beneath the slope including the highly tectonized deformational front on the upper plate of the subduction zone.

8.3 Conclusions of Chapter 5: Tectonostratigraphic Evolution of the Sandino Forearc Basin

The development of the Sandino basin is subdivided into five stages from its origin in the Late Cretaceous to the present day. Stage 1 begins with the formation of the forearc basin during subduction initiation in the Late Cretaceous following the accretion of an island arc terrane to the western margin of the Chortis block. As a result, an outer

arc high develops and the forearc basin subsides as it is infilled by deep water turbidites. This stable forearc configuration continues until the onset of Stage 2 during the Mid-Eocene. The second stage is marked by shoaling and carbonate deposition as the slope and outer shelf are uplifted as the result of a collision with a thickened subducting oceanic plate. The upper plate experiences accretion and underplating of the downgoing crustal material and the shelf undergoes a regional angular unconformity at the end of the stage during the early Late Oligocene at SB3. Stage 3 encompasses the Late Oligocene to Early Miocene and marks the onset of nearshore uplift and folding of the strata of the Central and Southern regions within the margin parallel depocenter. Clastic deposition dominates the basin during this stage. Changes to the basin that occur during the Mid-Miocene to Late Miocene stage 4 vary along-strike with subsidence dominating the Northern region and shortening prevalent in the Central, Southern, and Nicoya regions. Uplift and shortening in the Southern and Nicoya regions may record the deformation caused by the location of the Panama Fracture Zone (PFZ) triple junction ~8 Mya. The Pliocene to recent stage 5 is dominated by extensional and transtensional stresses as the PFZ triple junction migrates further to the southeast. Subsidence occurs throughout most of the shelf and slope and a forearc sliver translates parallel to the trench to the northwest.

8.4 CONCLUSIONS OF CHAPTER 6: SUBDUCTION EROSION VERSUS ACCRETION AT THE NICARAGUA CONVERGENT MARGIN

Despite its lack of an accretionary sedimentary wedge and pervasive extensional faults beneath the slope, the Nicaraguan margin otherwise does not behave as a typical subduction erosion-type margin. The Sandino basin displays episodic uplift at the outer arc as well as prograding clinoforms since the Late Cretaceous. Effects from terrane accretion and underplating appear to have overwhelmed any secondary effects from basal erosion of the upper plate due to subduction and therefore lead to a seaward retreat of the

trench and volcanic arc. Trenchward dipping normal faults observed on the slope likely initiated in the aftermath of a thickened downgoing plate entered the subduction zone and developed a slab-roll back scenario.

8.5 CONCLUSIONS OF CHAPTER 7: POTENTIAL FOR DECIPHERING A EUSTATIC SIGNAL WITHIN THE SANDINO BASIN

The Sandino basin offers a unique setting to study the feasibility of investigating eustasy at a convergent margin due to the variability of its tectonic setting along-strike. The Northern region of the basin has experienced a relatively stable regime since the Late Oligocene and contains an extraordinarily thick stratigraphic section for a forearc basin ($\geq$ 16 km). With better age control from modern ocean drilling techniques in conjunction with the high frequency MCS data obtained in 2004, sequence boundaries could be more accurately dated and compared to the independent global sea-level records. Mapped portions of sequence boundaries in the Northern region could then be compared to their expressions to the southeast where tectonism plays a more significant role in order to determine whether unconformities related to tectonism can be systematically distinguished from those controlled by changes in eustasy.

Bibliography

Alvarado, D., DeMets, C., Tikoff, B., Hernandez, D., Wawrzyniec, T. F., Pullinger, C., Mattioli, G., Turner, H. L., Rodriguez, M., and Correa-Mora, F., 2011, Forearc motion and deformation between El Salvador and Nicaragua: GPS, seismic, structural, and paleomagnetic observations: Lithosphere, v. 3, no. 1, p. 3-21.

Alvarado, G. E., Denyer, P., and Gazel, E., 2008, Endeavor research into evolving paradigms around ophiolites: the case of the oceanic igneous complexes of Costa Rica: Revista Geológica de América Central.

Barckhausen, U., Ranero, C. R., von Huene, R., Cande, S. C., and Roeser, H. A., 2001, Revised tectonic boundaries in the Cocos Plate off Costa Rica: Implications for the segmentation of the convergent margin and for plate tectonic models: Journal of Geophysical Research, v. 106, no. B9, p. 19207-19220.

Barckhausen, U. R., Cesar R; von Huene, R; Cande, Steven C; Roeser, Hans A, 2001, Revised tectonic boundaries in the Cocos Plate off Costa Rica - Implications for the segmentation of the convergent margin and for plate tectonic models: Journal of Geophysical Research, v. 106, no. B9, p. 207-220.

Berhorst, A., 2006, Die Struktur des aktiven Kontinentalhangs vor Nicaragua und Costa Rica: marin-seismische Steil-und Weitwinkelmessungen: Christian-Albrechts-Universität.

Boer, J. d., 1979, The outer arc of the Costa Rican orogen (oceanic basement complexes of the Nicoya and Santa Elena peninsulas: Tectonophysics, v. 56, p. 221-259.

Bourgois, J., Azema, J., Baumgartner, P. O., Tournon, J., Desmet, A., and Aubouin, J., 1984, The geologic history of the Caribbean-Cocos plate boundary with special reference to the Nicoya ophiolite complex (Costa Rica) and D.S.D.P. results (Legs 67 and 84 off Guatemala): A synthesis: Tectonophysics, v. 108, no. 1–2, p. 1-32.

Brown, K., and Westbrook, G., 1988, Mud diapirism and subcretion in the Barbados Ridge accretionary complex: the role of fluids in accretionary processes: Tectonics, v. 7, no. 3, p. 613-640.

Burbach, G. V., Frohlich, C., Pennington, W. D., and Matumoto, T., 1984, Seismicity and tectonics of the subducted Cocos Plate: Journal of Geophysical Research: Solid Earth, v. 89, no. B9, p. 7719-7735.

Burger, R. L., Fulthorpe, C. S., and Austin Jr, J. A., 2001, Late Pleistocene channel incisions in the southern Eel River Basin, northern California: implications for tectonic vs. eustatic influences on shelf sedimentation patterns: Marine Geology, v. 177, no. 3–4, p. 317-330.

Burger, R. L., Fulthorpe, C. S., Austin Jr, J. A., and Gulick, S. P. S., 2002, Lower Pleistocene to present structural deformation and sequence stratigraphy of the continental shelf, offshore Eel River Basin, northern California: Marine Geology, v. 185, no. 3–4, p. 249-281.

Cailleau, B., and Oncken, O., 2008, Past forearc deformation in Nicaragua and coupling at the megathrust interface: Evidence for subduction retreat?: Geochemistry, Geophysics, Geosystems, v. 9, no. 3, p. Q03016.

Calvo, C., 2003, Provenance of plutonic detritus in cover sandstone of Nicoya Complex, Costa Rica: Cretaceous unroofing history of a Mesozoic ophiolite sequence: GSA Bulletin, v. 115, no. 7, p. 832-844.

Christeson, G., McIntosh, K., Shipley, T., Flueh, E., and Goedde, H., 1999, Structure of the Costa Rica convergent margin, offshore Nicoya Peninsula: Journal of Geophysical Research: Solid Earth (1978–2012), v. 104, no. B11, p. 25443-25468.

Clift, P., and Vannucchi, P., 2004, Controls on tectonic accretion versus erosion in subduction zones: Implications for the origin and recycling of the continental crust: Reviews of Geophysics, v. 42, no. 2, p. RG2001.

Correa-Mora, F., DeMets, C., Alvarado, D., Turner, H. L., Mattioli, G., Hernandez, D., Pullinger, C., Rodriguez, M., and Tenorio, C., 2009, GPS-derived coupling estimates for the Central America subduction zone and volcanic arc faults: El Salvador, Honduras and Nicaragua: Geophysical Journal International, v. 179.

Corti, G., Carminati, E., Mazzarini, F., and Garcia, M. O., 2005, Active strike-slip faulting in El Salvador, Central America: Geology, v. 33, no. 12, p. 989-992.

Cowan, H., Prentice, C., Pantosti, D., Martini, P. d., Strauch, W., and Participants, W., 2002, Late Holocene Earthquakes on the Aeropuerto Fault, Managua, Nicaragua: Bulletin of the Seismological Society of America, v. 92, no. 5, p. 1694-1707.

Cramer, B., Toggweiler, J., Wright, J., Katz, M., and Miller, K., 2009, Ocean overturning since the Late Cretaceous: Inferences from a new benthic foraminiferal isotope compilation: Paleoceanography, v. 24, no. 4.

Crowe, J., and Buffler, R., 1985, Multichannel seismic records across the Middle America trench and Costa Rica–Nicaragua convergent margin, NCY-7 and NCI-1: Middle America Trench off western Central America, Ocean Drilling Program Regional Data Synthesis Series, Atlas, v. 7, p. 6-11.

DeMets, C., 2001, A new estimate for present-day Coco-Caribbean plate motion: Implications for slip along the Central American Volcanic arc: Geophysical Research Letters, v. 28, no. 21, p. 4043-4046.

DeMets, C., Jansma, P. E., Mattioli, G. S., Dixon, T. H., Farina, F., Bilham, R., Calais, E., and Mann, P., 2000, GPS geodetic constraints on Caribbean-North America plate motion: Geophysical Research Letters, v. 27, no. 3, p. 437-440.

DeMets, C., Mattioli, G., Jansma, P., Rogers, R. D., Tenorio, C., and Turner, H. L., 2007, Present motion and deformation of the Caribbean plate: Constraints from new GPS geodetic measurements from Honduras and Nicaragua: Geological Society of America Special Papers, v. 428, p. 21-36.

Dengo, G., 1962, Tectonic-igneous sequence in Costa Rica, *in* Engel, A. E. J., James, H. J., and Leonard, B. F., eds., Petrologic Studies: A volume to honor AF Budington. Geological Society of America Special Volume: New York, Geological Society of America, p. 133-161.

Denyer, P., and Baumgartner, P. O., 2006, Emplacement of Jurassic-Lower Cretaceous radiolarites of the Nicoya Complex (Costa Rica): Geologica Acta, v. 4, no. No. 1-2, p. 203-218.

Denyer, P., Baumgartner, P. O., and Gazel, E., 2006, Characterization and tectonic implications of Mesozoic-Cenozoic oceanic assemblages of Costa Rica and Western Panama: Geologica Acta, v. 4, no. No. 1-2, p. 219-235.

Dickinson, W. R., 1979, Structure and stratigraphy of forearc regions: The American Association of Petroleum Geologists bulletin, v. 63, no. 1, p. 2.

Donovan, D. T., and Jones, E. J. W., 1979, Causes of world-wide changes in sea level: Journal of the Geological Society, v. 136, no. 2, p. 187-192.

Ehrenborg, J., 1996, A new stratigraphy for the Tertiary volcanic rocks of the Nicaraguan Highland: GSA Bulletin, v. 108, no. No. 7, p. 830-842.

Elming, S.-A., Layer, P., and Ubieta, K., 2001, A paleomagnetic study and age determinations of Tertiary rocks in Nicaragua, Central America: Geophys. J. Int., v. 147, p. 294-309.

Frischbutter, A., 2002, Structure of the managua graben, Nicaragua, from remote sensing images: Geofisica Internacional, Universidad Nacional Autonoma de Mexico, v. 41, no. 2, p. 87-102.

Funk, J., Mann, P., McIntosh, K., and Stephens, J., 2009, Cenozoic tectonics of the Nicaraguan depression, Nicaragua, and Median Trough, El Salvador, based on seismic-reflection profiling and remote-sensing data: Geological Society of America Bulletin, v. 121, no. 11-12, p. 1491-1521.

Gazel, E., Denyer, P., and Baumgartner, P. O., 2006, Magmatic and geotectonic significance of Santa Elena Peninsula, Costa Rica: Geologica Acta, v. 4, no. No. 1-2, p. 193-2002.

GEBCO, 2008, British Oceanographic Data Centre. GEBCO Digital Atlas. GEBCO_08 Grid, version 20100927, http://www.gebco.net. .

Geldmacher, J., Hoernle, K., Van Den Bogaard, P., Hauff, F., and Klügel, A., 2008, Age and Geochemistry of the Central American Forearc Basement (DSDP Leg 67 and 84): Insights into Mesozoic Arc Volcanism and Seamount Accretion on the Fringe of the Caribbean LIP: Journal of Petrology, v. 49, no. 10, p. 1781-1815.

Gulick, S., Bangs, N., Shipley, T., Nakamura, Y., Moore, G., and Kuramoto, S., 2004, Three-dimensional architecture of the Nankai accretionary prism's imbricate thrust zone off Cape Muroto, Japan: Prism reconstruction via en echelon thrust propagation: Journal of Geophysical Research: Solid Earth (1978–2012), v. 109, no. B2.

Gurnis, M., 1992, Rapid continental subsidence following the initiation and evolution of subduction: Science, v. 255, no. 5051, p. 1556-1558.

Harlow, D. H., and White, R. A., 1985, Shallow earthquakes along the volcacnic chain in Central America: Evidence for oblique subduction: Earthquake Notes, v. 55, p. 28.

Hauff, F., Hoernle, K., van den Bogaard, P., Alvarado, G., and Garbe-Schönberg, D., 2000, Age and geochemistry of basaltic complexes in western Costa Rica: Contributions to the geotectonic evolution of Central America: Geochemistry, Geophysics, Geosystems, v. 1.

Hey, R., 1977, Tectonic evolution of the Cocos-Nazca spreading center: Geol Soc Am Bull, v. 88, no. 10, p. 1404-1420.

Hinz, K., von Huene, R., Ranero, C. R., and Group, P. W., 1996, Tectonic structure of the convergent Pacific margin offshore Costa Rica from multichannel seismic reflection data: Tectonics, v. 15, no. 1, p. 54-66.

Hoernle, K., Hauff, F., and van den Bogaard, P., 2004, 70 m.y. history (139–69 Ma) for the Caribbean large igneous province: Geology, v. 32, no. 8, p. 697-700.

Ibrahim, A.-B. K., Latham, G. V., and Ladd, J., 1979, Seismic refraction and reflection measurements in the Middle America Trench offshore Guatemala: Journal of Geophysical Research: Solid Earth, v. 84, no. B10, p. 5643-5649.

INE, 1993, Project CAM-009: Managua, Instituto Nicaragüense de Energía, p. 195.

INE, I. N. d. E., 1995, Geological field guide of Sandino basin onshore, Managua, Instituto Nicaraguense de Energia (INE).

Jarrard, R. D., 1986, Terrane motion by strike-slip faulting of forearc slivers: Geology, v. 14, no. 9, p. 780-783.

Jarvis, A., Reuter, H., Nelson, A., and Guevara, E., 2006, Hole-Filled SRTM for the Glove Version 3 (available from the CGIAR-CSI SRTM 90 m database).

Jordan, B. R., Sigurdsson, H., Carey, S. N., Rogers, R., and Ehrenborg, J., 2006, Geochemical correlation of Caribbean Sea tephra layers with ignimbrites in Central America: Geological Society of America Special Papers, v. 402, p. 175.

Jordan, B. R., Sigurdsson, H., Carey, S. N., Rogers, R., and Ehrenborg, J., 2007, Geochemical variation along and across the Central American Miocene paleoarc in Honduras and Nicaragua: Geochimica et cosmochimica acta, v. 71, no. 14, p. 3581-3591.

Kárason, H., and Van Der Hilst, R. D., 2000, Constraints on mantle convection from seismic tomography: The History and Dynamics of Global Plate Motions, p. 277-288.

Kidwell, S. M., 1993, Taphonomic expressions of sedimentary hiatuses: field observations on bioclastic concentrations and sequence anatomy in low, moderate and high subsidence settings: Geologische Rundschau, v. 82.

Kolb, W., and Schmidt, H., 1991, Depositional Sequences Associated with Equilibrium Coastlines in the Neogene of South-Western Nicaragua: Sedimentation, Tectonics and Eustasy: Sea-Level Changes at Active Margins, p. 259-272.

Kominz, M., Browning, J., Miller, K., Sugarman, P., Mizintseva, S., and Scotese, C., 2008, Late Cretaceous to Miocene sea-level estimates from the New Jersey and Delaware coastal plain coreholes: An error analysis: Basin Research, v. 20, no. 2, p. 211-226.

Kuijpers, E. P., 1980, The geologic history of the Nicoya Ophiolite Complex, Costa Rica, and its geotectonic significance: Tectonophysics, v. 68, no. 3–4, p. 233-255.

Ladd, J. W., and Schroder, S., 1985, Seismic stratigraphy of the continental shelf offshore Guatemala: Implications for vertical tectonics related to subduction: Initial Reorts of the Deep Sea Drilling Project, v. 84, p. 879-893.

LaFemina, P., Dixon, T. H., Govers, R., Norabuena, E., Turner, H., Saballos, A., Mattioli, G., Protti, M., and Strauch, W., 2009, Fore-arc motion and Cocos Ridge collision in Central America: Geochemistry, Geophysics, Geosystems, v. 10, no. 5, p. Q05S14.

LaFemina, P. C., Dixon, T. H., and Strauch, W., 2002, Bookshelf Faulting in Nicaragua: Geological Society of America, v. 30, no. 8, p. 751-754.

Lallemand, S. E., Schnürle, P., and Malavieille, J., 1994, Coulomb theory applied to accretionary and nonaccretionary wedges: Possible causes for tectonic erosion and/or frontal accretion: Journal of Geophysical Research, v. 99, no. B6, p. 12033-12012,12055.

Lonsdale, P., and Klitgord, K. D., 1978, Structure and tectonic history of the eastern Panama Basin: Geological Society of America Bulletin, v. 89, no. 7, p. 981-999.

Lundberg, N., 1982, Evolution of the slope landward of the Middle America Trench, Nicoya Peninsula, Costa Rica: Geological Society, London, Special Publications, v. 10, no. 1, p. 131-147.

Mann, P., 2007, Overview of the tectonic history of northern Central America: Geological Society of America Special Papers, v. 428, p. 1-19.

Matsumura, M., Hashimoto, Y., Kimura, G., Ohmori-Ikehara, K., Enjohji, M., and Ikesawa, E., 2003, Depth of oceanic-crust underplating in a subduction zone: Inferences from fluid-inclusion analyses of crack-seal veins: Geology, v. 31, no. 11, p. 1005-1008.

McBirney, A. R., and Williams, H., 1965, Volcanic History of Nicaragua: University of California Publications in Geological Sciences, v. 55.

McIntosh, K., Silver, E., and Shipley, T., 1993, Evidence and mechanisms for forearc extension at the accretionary Costa Rica convergent margin: Tectonics, v. 12, no. 6, p. 1380-1392.

McIntosh, K. D., Silver, E. A., Ahmed, I., Berhorst, A., Ranero, C. R., Kelly, R. K., and Flueh, E. R., 2007, The Nicaragua Convergent Margin: Seismic reflection imaging of the source of a tsunami earthquake, *in* Dixon, T., and Moore, J. C., eds., The Seismogenic Zone of Subduction Thrust Faults: New York, Columbia Univ. Press, p. 257–287.

Meschede, M., and Barckhausen, U., 2000, Plate Tectonic Evolution of the Cocos-Nazca Spreading Center: *Proceedings of the Ocean Drilling Program, Scientific Results. College Station TX, Texas A&M*, v. Leg 170, no. Silver, E.A., Kimura, G., and Shipley, T.H. (Eds.)

Miller, K., Mountain, G., Wright, J., and Browning, J., 2011, A 180-million-year record of sea level and ice volume variations from continental margin and deep-sea isotopic records: Oceanography, v. 24, no. 2, p. 40-53.

Miller, K. G., Kominz, M. A., Browning, J. V., Wright, J. D., Mountain, G. S., Katz, M. E., Sugarman, P. J., Cramer, B. S., Christie-Blick, N., and Pekar, S. F., 2005, The Phanerozoic record of global sea-level change: Science, v. 310, no. 5752, p. 1293-1298.

Molnar, P., and Sykes, L. R., 1969, Tectonics of the Caribbean and Middle America regions from focal mechanisms and seismicty: Geological Society of America Bulletin, v. 80, p. 1639-1684.

Norabuena, E., Dixon, T. H., Schwartz, S., DeShon, H., Newman, A., Protti, M., Gonzalez, V., Dorman, L., Flueh, E. R., Lundgren, P., Pollitz, F., and Sampson, D., 2004, Geodetic and seismic constraints on some seismogenic zone processes in Costa Rica: Journal of Geophysical Research, v. 109, no. B11403.

Phipps Morgan, J., Ranero, C., and Vannucchi, P., 2008, Intra-arc extension in Central America: Links between plate motions, tectonics, volcanism, and geochemistry: Earth and Planetary Science Letters, v. 272, no. 1, p. 365-371.

Plank, T., Balzer, V., and Carr, M., 2002, Nicaraguan volcanoes record paleoceanographic changes accompanying closer of the Panama gateway: Geology, v. 30, no. 12, p. 1087-1090.

Protti, M., Guendel, F., and McNally, K., 1995, Correlation between the age of the subducting Cocos plate and the geometry of the Wadati-Benioff zone under Nicaragua and Costa Rica: Geologic and Tectonic Development of the Caribbean Plate Boundary in Southern Central America, p. 309-326.

Protti, M., Gundel, F., and McNally, K., 1994, The geometry of the Wadati-Benioff zone under southern Central America and its tectonic significance: results from a high-resolution local seismographic network: Physics of the Earth and Planetary Interiors, v. 84, p. 271-287.

Ranero, C. R., Huene, R. v., Flueh, E., Duarte, M., Baca, D., and McIntosh, K., 2000, A cross section of the convergent Pacific margin of Nicaragua: Tectonics, v. 19, no. 2, p. 335-357.

Ranero, C. R., and von Huene, R., 2000, Subduction erosion along the Middle America convergent margin: Nature, v. 404, no. 6779, p. 748-752.

Reyners, M., Eberhart-Phillips, D., and Bannister, S., 2011, Tracking repeated subduction of the Hikurangi Plateau beneath New Zealand: Earth and Planetary Science Letters, v. 311, no. 1–2, p. 165-171.

Rogers, R. D., Karason, H., and Hilst, R. D. v. d., 2002, Epeirogenic uplift above a detached slab in northern Central America: Geological Society of America, v. 30, no. no. 11, p. 1031-1034.

Saginor, I., Gazel, E., Carr, M. J., Swisher Iii, C. C., and Turrin, B., 2011, New Pliocene–Pleistocene 40Ar/39Ar ages fill in temporal gaps in the Nicaraguan volcanic record: Journal of Volcanology and Geothermal Research, v. 202, no. 1–2, p. 143-152.

Sallarès, V., Dañobeitia, J. J., Flueh, E. r., and Leandro, G., 1999, Seismic velocity structure across the Middle American landbridge in northern Costa Rica: Journal of Geodynamics, v. 27, no. 3, p. 327-344.

Sallarès, V., Meléndez, A., Prada, M., Ranero, C. R., McIntosh, K., and Grevemeyer, I., 2013, Overriding plate structure of the Nicaragua convergent margin: Relationship to the seismogenic zone of the 1992 tsunami earthquake: Geochemistry, Geophysics, Geosystems.

Sandwell, D., and Smith, W., 1997, Marine gravity anomaly from Geosat and ERS 1 satellite altimetry: Journal of Geophysical Research, v. 102, no. B, p. 10039-10054.

Sandwell, D. T., and Smith, W. H., 2009, Global marine gravity from retracked Geosat and ERS-1 altimetry: Ridge segmentation versus spreading rate: Journal of Geophysical Research: Solid Earth (1978–2012), v. 114, no. B1.

Scherwath, M., Kopp, H., Flueh, E. R., Henrys, S. A., Sutherland, R., Stagpoole, V. M., Barker, D. H. N., Reyners, M. E., Bassett, D. G., Planert, L., and Dannowski, A., 2010, Fore-arc deformation and underplating at the northern Hikurangi margin, New Zealand: Journal of Geophysical Research: Solid Earth (1978–2012), v. 115, no. B6.

Schmidt, H., and Seyfried, H., 1991, Depositional sequences and sequence boundaries in fore-arc coastal embayments: case histories from Central America: Sedimentation, Tectonics and Eustasy: Sea-Level Changes at Active Margins, p. 241-258.

Sella, G., Dixon, T., and Mao, A., 2002, REVEL: A model for Recent plate velocities from space geodesy: Journal of Geophysical Research.

Seyfried, H., Astorga, A., Ammann, H., Calvo, C., Kolb, W., Schmidt, H., and Winsemann, J., 1991, Anatomy of an evolving island arc: tectonic and eustatic control in the south Central American fore-arc area.

Shipley, T. H., Stoffa, P. L., and Dean, D. F., 1990, Underthrust sediments, fluid migration paths, and mud volcanoes associated with the accretionary wedge off Costa Rica: Middle America Trench: Journal of Geophysical Research, v. 95, no. B6, p. 8743-8752.

Sigurdsson, H., Kelley, S., Leckie, R., Carey, S., Bralower, T., and King, J., 2000, History of circum-Caribbean explosive volcanism: 40Ar/39Ar dating of tephra layers: Proceedings of the Ocean Drilling Program, Scientific Results. College Station TX, Texas A&M, v. 165, p. 299-314.

Sinton, C. W., Duncan, R. A., and Denyer, P., 1997, Nicoya Peninsula, Costa Rica: A single suite of Caribbean oceanic plateau magmas: Journal of Geophysical Research: Solid Earth, v. 102, no. B7, p. 15507-15520.

Struss, I., Artiles, V., Cramer, B., and Winsemann, J., 2008, The Petroleum System In The Sandino Forearc Basin, Offshore Western Nicaragua: Journal of Petroleum Geology, v. 31, no. 3, p. 221-224.

Sutherland, R., Stagpoole, V., Uruski, C., Callum, K., Bassett, D., Henrys, S., Scherwath, M., Kopp, H., Field, B., Toulmin, S., Barker, D., Bannister, S., Davey, F., TimothyStern, and Flueh, E. R., 2009, Reactivation of tectonics, crustal underplating, and uplift after 60 Myr of passive subsidence, Raukumara Basin, Hikurangi-Kermadec fore arc, New Zealand: Implications for global growth and recycling of continents, Tectonics, Volume 28.

Syracuse, E. M., and Abers, G. A., 2006, Global compilation of variations in slab depth beneath arc volcanoes and implications: Geochemistry, Geophysics, Geosystems, v. 7, no. 5.

Turner, H. L., LaFemina, P., Saballos, A., Mattioli, G. S., Jansma, P. E., and Dixon, T., 2007, Kinematics of the Nicaraguan forearc from GPS geodesy: Geophysical Research Letters, v. 34.

Van Wagoner, J., Posamentier, H., Mitchum, R., Vail, P., Sarg, J., Loutit, T., and Hardenbol, J., 1988, An overview of the fundamentals of sequence stratigraphy and key definitions: Sea-Level Changes: An Integrated Approach: SEPM, Special Publication, v. 42, p. 39-45.

Vogt, K., and Gerya, T. V., 2012, From oceanic plateaus to allochthonous terranes: Numerical Modelling: Gondwana Research.

Von Huene, R., Ranero, C. R., and Vannucchi, P., 2004, Generic model of subduction erosion: Geology, v. 32, no. 10, p. 913-916.

von Huene, R., Ranero, C. R., Weinrebe, W., and Hinz, K., 2000, Quaternary convergent margin tectonics of Costa Rica, segmentation of the Cocos Plate, and Central American volcanism: Tectonics, v. 19, no. 2, p. 314-334.

Walther, C. H. E., Flueh, E. R., Ranero, C. R., Huene, R. v., and Strauch, W., 2000, Crustal structure across the Pacific margin of Nicaragua: Evidence for ophiolitic basement and a shallow mantle sliver: Geophys. J. Int., v. 141, p. 749-777.

Weinberg, R. F., 1992, Neotectonic development of western Nicargua: Tectonics, v. 11, p. 1010-1017.

Weyl, R., 1980, Geology of Central America: Berlin, Gebruder Borntraeger, p. 371.

Wilson, D. S., 1996, Fastest known spreading on the Miocene Cocos-Pacific Plate Boundary: Geophysical Research Letters, v. 23, no. 21, p. 3003-3006.

Wilson, D. S., and Hey, R. N., 1995, History of rift propagation and magnetization intensity for the Cocos-Nazca spreading center: Journal of Geophysical Research, v. 100, no. B6, p. 10041-10010,10056.

Wortel, R., and Cloetingh, S., 1981, On the origin of the Cocos-Nazca spreading center: Geology, v. 9, no. 9, p. 425-430.

Yilmaz, O., 2001, Seismic data analysis: Processing, inversion, and interpretation of seismic data, v. 1, p. 1000.